

Diffuse supernova neutrinos at underground laboratories

Cecilia Lunardini*

Arizona State University, Tempe, AZ 85287-1504 and

RIKEN BNL Research Center, Brookhaven National Laboratory, Upton, NY 11973

I review the physics of the Diffuse Supernova Neutrino flux (or Background, DSNB), in the context of future searches at the next generation of neutrino telescopes. The theory of the DSNB is discussed in its fundamental elements, namely the cosmological rate of supernovae, neutrino production inside a core collapse supernova, redshift, and flavor oscillation effects. The current upper limits are also reviewed, and results are shown for the rates and energy distributions of the events expected at future 0.1- 1 Mt mass detectors using water, liquid argon and liquid scintillator. Perspectives are given on the significance of future observations of the DSNB, both at the discovery and precision phases, for the investigation of the physics of supernovae and of the properties of the neutrino.

Contents

I. Introduction	2
II. Diffuse supernova neutrinos: the essentials	3
III. The theory: diffuse neutrinos from supernovae	4
A. Core collapse supernovae and their cosmological rates	4
B. Neutrinos from supernovae	5
C. Neutrino flavor conversion	6
D. Constraints from SN1987A	8
E. Diffuse flux at Earth	9
1. Generalities	9
2. Dependence on the original neutrino spectrum	10
3. Dependence on the core collapse rate	10
4. The $\bar{\nu}_e$ and ν_e fluxes in a detector	11
5. Diffuse flux from failed supernovae	11
IV. Detection: the diffuse neutrino flux at neutrino telescopes	12
A. The energy window	12
B. Detection concepts	12
C. Upper limits	14
1. Data and flux constraints	14
2. Implications of the SK limit	15
D. Water Cherenkov detectors towards megaton scale	15
1. Number of events	15
2. Technical considerations	16
E. Reducing backgrounds with liquid scintillator and Gadolinium	17
1. GADZOOKS	17
2. Liquid scintillator at the 50 kt scale	18
F. Liquid argon for ν_e detection	18
1. Numbers of events	18
2. technical considerations	19
V. Perspectives: what can be learned and how?	19
A. What can and can not be learned	19
B. Testing the physics of supernovae: neutrino spectra	20
C. Testing neutrino flavor conversion	21
D. Sensitivity to neutrino exotica	22
E. Directions for improvement	23
1. Phenomenology of the DSNB	23
2. Experimental searches	23
F. Final considerations	24
Acknowledgments	24

*Electronic address: Cecilia.Lunardini@asu.edu

References	24
Figures	28
Tables	53

I. INTRODUCTION

The discovery of neutrino oscillations in 2003 (Eguchi *et al.*, 2003), marks the end of a chapter in neutrino physics, and the opening of a new course in this field. This new chapter will be powered by a new array of neutrino telescopes, and focuses on neutrino sources of increasing distance from Earth, increasing energy, and increasing physical complexity.

The still mysterious core collapse supernovae are among these sources. After the handful of neutrino data from SN1987A, the scientific community is still waiting for the next detection of supernova neutrinos, to have the opportunity to learn about the physics of core collapse, to test neutrino properties, and to answer a large number of questions regarding new particles and new forces of nature. Considering that supernovae in our galactic neighborhood are rare (1-3 per century, see e.g. Ando *et al.* (2005); Arnaud *et al.* (2004)), it is likely that the opportunity will first be offered by the *diffuse* supernova neutrino flux (commonly called “diffuse supernova neutrino background”, DSNB). This flux receives contributions from all the supernovae in the universe and therefore is practically constant in time¹, requiring only the right experimental sensitivity to be seen. Once observed, it will turn the field of supernova neutrinos from the realm of rare events to the territory of a moderately paced and steady progress.

In addition to testing the variety of physics already probed by SN1987A – like neutrino masses and mixings, neutrino spectra formation in the star, and a number of exotica – the diffuse flux will offer other, complementary, information. Most importantly, the diffuse flux reflects the whole supernova population of the universe, comprised of progenitor stars of different mass and distance. Thanks to the fast rising of the supernova rate with the redshift, a substantial fraction of the DSNB at Earth originates at cosmological distances. This opens the exciting possibility to do cosmology with neutrinos, and test not only the supernova rate, but also the rate of star formation, of which supernovae are tracers.

Since the original idea that diffuse supernova neutrinos might be detectable (Bisnovatyi-Kogan and Seidov, 1982; Krauss *et al.*, 1984), the physics of the DSNB has matured considerably. After early upper limits that exceeded the predictions by orders of magnitude (Aglietta *et al.*, 1992; Zhang *et al.*, 1988), a turning point happened when SuperKamiokande placed what is currently the best limit (Malek *et al.*, 2003), a bound that touches the interval of theoretical predictions², $\Phi \sim 0.1 - 1 \text{ cm}^{-2}\text{s}^{-1}$ (above 19.3 of neutrino energy, see fig. 2), thus rising the hopes that the DSNB might be detected soon. The SuperKamiokande result has motivated more detailed theoretical predictions of the DSNB, which now include several neutrino oscillation effects³, supernova rate functions motivated by different data sets⁴, neutrino spectra from several numerical calculations (Ando and Sato, 2004; Horiuchi *et al.*, 2009) and inspired by SN1987A as well⁵, and even possible new non-standard physics⁶ and new supernova types⁷. Studies show that the current bound implies conditional constraints on the supernova rate (Strigari *et al.*, 2005) and on the neutrino flux parameters (Yuksel *et al.*, 2006), and discuss what will be learned from a future detection on the neutrino spectra (Lunardini, 2007b).

While developing the phenomenology of the DSNB, the neutrino community looks ahead to the next generation of large scale detectors⁸, of which some will expand existing projects, while others will be in completely new multi-disciplinary facilities, like the Deep Underground Science and Engineering Laboratory (DUSEL) now in its infancy

¹ Fluctuations in time could be seen due to individual supernovae at several megaparsecs of distance (Ando *et al.*, 2005).

² For predictions prior to the SuperKamiokande limit see, e.g.: Hartmann and Woosley (1997); Kaplinghat *et al.* (2000); Malaney (1997); Totani and Sato (1995); Totani *et al.* (1996); Woosley *et al.* (1986).

³ Oscillation effects are discussed in detail in: Ando and Sato (2003, 2004); Chakraborty *et al.* (2008); Cocco *et al.* (2004); Fogli *et al.* (2005); Galais *et al.* (2009); Lunardini (2006b).

⁴ For works with particular focus on the supernova rate, see e.g. Ando (2004); Ando and Sato (2004); Ando *et al.* (2003); Daigne *et al.* (2005); Iocco *et al.* (2005); Strigari *et al.* (2004).

⁵ The connection with SN1987A was first made by Fukugita and Kawasaki (2003), followed by detailed studies by Horiuchi *et al.* (2009); Lunardini (2006b); Yuksel and Beacom (2007).

⁶ See for example: Ando (2003); Fogli *et al.* (2004); Goldberg *et al.* (2005); Volpe and Welzel (2007).

⁷ Studies appeared recently, see e.g.: Daigne *et al.* (2005); Lien *et al.* (2010); Lunardini (2009).

⁸ For the main proposals, see de Bellefon *et al.* (2006); Cline *et al.* (2006); Ereditato and Rubbia (2006); Jung (1999); Marrodan Undagoitia *et al.* (2006); Nakamura (2003); Rubbia (2009b); Wurm *et al.* (2007).

in the USA⁹. For the new neutrino telescopes, observing the DSNB is an important item of the agenda, to the point that technical upgrades are sometimes driven by this specific goal (Beacom and Vagins, 2004). For all detection technologies backgrounds are the main limiting factors, as they often restrict the sensitive energy window considerably (to the 20-40 MeV interval, in the case of a water Cherenkov detector) and even in the energy window they limit the benefits of the larger detector mass.

Interestingly, searches for the DSNB show how, in the new chapter of neutrino astrophysics, what were once sought after signals – such as solar and atmospheric neutrinos – will become well known backgrounds that will have to be reduced or subtracted. This shift in the focus of neutrino experiments might have interesting implications on what characteristics might define an ideal detector several decades from now.

In this time of intense activity on the diffuse supernova neutrino flux, this review may offer a timely summary as well as a useful perspective on this new direction of research, within the activity of scoping of the next generation of neutrino telescopes. The paper opens with a section of essential facts (sec. II), which are then developed in sec. III for the theory and IV for detection aspects. A section of discussion of the physics potential of the DSNB follows in closing (sec. V).

Many of the numerical results (figures and tables) that appear here were prepared specifically for this review – and not taken from previous literature – for the sake of consistency in the graphics styles and in the sets of input parameters. The original works where analogous results appear will be referenced as accurately as possible, with apologies in advance for involuntary omissions.

II. DIFFUSE SUPERNOVA NEUTRINOS: THE ESSENTIALS

This section gives a minimal introduction to the subject of diffuse supernova neutrinos. It might be useful to the reader who needs only the essential information, and to others as a summary of the reminder of the review.

Stars with masses larger than $\sim 8M_\odot$ (with $M_\odot = 1.99 \cdot 10^{30}$ Kg the mass of the Sun) end their lives with the gravitational collapse of their core, followed first by neutrinos emission over a time scale of about 10 s, and then by a shock-driven, very luminous, explosion called a supernova (SN). These core collapse supernovae¹⁰ are relatively rare phenomena: their rate in the universe today (redshift $z = 0$) is $R_{SN}(0) \sim 10^{-4} \text{ yr}^{-1} \text{ Mpc}^{-3}$. Interestingly, the supernova rate is a growing function of the redshift, z , signifying that supernovae were more frequent in the past (sec. III.A).

The matter inside a supernova is dense enough (reaching nuclear density in the core, $\rho \simeq 10^{14} \text{ g cm}^{-3}$) to host a thermal population of neutrinos of all species ($\nu_e, \bar{\nu}_e, \nu_\mu, \nu_\tau, \bar{\nu}_\mu, \bar{\nu}_\tau$) which then diffuse out and reach the Earth, carrying information on the stellar temperature in their nearly thermal energy spectrum, which peaks at $\sim 10 - 20$ MeV. It is expected that ν_e and $\bar{\nu}_e$ have colder spectra than the other species, as they are more strongly coupled to matter (sec. III.B). Neutrinos dominate the energetics of a supernova: they carry away about 99% of the gravitational binding energy released in the collapse, $E_b \simeq 3 \cdot 10^{53} \text{ ergs}$ ($= 3 \cdot 10^{46} \text{ J}$), which is roughly equipartitioned between the six neutrino species.

On the way between their production point and a detector on Earth, the neutrinos undergo redshift of energy and flavor conversion (oscillations), so that the flux of neutrinos (antineutrinos) of a given flavor in a detector is a linear combination of the fluxes of neutrinos (antineutrinos) originally produced in different flavors (sec. III.C). If all supernovae are outside our immediate galactic neighborhood (farther than few megaparsecs), the flux we receive from each of them is practically infinitesimal, but the total, diffuse, flux from all supernovae combined is in principle observable. In terms of the (comoving) supernova rate, $R_{SN}(z)$, the diffuse flux of $\bar{\nu}_e$ in a detector at Earth, differential in energy, surface and time, is given by:

$$\Phi_{\bar{e}}(E) = \frac{c}{H_0} \int_0^{z_{max}} R_{SN}(z) F_{\bar{e}}(E') \frac{dz}{\sqrt{\Omega_m(1+z)^3 + \Omega_\Lambda}} \quad (1)$$

(see e.g. Ando and Sato (2004)), where $F_{\bar{e}}(E')$ is the contribution of an individual supernova, inclusive of neutrino oscillations and of the redshift of energy, $E' = E(1+z)$, and differential in E' . Ω_m and Ω_Λ are the fractions of the cosmic energy density in matter and dark energy respectively; c is the speed of light and H_0 is the Hubble constant. z_{max} is the maximum redshift for which there is substantial star formation, $z_{max} \sim 5$ (sec. III.A).

⁹ For the main vision and details, see various authors (2008); Barger *et al.* (2007); Svoboda (2008).

¹⁰ Core collapse supernovae are astronomically classified as type II, Ib and Ic. Type Ia supernovae are of entirely different nature and do not involve a collapse of the stellar core.

Estimates (fig. 1) show that for realistic neutrino spectra and luminosities, the DSNB peaks around $5 - 7$ MeV of energy, where it can be as large as $\Phi \sim 5 \text{ cm}^{-2}\text{s}^{-1}\text{MeV}^{-1}$ for each neutrino species. It decays exponentially with energy above the peak. The flux in each neutrino type is typically in the range $12 - 20 \text{ cm}^{-2}\text{s}^{-1}$ if integrated over all energies, and $\sim 0.2 - 1 \text{ cm}^{-2}\text{s}^{-1}$ in the energy window of current experimental interest: $E \sim 18 - 35$ MeV. This window is determined by backgrounds such as spallation and solar neutrinos at low energy, and atmospheric neutrinos at high energy (sec. IV.A).

Experimentally, many upper bounds on the DSNB exist (fig. 1; sec. IV.C). The strongest is on the $\bar{\nu}_e$ component, from the positron search at SuperKamiokande (SK) (Malek *et al.*, 2003):

$$\Phi_{\bar{\nu}_e}(E > 19.3 \text{ MeV}) < 1.4 - 1.9 \text{ cm}^{-2}\text{s}^{-1} \quad \text{at } 90\% \text{C.L.}, \quad (2)$$

where the interval accounts for varying the neutrino spectrum (Lunardini and Peres, 2008). This limit is between a factor of 1 and 4 or so from theoretical predictions (fig. 2), and thus suggests the detectability of the DSNB at current, or, more likely, near future detectors. Current projects for new neutrino telescopes include a ~ 1 Mt water Cherenkov detector (de Bellefon *et al.*, 2006; Jung, 1999; Nakamura, 2003), a 50 kt liquid scintillator one (Marrodan Undagoitia *et al.*, 2006; Wurm *et al.*, 2007) and a 0.1 kt liquid argon experiment (Cline *et al.*, 2006; Ereditato and Rubbia, 2006; Rubbia, 2009b) (secs. IV.D-IV.E). They are largely complementary in their capability for the DSNB: the Mt water Cherenkov design will have the largest statistics ($\sim 30 - 230$ events for a $2 \text{ Mt} \cdot \text{yr}$ exposure, sec. IV.D), while a solution of water and Gadolinium as well as liquid scintillator allow to reduce background, and liquid argon has a unique sensitivity to electron neutrinos.

The first phase of the DSNB detection will probably be a test of the theoretically predicted event rates, and will constrain the multi-dimensional space of the parameters that govern the DSNB. A more mature phase will require high energy resolution and lower energy thresholds (compared to SK) as key elements. It would allow to reconstruct the energy spectrum of at least some flavor components of the DSNB and therefore infer information – even though in a model dependent way – on the spectrum of the neutrinos that emerge from an individual supernova (sec. V.B). Tests of the cosmological supernova rate, $R_{SN}(z)$, will be complementary to, but probably not as sensitive as, astrophysical ones (sec. V). Neutrino oscillation effects will be probed at a basic level, limited by the high energy thresholds and by the integration over z washing out interesting spectral features (sec. V.C). Several exotica will be probed, improving on the many strong constraints already placed by SN1987A, especially thanks to the longer propagation distances involved.

III. THE THEORY: DIFFUSE NEUTRINOS FROM SUPERNOVAE

A. Core collapse supernovae and their cosmological rates

How common are supernovae in the universe? The question of the rate of stellar death by core collapse is interestingly related to the question of stellar birth. Indeed, supernova progenitors have a typical life span of $\sim 10^7$ years, much smaller than the characteristic time of formation of a star. Thus, it is expected that the supernova rate (SNR) as a function of the redshift z , should be proportional to the cosmological star formation rate (SFR), defined as the mass that forms stars per unit of (comoving) volume per unit time. Assuming that stars are distributed in mass according to the Salpeter Initial Mass Function, $\phi(m) \propto m^{-2.35}$ (Salpeter, 1955), this proportionality between the supernova rate $R_{SN}(z)$ and the star formation rate $R_{SF}(z)$ reads:

$$R_{SN}(z) = \frac{\int_{8M_{\odot}}^{125M_{\odot}} dm \phi(m)}{\int_{0.5M_{\odot}}^{125M_{\odot}} dm m \phi(m)} R_{SF}(z) \simeq 0.0122 M_{\odot}^{-1} R_{SF}(z), \quad (3)$$

where a cutoff of $0.5M_{\odot}$ has been assumed and $125M_{\odot}$ is a tentative upper limit for the occurrence of normal core collapse supernovae (as opposed to pair instability ones or black-hole forming events). The exact value of this limit does not influence results appreciably.

The SFR is fairly well known, even though with some uncertainties, especially on the normalization. Different tracers of star formation, such as ultraviolet and far-infrared radiation, indicate that the SFR grows with z (see e.g., Hopkins (2006) for a review). Fig. 3 shows the data and two commonly used functional fits, a piecewise one and a continuous one from Cole *et al.* (2001):

$$R_{SF}(z) \propto \begin{cases} (1+z)^{\beta} & z < 1 \\ (1+z)^{\alpha} & 1 < z < 4.5 \\ (1+z)^{\gamma} & 4.5 < z \end{cases} \quad (4)$$

$$R_{SF}(z) \propto \frac{a + bz}{1 + (z/c)^d},$$

where $\alpha, \beta, \gamma, a, b, c, d$ are fit parameters. In the next sections the piecewise form will be used, for its transparency and easier comparison with other literature (e.g. Lunardini (2006b)). Fig. 3, as well as the detailed statistical analysis in Hopkins (2006), show that the SFR is about $R_{SF}(0) = 0.015 M_{\odot} \text{yr}^{-1} \text{Mpc}^{-3}$ today, grows with power $\beta \simeq 3$ ($\beta = 3.28$ best fit) up to $z \simeq 1$, flattens at larger redshift ($\alpha = -0.26$ best fit) and decreases at $z \gtrsim 4.5$ ($\gamma = -7.8$ best fit). The corresponding best fit SNR, obtained via Eq. (3), can be written as:

$$R_{SN}(z) = R_{-4} 10^{-4} \text{ yr}^{-1} \text{Mpc}^{-3} \begin{cases} (1+z)^{3.28} & z < 1 \\ (1+z)^{-0.26} & 1 < z < 4.5 \\ (1+z)^{-7.8} & 4.5 < z \end{cases} \quad (5)$$

with $R_{-4} \sim 1$ describing the uncertainty in the normalization. It is plotted in fig. 4 (left panel, upper dashed line).

Fig. 4 also shows the *direct* measurements of the SNR as of 2005 (Cappellaro *et al.*, 1999, 2005; Dahlen *et al.*, 2004) and their piecewise fitting curve (Lunardini, 2006b). For the same fit, fig. 5 gives the allowed region of the parameters $R_{SN}(0)$ and β ; the correlation between the two quantities is evident in the figure. The comparison between the SNR obtained directly and that derived from the SFR (fig. 4, left) shows a discrepancy in the normalization of the SNR, which can be interpreted as a measure of the systematic errors involved. Note that the discrepancy should be lessened if the 2008 data were included (fig. 4, right).

B. Neutrinos from supernovae

Core collapse supernovae are the only site in the universe today where the matter density is large enough to have the buildup of a thermal gas of neutrinos. Thanks to their lack of electromagnetic interaction, these neutrinos can diffuse out of the star over a time scale of few seconds, much shorter than the diffusion time of photons. This makes the neutrinos the principal channel of emission of the $\mathcal{O}(10^{53})$ ergs of gravitational energy that is liberated in the collapse. The energy spectrum of neutrinos of each flavor is expected to be thermal near the surface of decoupling from matter (“neutrinosphere”), but then it changes due to propagation effects. One of these effects is scattering. Numerical modeling indicates that, after scattering right outside the decoupling region, neutrinos of a given flavor w ($w = e, \mu, \tau$) have energy spectrum:

$$\frac{dN_w}{dE} \simeq \frac{(1 + \alpha_w)^{1+\alpha_w} L_w}{\Gamma(1 + \alpha_w) E_{0w}^2} \left(\frac{E}{E_{0w}} \right)^{\alpha_w} e^{-(1+\alpha_w)E/E_{0w}}, \quad (6)$$

(Keil *et al.*, 2003), where E is the neutrino energy, L_w is the (time-integrated) luminosity in the species w and E_{0w} is the average energy of the spectrum. The quantity α_w is a numerical parameter, $\alpha_w \sim 2 - 5$ (Keil *et al.*, 2003), describing the shape of the spectrum. Considering typical temperatures of matter near the collapsed core, one expects average energies in the 10-20 MeV range. The non-electron neutrino flavors, $\nu_{\mu}, \nu_{\tau}, \bar{\nu}_{\mu}$ and $\bar{\nu}_{\tau}$ (each of them denoted as ν_x from here on¹¹), interact with matter more weakly than ν_e and $\bar{\nu}_e$ (via neutral current processes only), and therefore decouple from matter in a denser and hotter region. Additionally, an asymmetry exist in the coupling with matter of ν_e and $\bar{\nu}_e$: these are kept in thermalized by charged current interaction on neutrons and protons respectively, and the overabundance of neutrons relative to protons implies a lower decoupling temperature for ν_e . Therefore, we expect a hierarchy of average energies:

$$E_{0e} < E_{0\bar{e}} < E_{0x}. \quad (7)$$

While the basic spectral features and the total neutrino luminosity are generic predictions, a detailed study of neutrino emission in a supernova requires complex numerical calculations, that have been performed by several groups in the quest of reproducing the observed explosion that follows the collapse (see e.g. Cardall *et al.* (2005) for a review). For illustration, here I use three different results, summarized in Table I. They are from the Lawrence Livermore group (LL, Totani *et al.* (1998)), from Burrows, Thompson and Pinto (Arizona group, TBP, Thompson *et al.* (2003)) and from Keil, Raffelt and Janka (Garching group, KRJ, “accretion phase model II” in Keil *et al.* (2003)). They have been used extensively to model the diffuse flux (see e.g. Ando and Sato (2004)) and so their use facilitates the comparison with previous literature. While updated calculations exist¹², these three models are still representative of the variety of results currently available.

¹¹ For the energies of interest here, the produced fluxes of ν_{μ}, ν_{τ} are equal with very good approximation. They are also nearly equal to the fluxes of $\bar{\nu}_{\mu}$ and $\bar{\nu}_{\tau}$, up to corrections due to weak magnetism (Horowitz, 2002).

¹² For recent examples see e.g., Fischer *et al.* (2009); Huedepohl *et al.* (2009); Marek and Janka (2009); Ott *et al.* (2008).

From Table I one sees major differences between the predictions of the three groups, especially between the LL model and the other two. The LL calculation follows the neutrino emission in its entire time duration, and obtains an explosion. It finds a nearly exact equipartition of the (time integrated) luminosity between the different neutrino species. However, the intensive calculation of the evolution up to several seconds post-bounce came at the price of a relatively simplified treatment of neutrino transport, where several relevant processes were not included.

The TBP hydrodynamic calculation simulates the neutrino emission up to 0.25 s post-bounce and includes relevant processes such as neutrino bremsstrahlung and neutrino-nucleon scattering with nucleon recoil. Results show softer energy spectra for neutrinos of all flavors and a deviation from equipartition of luminosities. Due to the short simulation time, these results are not immediately applicable to the diffuse flux, however they can be used as a rough representation of the tendency of models with more sophisticated neutrino transport to give lower neutrino average energies. The deviation from the equipartition of luminosities is not adopted here, however, as its validity for the total flux has not been established. Equipartition will be used.

The KRJ calculation uses a Monte Carlo method. Neutrino transfer is solved in a static background (not coupled to the hydrodynamics) up to 150 ms post-bounce. Many relevant neutrino processes are included, and ν_μ and ν_τ elastic scattering on nucleons are found to be the main source of opacity. Results indicate that the ν_x and $\bar{\nu}_e$ spectra might be very similar, with only a weak hierarchy compared to the other models. A strong deviation of the equipartition of luminosity is found in favor of the electron flavors, but again equipartition is assumed here due to the lack of investigation on longer evolution times.

The models discussed so far refer to the most common scenario for a supernova: a collapse that leads to the formation of a neutron star (“neutron star-forming collapses”, NSFCs). Recently, detailed studies have appeared¹³ on the rarer case of *direct* collapse into a black hole without explosion, i.e., a *failed supernova*. This is the fate of stars with $M \gtrsim 25 - 40 M_\odot$, which comprise a 9 - 22% fraction of all supernova progenitors (Lunardini, 2009). It was shown that the neutrino emission from these direct black hole-forming collapses (DBHFCs) is somewhat more luminous and decidedly more energetic than for neutron star-forming collapses – depending on the equation of state (EoS) of nuclear matter – due to the rapid contraction of the newly formed protoneutron star preceding the black hole formation. This suggests that the hotter contribution of black hole-forming collapses to the DSNB might exceed that of neutron star-forming ones in part of the energy spectrum (Lunardini, 2009).

Fig. 6 shows the neutrino fluxes emitted in a direct black hole-forming collapse, taken from fig. 5 of Nakazato *et al.* (2008). They were obtained for the $40 M_\odot$ progenitor in Woosley and Weaver (1995) with the stiffer Shen *et al.* (S) EoS (Shen *et al.*, 1998) (incompressibility $K = 281$ MeV) and the softer Lattimer-Swesty (LS) one (Lattimer and Swesty, 1991) (with $K = 180$ MeV, see Nakazato *et al.* (2008)). It appears that average energies are $E_0 \sim 20 - 24$ MeV for all neutrino flavors, with a stiffer EoS corresponding to more energetic neutrino spectra. Notice how the ν_e and $\bar{\nu}_e$ components are especially luminous due to the high rate of capture of electrons and positrons on nuclei.

C. Neutrino flavor conversion

For a long time a mere hypothesis, neutrino flavor conversion is now a reality well established experimentally (Ahmad *et al.*, 2001; Eguchi *et al.*, 2003). The leading mechanism driving conversion is neutrino oscillations due to the neutrino being massive and having non-zero mixing between the neutrino mass eigenstates, ν_i ($i = 1, 2, 3$) with masses m_i , and the flavor eigenstates, ν_α ($\alpha = e, \mu, \tau$): $\nu_\alpha = \sum_i U_{\alpha i} \nu_i$. The standard parameterization of the mixing matrix (see e.g. Krastev and Petcov (1988)) is in terms of three mixing angles: $\theta_{12}, \theta_{23}, \theta_{13}$. Oscillation effects depend on these angles and on the mass squared differences, $\Delta m_{ij}^2 = m_i^2 - m_j^2$, as well as on the neutrino energy and on the density and composition of the medium of propagation due to forward scattering on the matter constituents (refraction).

After a first, intense phase of neutrino experiments on solar, atmospheric, reactor and accelerator neutrinos, measurements are available for the quantities $\theta_{12}, \theta_{23}, \Delta m_{21}^2$ and $|\Delta m_{31}^2|$ (see e.g., Schwetz *et al.* (2008)):

$$\begin{aligned} |\Delta m_{31}^2| &= (2.40^{+0.12}_{-0.11}) \cdot 10^{-3} \text{eV}^2 & \tan^2 \theta_{23} &= 1.0^{+0.32}_{-0.22} \\ \Delta m_{21}^2 &= (7.59^{+0.21}_{-0.21}) \cdot 10^{-5} \text{eV}^2, & \tan^2 \theta_{12} &= 0.468^{+0.042}_{-0.033}. \end{aligned} \quad (8)$$

Current data are not sufficient to distinguish the sign of Δm_{31}^2 : The two possibilities, $\Delta m_{32}^2 \approx \Delta m_{31}^2 > 0$ and $\Delta m_{32}^2 \approx \Delta m_{31}^2 < 0$, are referred to as *normal* and *inverted* mass hierarchy/ordering. The angle θ_{13} , which describes

¹³ Starting from the first study of 2004, the main references are: Fischer *et al.* (2008); Liebenroerfer *et al.* (2004); Nakazato *et al.* (2008); Sumiyoshi *et al.* (2007, 2008, 2006).

the electron flavor content of ν_3 , is not measured, but known to be small (Apollonio *et al.*, 1999; Boehm *et al.*, 2000):

$$\sin^2 \theta_{13} \lesssim 0.02 . \quad (9)$$

With these information, it has been possible to study flavor conversion of supernova neutrinos in detail, uncovering a very rich pattern. One can distinguish four spatially separated stages of conversion, that contribute to the final ν_e and $\bar{\nu}_e$ survival probabilities (Table II):

- Within ~ 200 Km radius in the star, flavor oscillations occur due to neutrino-neutrino coherent scattering¹⁴ when the density of neutrinos exceeds that of electrons (Esteban-Pretel *et al.*, 2008). This should be the case $\sim 1 - 5$ s after the core bounce. The net effect is a swap of the spectra of the electron and non-electron neutrinos and antineutrinos for the inverted mass hierarchy and above a certain critical energy, E_c . E_c is very small for antineutrinos, while for neutrinos it depends on the fluxes of ν_e , and $\bar{\nu}_e$ and ν_x ($\nu_x = \nu_\mu, \nu_\tau, \bar{\nu}_\mu, \bar{\nu}_\tau$) as:

$$\int_{E_c}^{\infty} (F_e^0 - F_x^0) = \int_0^{\infty} (F_e^0 - F_x^0) , \quad (10)$$

with $E_c \simeq 3 - 10$ MeV as typical values (Duan *et al.*, 2007b).

- At larger radii, where neutrino-neutrino coherent scattering is negligible, conversion is driven by coherent scattering on electrons, according to the Mikheev-Smirnov-Wolfenstein effect (MSW) (Mikheev and Smirnov, 1985; Wolfenstein, 1978), that was first elaborated in the context of solar neutrino and then applied to supernova neutrinos (Mikheev and Smirnov, 1986). In essence, the MSW effect is the idea that a small neutrino mixing induces more than 50% change of flavor if neutrinos propagate in matter and:
 - (i) the matter density along the neutrino trajectory varies slowly enough that there are no quantum transitions between different eigenstates of the Hamiltonian (*adiabatic propagation*). Under this condition, a neutrino that is produced in given eigenstate of the Hamiltonian in matter, $\nu_{i,m}$ will remain in such state while the flavor composition of the state itself varies as an effect of the varying matter density along the neutrino trajectory. At emergence from the star, the neutrino is in the vacuum state ν_i , whose flavor composition is described by the mixing matrix. The process results in a strong change of flavor if
 - (ii) the neutrinos cross a region where the density is such (*resonance density*) that a cancellation occurs between the matter and kinetic terms of the Hamiltonian, thus producing a resonant behavior.

Two MSW resonances relevant for ν_e and $\bar{\nu}_e$ conversion are realized inside a supernova, corresponding to the two independent mass squared splittings (fig. 7). The first resonance occurs at $\rho \sim 10^3 \text{ g} \cdot \text{cm}^{-3}$; it depends on θ_{13} and on the neutrino mass hierarchy: it affects neutrinos (antineutrinos) if the mass hierarchy is normal (inverted). The adiabaticity of the conversion in this resonance is described by the probability of quantum transitions, P_H (where H stands for “high” matter density). For small mixing angles (which is the case here) P_H can be calculated using the well known Landau-Zener formalism and a model for the electron density profile of the star. Using a power law profile,

$$\rho(r) = 10^{13} C \left(\frac{10 \text{ km}}{r} \right)^3 \text{ g} \cdot \text{cm}^{-3} \quad C \simeq 1 - 15 \quad (11)$$

(Lunardini and Smirnov, 2003), one gets:

$$P_H = \exp \left[- \left(\frac{E_{na}}{E} \right)^{2/3} \right] , \quad (12)$$

$$E_{na} \simeq 1.08 \cdot 10^7 \text{ MeV} \left(\frac{|\Delta m_{32}^2|}{10^{-3} \text{ eV}^2} \right) C^{1/2} \sin^3 \theta_{13} \quad (13)$$

(Lunardini and Smirnov, 2003). Evaluating this formula shows that the conversion is adiabatic ($P_H \simeq 0$) for $\sin^2 \theta_{13} \gtrsim 3 \cdot 10^{-4}$ or so and completely non-adiabatic ($P_H \simeq 1$) for $\sin^2 \theta_{13} \lesssim 3 \cdot 10^{-6}$ (fig. 8) (Dighe and Smirnov, 2000; Lunardini and Smirnov, 2003).

¹⁴ See e.g. Duan *et al.* (2006a,b, 2007a, 2006c); Esteban-Pretel *et al.* (2007); Fogli *et al.* (2007); Hannestad *et al.* (2006); Raffelt and Smirnov (2007).

- The second resonance is at $\rho \sim 10 \text{ g} \cdot \text{cm}^{-3}$ and is described by the parameters θ_{12} and Δm_{21}^2 , known as the LMA (Large Mixing Angle MSW) solution of the solar neutrino problem. The resonance is adiabatic and it affects neutrinos. Antineutrinos undergo non-resonant conversion, thanks to θ_{12} being large.
- A fourth stage of oscillations happens inside the Earth, where the physical conditions resemble those of the second resonance. While potentially important for neutrinos from a galactic supernova, these oscillations affect the DSNB by less than few per cent (Lunardini, 2006a), so they will not be discussed here.

The fluxes of ν_e and $\bar{\nu}_e$ after oscillations are a mixture of the original fluxes in these flavors and of the original muon and tau component. Up to a geometric factor due to the distance from the star (omitted here for simplicity), they are described by the survival probabilities, p, \bar{p} as:

$$F_e = pF_e^0 + (1 - p)F_x^0, \quad (14)$$

$$F_{\bar{e}} = \bar{p}F_{\bar{e}}^0 + (1 - \bar{p})F_x^0. \quad (15)$$

The oscillated fluxes, $F_e, F_{\bar{e}}$, are more energetic than the original ones due to the higher average energy of F_x^0 . This spectral hardening is one of the main signature of neutrino flavor conversion in a supernova. The calculation of p and \bar{p} is at times complex, and for this we refer to the literature (e.g., Dasgupta *et al.* (2008); Dighe and Smirnov (2000); Duan *et al.* (2007c); Lunardini and Smirnov (2003)). Here the results are shown in Table II. It appears that p and \bar{p} are in the ranges:

$$\begin{aligned} p &= 0 - \sin^2 \theta_{12} \simeq 0 - 0.32, \\ \bar{p} &= 0 - \cos^2 \theta_{12} \simeq 0 - 0.68. \end{aligned} \quad (16)$$

In general, both quantities vary with the neutrino energy due to the spectral swap at $E = E_c$ and to the energy dependence of P_H . However, in many situations of interest the probabilities are constant in energy. This is the case if $\sin^2 \theta_{13} \gtrsim 3 \cdot 10^{-4}$ or $\sin^2 \theta_{13} \lesssim 3 \cdot 10^{-6}$ (see fig. 8) and if the neutrino energy is above E_c , which is typically the case for the DSNB in the energy window for detection.

As a final remark, it should be noted that the phenomenology of oscillations induced by neutrino-neutrino scattering is still in the phase of initial exploration, and therefore the results in Table II may change as studies progress. For example, recently it has been understood that multiple spectral swaps due to neutrino-neutrino scattering can occur (Dasgupta *et al.*, 2009). One should also consider that p and \bar{p} change over the duration of a neutrino burst due to the time evolution of the neutrino spectra and luminosities (which affect the neutrino-neutrino refraction effects) and to shockwave-modulated oscillations (Ando and Sato, 2003; Galais *et al.*, 2009). Therefore the expressions in Table II may not be entirely applicable to the DSNB. Variations between individual supernovae (e.g., in the matter density profile, see Nakazato *et al.* (2008)) may further complicate the description of conversion effects for the DSNB. In view of these uncertainties, it is adequate and convenient – for the sake of generality – to describe the effects of oscillations on the DSNB in terms of p and \bar{p} intended as averaged over time and over the supernova population. I neglect their energy dependence for the reasons discussed so far, and vary them in the numerical intervals (16), which are guaranteed to be valid by the adiabaticity of the lower density resonance and in the absence of turbulence (see e.g. Kneller and Volpe (2010)).

D. Constraints from SN1987A

It is interesting to check how predictions compare with the only data we currently have on supernova neutrinos – those from SN1987A – and what these data alone tell us without theoretical priors (Fukugita and Kawasaki, 2003; Lunardini, 2006b). Fig. 9 shows the data published by the Kamiokande-II and IMB experiments (Bionta *et al.*, 1987; Hirata *et al.*, 1987) and the best fits from a maximum likelihood analysis of the two datasets separately and combined (Lunardini, 2006b). The analysis was carried out assuming that all the events were from inverse beta decay ($\bar{\nu}_e + p \rightarrow n + e^+$) for the inverted mass hierarchy and with five fit parameters: $L_{\bar{e}}, L_x, E_{0\bar{e}}, E_{0x}, \theta_{13}$. Varying the mixing angle θ_{13} covers the entire range of possible values of \bar{p} (table II), thus effectively including the case of normal hierarchy. For simplicity, $\alpha_{\bar{e}} = \alpha_x = 2.3$ (which give a spectral shape close to Fermi-Dirac) was held fixed. The figure shows that the two datasets are compatible, in spite of the tension in their favoring different neutrino energy spectra. The best fit of all the data together is realized for maximum permutation of fluxes ($\bar{p} = 0.68$) and:

$$\begin{aligned} E_{0\bar{e}} &= 4.2 \text{ MeV} & L_{\bar{e}} &= 4.4 \cdot 10^{53} \text{ ergs} \\ E_{0x} &= 14.9 \text{ MeV} & L_x &= 0.8 \cdot 10^{53} \text{ ergs}, \end{aligned} \quad (17)$$

where the $\bar{\nu}_e$ parameters are somewhat in tension with the theoretical expectations for the unusually low average energy and the very large luminosity.

The region of the parameter space allowed at different confidence levels is large and is shown in fig. 10, where the hierarchy $E_{0\bar{e}} \leq E_{0x}$ (Eq. (7)) has been imposed. A comparison between this figure and Table I shows that the data are compatible with numerical predictions (only marginally for the LL model), but at the same time allow much softer neutrino spectra, which thus remain a possibility on the basis of data alone. How these softer spectra impact the DSNB is discussed in sec. III.E.4.

E. Diffuse flux at Earth

1. Generalities

Armed with the ingredients discussed so far, one can calculate the DSNB expected at Earth, using Eq. (1). Here I first discuss a scenario in which a number of approximations and simplifying assumptions hold:

- all the neutrinos are from neutron star-forming collapses (Table I)
- the neutrino emission is identical for all neutron star-forming progenitors, which is a condition for the validity of Eq. (1). The generalization to a mixed population (neutron star-forming and black hole-forming) will be discussed in sec. III.E.5.
- the total neutrino luminosity is fixed and equipartitioned among the flavors: $L_e = L_{\bar{e}} = L_x = 0.5 \cdot 10^{53}$ ergs.
- the piecewise form of the SNR, Eq. (5), is used, with $R_{-4} = 1$.¹⁵
- the survival probabilities p, \bar{p} are constant in energy, which is valid in several representative cases (sec. III.C).
- due to backgrounds, the energy thresholds that are considered realistic for the detection of the DSNB are $E_{th} \simeq 11 - 20$ MeV (see sec. IV). These will be the focus of the discussion.

Under these conditions, one can write the $\nu_e, \bar{\nu}_e$ component of the DSNB as:

$$\begin{aligned}\Phi_e(E) &= p\Phi_e^0(E) + (1-p)\Phi_x^0(E) , \\ \Phi_{\bar{e}}(E) &= \bar{p}\Phi_{\bar{e}}^0(E) + (1-\bar{p})\Phi_x^0(E) ,\end{aligned}\tag{18}$$

where

$$\Phi_w^0(E) = \frac{c}{H_0} \int_0^{z_{max}} R_{SN}(z) F_w^0(E') \frac{dz}{\sqrt{\Omega_m(1+z)^3 + \Omega_\Lambda}} ,\tag{19}$$

is the component of the DSNB of the species w in absence of oscillations and $E' = E(1+z)$ (sec. III.C). While unphysical, $\Phi_e^0, \Phi_{\bar{e}}^0, \Phi_x^0$ are useful to understand the main features of the DSNB and to calculate results for several different oscillations scenarios.

For applications, it is interesting to study the integrated fluxes (oscillated and unoscillated) above a threshold E_{th} :

$$\phi_w(E_{th}) = \int_{E_{th}}^\infty \Phi_w(E) dE , \quad \phi_w^0(E_{th}) = \int_{E_{th}}^\infty \Phi_w^0(E) dE .\tag{20}$$

¹⁵ Results can be rescaled to reproduce those of other literature, e.g. Ando and Sato (2004) ($R_{-4} = 0.87$), Lunardini (2006b) ($R_{-4} = 0.67$, best fit) and Hopkins and Beacom (2006) ($R_{-4} = 1.84$).

2. Dependence on the original neutrino spectrum

Here I describe how the neutrino fluxes at production, F_w^0 , influence the DSNB. For simplicity, I consider the unoscillated fluxes Φ_w^0 and ϕ_w^0 ; as their features apply to the oscillated ones through the combination (18).

The integral in Eq. (19) can not be calculated exactly, and so one can resort to certain approximations or to numerical calculation. The following approximation is valid at high energy ($\gtrsim 15 - 20$ MeV) (Lunardini, 2007a):

$$\Phi_w^0 \simeq R_{SN}(0) \frac{c}{H_0} \frac{L_w}{\Gamma(2 + \alpha_w) \epsilon_w^2} e^{-\frac{E}{\epsilon_w}} \sum_{k=0}^{\eta_w} \left[\left(\frac{E}{\epsilon_w} \right)^{\alpha_w - 1 - k} \frac{\eta_w!}{(\eta_w - k)!} \right], \quad (21)$$

where Γ stands for the Gamma function, $\eta_w \equiv \alpha_w + \beta - 3\Omega_m/2$ (β is the power of growth of the SFR and SNR with z , Eq. (4)) and $\epsilon = E_{0w}/(1 + \alpha_w)$. The dependence on the parameters α and γ of the SFR is neglected. The expression (21) exceeds the exact result by up to 40% above 19 MeV of energy. It has also been observed (Lunardini, 2007a; Malek, 2003) that a simple exponential form, $\Phi_w^0 = \Phi_w^0(0) e^{-E/\langle E \rangle_w}$ (with $\langle E \rangle_w \sim \epsilon_w$) is adequate for realistic parameters and for $E \gg \langle E \rangle_w$. In what follows, exact, numerically calculated results will be discussed.

Fig. 11 illustrates Φ_w^0 ($w = e, \bar{e}, x$) for different values of the parameters E_{0w}, α_w of the original flux F_w^0 . It appears that Φ_w^0 has a peak value of $\sim 1 - 5 \text{ cm}^{-2} \text{s}^{-1} \text{MeV}^{-1}$ at 4-7 MeV, with an exponential decay at higher energy. As expected from Eq. (21), the decay is faster for smaller ϵ , corresponding to lower average energy E_{0w} and/or larger α_w . For $\alpha_w = 3.8$, varying E_{0w} between 9 and 18 MeV corresponds to a variation of the diffuse flux at 20 MeV by more than one order of magnitude, while variations are more modest (a factor of 2 or so) when varying α_w between 2 and 5 with E_{0w} fixed. The dependence on the parameters becomes stronger with increasing neutrino energy.

For further illustration, the fluxes $\Phi_e^0, \Phi_{\bar{e}}^0, \Phi_x^0$ for the LL, TBP and KJR models (Table I) are presented in fig. 12. Notice that the ν_x flux can easily be one order of magnitude larger than the ν_e one at 30-40 MeV. This already gives an idea of how flavor conversion can strongly enhance the potential of detection of the electron flavor components above realistic thresholds (sec. III.E.4).

The characteristics of the integrated flux ϕ_w^0 reflect those already noted for the energy spectrum: for $E_{th} \gtrsim 10$ MeV, ϕ_w^0 increases with the increasing average energy E_{0w} and with decreasing values of α_w . Fig. 13 illustrates this for $E_{th} = 19.3, 11.3$ MeV, that are both relevant for water Cherenkov detectors (sec. IV). In the figure one notes the dramatic increase (up to one order of magnitude!) of the flux as the energy cut is lowered, thus approaching the peak of the spectrum.

This is further illustrated in Table III, where the values of $\phi_e^0, \phi_{\bar{e}}^0, \phi_x^0$ are given for the LL, TBP, KRJ models. The Table evidences the large differences between the fluxes in the different flavors and in the different models. Among the total fluxes, integrated over all energies, the ν_e flux is larger: indeed, it has the same total luminosity than the other flavors, but each ν_e carries on average a lower energy. When the integration is restricted to increasingly high energy, the ν_x unoscillated flux starts to dominate, being higher than the ν_e flux by a factor of 3-14. For the LL model, which has the most energetic ν_x , ϕ_x^0 approaches the current SK limit, Eq. (2), thus confirming that experiments are already probing the interesting region of the parameters. For example, with a neutrino spectrum equally or more energetic than the LL one, one can constrain the SNR normalization (Strigari *et al.*, 2005).

3. Dependence on the core collapse rate

It is interesting to study what fraction of the DSNB is due to sources at cosmological distance, i.e., $z \gtrsim 1$. Fig. 14 addresses this question, showing the contributions to the flux of sources in bins of the form $[z, z + 1]$, for the unoscillated $\bar{\nu}_e$ flux obtained with the LL model and the SNR in Eq. (5). It appears that the flux above ~ 20 MeV is practically all due to supernovae at $z < 1$, while the contribution of more distant sources becomes increasingly important at decreasing energy: sources at $z \sim 2$ should be included to reproduce the flux at 10 MeV, and at 2 MeV the dominant contribution is from sources at $z > 3$. This feature is explained with the larger redshift of the energy of neutrinos emitted at larger distances. If we consider the total flux of neutrinos of all energies, the contributions of the first three redshift bins are about $\sim 40\%, 35\%, 14\%$, while the remaining bins contribute for less than $\sim 10\%$. See Ando and Sato (2004) for further details.

How does the DSNB depend on the SNR parameters, $\beta, R_{SN}(0)$ ¹⁶? This question is especially relevant if one considers the region allowed by supernova observations only (fig. 5), which is wider than that allowed by measurements of the star formation rate and exhibits a correlation between the normalization, $R_{SN}(0)$ and the power β . Fig. 15

¹⁶ The dependence on α and γ in Eq. (4) is weak, and negligible in first approximation.

shows the unoscillated $\bar{\nu}_e$ flux obtained with the LL model and with a set of point in the space $(\beta, R_{SN}(0))$ that roughly map the 90% C.L. region in fig. 5 (see caption of fig. 15 for details). One can see that larger β (faster growth of the SNR with z) corresponds to less energetic spectrum, reflecting the increased contribution to the flux of the more redshifted neutrinos from cosmological sources. At certain points of the energy spectrum, the flux can vary by up to a factor of 4 as an effect of the variation of the SNR parameters, however the variation is always close to a factor of 2 for the integrated fluxes above various thresholds.

4. The $\bar{\nu}_e$ and ν_e fluxes in a detector

When oscillation effects are included, the $\bar{\nu}_e$ and ν_e components of the DSNB receive a contribution from the original ν_x flux produced inside the star, eq. (18). The oscillated ν_e and $\bar{\nu}_e$ fluxes are described in figs. 16 and 17 and in Tables IV and V for the LL, TBP and KRJ models, as well as for the flux that best fits the SN1987A data (Eq. (17)). All results refer to the extreme values of the survival probabilities p, \bar{p} , as they illustrate the maximum range of variation of the DSNB with the varying oscillations parameters. Intermediate cases can be calculated from the unoscillated fluxes in the different flavors (sec. III.E.2, Table III).

From the energy spectra in fig. 16 one can see that large variations (up to a factor of 3 or so) in the $\bar{\nu}_e$ flux can be expected for each model above 19.3 MeV as a consequence of the wide range of variation of \bar{p} . The ν_e flux instead is always within 30-40% from the unoscillated flux Φ_x^0 as a consequence of the small component due to Φ_e^0 , $p \leq 0.32$. Thanks to the larger contribution of the ν_x original flux, the ν_e spectrum is always more energetic than the $\bar{\nu}_e$ one. The ν_e and $\bar{\nu}_e$ diffuse fluxes can be equal in the limiting case $p = \bar{p} = 0$, which is realized, for the energies of interest, if the mass hierarchy is inverted and $\sin^2 \theta_{13} \lesssim 3 \cdot 10^{-6}$ ($P_H = 1$) due to neutrino-neutrino scattering (see Table II).

Large variations in the flux are also seen for fixed p, \bar{p} and varying spectral model, as already commented about the unoscillated fluxes. Expectedly, the LL model gives a flux that is much larger (up to one order of magnitude at 50 MeV) than the other models. For the SN1987A best fit spectrum the DSNB has a high peak at 2 MeV, reflecting the very high $\bar{\nu}_e$ original flux, and exceeding the other predictions by two orders of magnitude. For the energies of interest here, however, the flux is intermediate between the TBP and KRJ models.

The integrated fluxes are given in fig. 17 and in Tables IV and V for completeness. They reflect the features already noted for the unoscillated fluxes: the fast (exponential) decay of the flux with the increase of threshold energy E_{th} , and the variation by a factor of ~ 2 of the flux at high energy depending on the spectral model. Again, the ν_e flux is generally larger above realistic thresholds due to the larger flavor permutation.

5. Diffuse flux from failed supernovae

Analogously to what done so far for neutrinos from neutron star-forming collapses, one can calculate the diffuse flux of neutrinos from black hole-forming ones, Φ_{BH} (Lunardini, 2009), using the spectra in fig. 6 and considering that neutron star-forming (black hole-forming) collapses amount to a fraction $f_{NS} = 0.78 - 0.91$ ($1 - f_{NS} = 0.09 - 0.22$) of the total (sec. III.B).

Results are given in fig. 18 and 19 for the $\bar{\nu}_e$ and ν_e component of Φ_{BH} respectively and the extreme values of \bar{p}, p (assumed to be the same for both types of collapses) and of f_{NS} . For comparison, examples of diffuse flux from neutron star-forming collapses are shown; they were calculated using the parameters $E_{0e} = 9$ MeV, $E_{0\bar{e}} = 15$ MeV, $E_{0x} = 18$ MeV, $L_e = L_{\bar{e}} = L_x = 5 \cdot 10^{52}$ ergs, $\alpha_{\bar{e}} = \alpha_e = 3.5$ and $\alpha_x = 2.5$, that correspond to spectra intermediate between the KJR and LL model. As expected, Φ_{BH} has hotter spectrum compared to the flux from neutron star-forming collapses, and thus it is increasingly important at higher energy. Oppositely to the case of neutrinos from neutron star-forming collapses, Φ_{BH} is larger for minimal permutation ($\bar{p} = 0.68$, $p = 0.32$) (Nakazato *et al.*, 2008), because of the especially luminous original $\bar{\nu}_e$ and ν_e fluxes (fig. 6). The dependence of the original fluxes on the EoS is evident in Φ_{BH} .

Fig. 18 evidences that Φ_{BH} might dominate already at $E \sim 22$ MeV, implying a strong effect at SuperKamiokande. For the most favorable parameters the total flux from both types of collapses above 19.3 MeV is more than twice as large as the case of 100% neutron star-forming collapses. It reaches the value $\phi_{BH} \simeq 0.89 \text{ cm}^{-2}\text{s}^{-1}$, tantalizingly close to the current upper limit. It is more likely, however, that Φ_{BH} becomes dominant only above 30-40 MeV, as the figure shows. If so, its effect would be below the sensitivity of SK – which would therefore place limits on neutrinos from failed supernovae – but might be visible at the more massive and more sensitive detectors of the next generation.

IV. DETECTION: THE DIFFUSE NEUTRINO FLUX AT NEUTRINO TELESCOPES

A. The energy window

A fortunate circumstance makes the DSNB detectable: the fact that part of it falls in a relatively quiet region of the neutrino spectrum, and precisely above the typical energies of neutrinos from nuclear processes ($E_{nuc} \lesssim 18$ MeV) and below the higher energies of neutrinos from cosmic rays (atmospheric neutrinos, $E_{atm} \gtrsim 10^2$ MeV). These neutrino fluxes are for the most part ineliminable backgrounds, and thus place a natural limit to the sensitivity of any experiment to the DSNB. Here I discuss the generalities of the ν_e and $\bar{\nu}_e$ components of these backgrounds, which dominate the relevant detection channels. They are shown in fig. 20. Detector-specific backgrounds are discussed in secs. IV.D-IV.F.

- *solar neutrinos*. Electron, muon and tau neutrinos from the sun (with ν_μ, ν_τ generated by oscillations of originally produced ν_e s) extend to ~ 16 MeV energy if they come from the 8B chain, and even to ~ 19 MeV if produced through the *hep* process. Reaching $\sim 10^2 \text{ cm}^{-2}\text{s}^{-1}\text{MeV}^{-1}$, the *hep* flux dominates over the DSNB in the whole energy range nearly up to its endpoint. Its ν_e component is shown in fig. 20, where the effect of oscillations in the Sun has been included using the best fit oscillation parameters in Eq. (8).
- *reactor antineutrinos*. Nuclear powerplants are a copious source of electron antineutrinos of energies up to ~ 14 MeV. This reactor flux acquires a muon and tau component on the way to a detector due to oscillations (Araki *et al.*, 2005b). Very important as a signal for oscillation tests, the reactor antineutrino flux is a serious obstacle to the study of diffuse antineutrinos from supernovae. For example, at the Kamioka site the reactor flux is as high as $\sim 10^2 \text{ cm}^{-2}\text{s}^{-1}\text{MeV}^{-1}$ at 8 MeV, and dominates over the DSNB below ~ 12 MeV (fig. 20). The lower reactor flux in less nuclearized areas would allow a slightly larger energy window for the DSNB, down to 9 MeV for Homestake (where the reactor flux is lower by a factor of ~ 30 compared to Kamioka) and even to 8.2 MeV for a detector in New Zealand (table VI). Even in the best case, however, the reactor flux obscures the peak of the DSNB.
- *geoneutrinos*. Even in the ideal scenario of complete absence of reactors, there is still another low energy background: a flux of $\bar{\nu}_e$ from the natural radioactivity of the Earth. These geoneutrinos have been seen by KamLAND (Araki *et al.*, 2005a) and Borexino (Bellini *et al.*, 2010), and – according to calculations (Krauss *et al.*, 1984) – they should dominate over the DSNB below 3.26 MeV, where the spectrum of $\bar{\nu}_e$ from ${}^{214}Bi$ ends. This is sufficiently low to expose the peak of the DSNB at 5-7 MeV; however this is a highly speculative scenario and is presented here only as motivation for minimizing the reactor flux.
- *atmospheric neutrinos*. Collisions of cosmic rays with the Earth's atmosphere generate a shower of $\nu_e, \bar{\nu}_e, \nu_\mu, \bar{\nu}_\mu$ (and $\nu_\tau, \bar{\nu}_\tau$ via oscillations) that appears in neutrino detectors primarily in the energy window $0.1 - 10^3$ GeV. Still, a low energy tail of this atmospheric flux extends down to few MeV. The spectrum of ν_e s and $\bar{\nu}_e$ s in this tail (Battistoni *et al.*, 2005) is shown in fig. 20. Oscillation effects have not been taken into account, since they are at the level of 5-10% at these energies (Peres and Smirnov, 2009). The figure shows that typically the atmospheric flux exceeds the DSNB above ~ 30 MeV or so depending on the intensity and spectrum of the DSNB. It should also be noticed that the atmospheric neutrino flux is location-dependent due to the dependence of the cosmic ray flux on the latitude, and increases as one moves towards the magnetic poles of our planet. For example, the atmospheric flux is about ~ 1.5 times higher at Homestake than at Kamioka (Wurm *et al.*, 2007), resulting in a smaller energy window for the DSNB. This appears in fig. 20 and in Table VI (Wurm *et al.*, 2007), which gives the energy windows for $\bar{\nu}_e$ detection in different locations.

It is interesting to consider whether the fluxes discussed here are truly ineliminable backgrounds or can in principle be distinguished from the DSNB. While the answer ultimately depends on technology, here I observe that only the atmospheric neutrino flux is truly similar to the DSNB: it shares the same energy window, has similar flavor composition, and has the same isotropic distribution in direction. The other fluxes are not isotropic, and therefore can be distinguished *in principle*, while most likely not in practice.

Besides the neutrino fluxes discussed here, one should consider a number of non-neutrino processes and various instrumental effects that also constitute background for a given detector and that generally restrict the energy window compared to what discussed here. These backgrounds are described in sec. IV.B.

B. Detection concepts

Neutrinos in a detector are studied through the products of their interaction with electrons and nuclei. For a charged current process of the type $\nu_e + {}^A_Z X \rightarrow {}^A_{Z+1} Y + e^-$, the rate of events with electrons of *observed* kinetic energy

E_e is

$$\frac{dN_e}{dE_e} = N_T \int_{-\infty}^{+\infty} dE'_e \mathcal{R}(E_e, E'_e) \mathcal{E}(E'_e) \int dE \Phi_e(E) \frac{d\sigma(E'_e, E)}{dE'_e}, \quad (22)$$

where E'_e is the *true* energy of the electron, N_T is the number of target nuclei in the fiducial volume and \mathcal{E} represents the detection efficiency. Here $d\sigma(E'_e, E)/dE'_e$ is the differential cross section of the detection reaction and $\mathcal{R}(E_e, E'_e)$ is the energy resolution function. An expression analogous to (22) holds for the events due to the $\bar{\nu}_e$ flux, $\Phi_{\bar{e}}$.

From what discussed so far, it appears that the detection of diffuse supernova neutrinos requires a detector with: (i) large mass (at least comparable with SK, 50 kt), (ii) high detection cross section (iii) good energy resolution (to identify and study the DSNB energy window) and (iv) excellent discrimination of the signal over the background. Currently neutrino telescopes are entering their mature phase, and several technologies are now available to achieve these requirements. They are illustrated in Table VII, and reviewed briefly in this section. A more detailed discussion on specific designs is given in secs. IV.D-IV.E.

- **Water and water-based detectors.** Water Cherenkov detection is probably the oldest and best known technology. It has already been used successfully to detect supernova neutrinos in the SN1987A event (Bionta *et al.*, 1987; Hirata *et al.*, 1987). SK has proven the feasibility of this technology for tens of kilotons mass, and – thanks to its robustness and contained cost – masses up to 1 Mt are considered realistic (sec. IV.D).

In water, supernova neutrinos undergo several scattering processes with the production of an electron or positron (energies are sub-threshold for muon and tau production) that can be detected through its Cherenkov cone. These processes (Table VII) are elastic scattering of neutrinos of all flavors on electrons and charged-current interactions of ν_e and $\bar{\nu}_e$ on hydrogen and oxygen nuclei. Their cross sections are shown in fig. 21. In realistic energy windows, inverse beta decay ($\bar{\nu}_e + p \rightarrow n + e^+$) exceeds all other channels by at least one order of magnitude in cross section, and therefore it dominates a signal from the DSNB. All other channels can be neglected in first approximation.

The energy resolution $\mathcal{R}(E_e, E'_e)$ of a water Cherenkov detector depends on photocatode coverage. For example, the resolution of SK is well modeled by a Gaussian function of width $\Delta/\text{MeV} \simeq (0.5 - 0.6) \times \sqrt{E_e/\text{MeV}}$ (Fogli *et al.*, 2005; Suzuki, 2004), corresponding to a resolution of $\sim 11 - 13\%$ at 20 MeV. At energies above 5-7 MeV, the (hardware) detection efficiency is very good, being close to 100% at SK (Smy, 2010).

The DSNB detection in water is background-dominated. Among backgrounds from other neutrino fluxes, events from solar neutrinos can be subtracted very effectively: they are due mostly to elastic scattering on electrons, which is directional (the emitted electron is nearly collinear with the incoming neutrino) and therefore pointing back to the Sun. The events from reactors and atmospheric neutrinos instead are mostly due to interactions with nuclei; they have little directional information, and thus are likely ineliminable backgrounds. Water detectors are also limited by other two backgrounds: events from spallation and events due to atmospheric invisible muons¹⁷ in the detector. At SK, most spallation events are excluded by a combination of an energy cut and of other techniques (see sec. IV.D.2), while invisible muons are included in data analyses (see sec. IV.C).

A relatively recent chapter in the development of water-based detectors is the idea to use of a Gadolinium compound dissolved in water for enhanced signal discrimination over background (Beacom and Vagins, 2004). Gadolinium is a strong neutron capturer, already used in the past for the detection of reactor neutrinos (see e.g. Apollonio *et al.* (1999)). The capture of a neutron on Gd is followed by gamma ray emission from de-excitation; the detection in coincidence of the gamma ray and positron from inverse beta decay allows to distinguish this process from spallation and from invisible muons in most cases¹⁸. This results in a strong reduction of backgrounds, by a factor of ~ 5 for invisible muons and by at least an order of magnitude for spallation (Beacom and Vagins, 2004; Fogli *et al.*, 2005). Therefore, the energy window would extend down to the barrier posed by reactor neutrinos. Feasible at tens of kilotons scale, the water+Gadolinium technology might be impractical at larger masses. Still, it is a very attractive idea for a fast and cost-effective enhancement of current detectors (see sec. IV.E).

¹⁷ The wording “invisible muon” denotes a muon whose only signature in the detector is the track of the electron (or positron) produced by its decay. See e.g. Malek (2003).

¹⁸ A fraction of spallation and invisible muon events is accompanied by neutrons, and of these, some will be indistinguishable from inverse beta decay events in water with Gd. Still the reduction in background is expected to be substantial (Smy, 2010).

- Liquid scintillator. Another well known technology, liquid scintillator detection has been used extensively in studies of neutrinos of all types, including neutrinos from galactic supernovae (Alekseev *et al.*, 1987; Dadykin *et al.*, 1987; Selvi, 2007). Current liquid scintillator detectors reach 1 kt mass, and a scaling of one order of magnitude is envisioned (Marrodan Undagoitia *et al.*, 2006; Wurm *et al.*, 2007). Made of organic materials of the type C_nH_{2n} , scintillator can detect supernova neutrinos via elastic scattering on electrons and scattering on hydrogen and carbon nuclei (Table IV.B). Like in water, inverse beta decay dominates the event rates. Compared to water, scintillator offers better background discrimination and better energy resolution. Spallation and invisible muons¹⁹ are distinguished, for the most part, from inverse beta decay because the latter is accompanied by a gamma ray from the neutron capture on a free proton, $n(p, d)\gamma$. The coincident positron can be detected with energy resolution up to six times better than water: $\Delta/\text{MeV} = 0.10\sqrt{E_e/\text{MeV}}$, i.e., about 2% at 20 MeV (Wurm *et al.*, 2007). The same scaling to Mt mass as water detectors does not appear realistic, however. Thus, scintillator detectors might be ultimately limited by low statistics (sec. IV.E).
- Liquid Argon (LAr). A newcomer in the panorama of neutrino detection, the liquid argon technology has only been explored at the prototype level with the 600 tons ICARUS project (Amerio *et al.*, 2004). Currently, ICARUS has uncertain fate due to funding issues, but has already left a fruitful legacy of new projects of up to 100 kt mass (Cline *et al.*, 2006; Rubbia, 2009b) (Table VII). A LAr detector operates by imaging the tracks left by charged, ionizing particles, using the Time Projection Chamber (TPC) method. This imaging capability – similar to that of a bubble chamber (Cline *et al.*, 2006; Rubbia, 2009b) – allows very good particle and process identification, as well as very good energy resolution. Of the several detection processes, given in Table VII (see fig. 23), charged current scattering of ν_e on the ^{40}Ar nucleus dominates, making liquid argon absolutely unique for its potential to detect the ν_e component of the DSNB. Neutral current scatterings on ^{40}Ar are not relevant for the detection of the DSNB because their signature – the emission of gamma rays below 11 MeV energy from the deexcitation of the daughter nucleus – would be completely buried by solar neutrinos (Cocco *et al.*, 2004). Electron scattering is subdominant due to its smaller cross section.

The energy window for the DSNB at LAr is determined by atmospheric and solar neutrinos (sec. IV.A), under the sensible assumption that other backgrounds can be effectively separated²⁰. A full determination of backgrounds (including rare events, since the DSNB detection rate would be low) will come from extensive R&D studies that are currently ongoing. Until then, the discussion of DSNB detection at LAr will necessarily be indicative.

C. Upper limits

1. Data and flux constraints

So far, the DSNB has escaped detection. Thanks to their larger volumes, currently active detectors²¹ have improved dramatically on the bounds set by the previous generation of experiments (Aglietta *et al.*, 1992; Zhang *et al.*, 1988). Table VIII summarizes the most stringent upper limits (see also fig. 1 for a graphical representation).

The strongest bounds on all neutrino flavors were established by the 1496 days search at SK (Malek *et al.*, 2003) for events with energy between the threshold of 18 MeV (established after a spallation cut) and 80 MeV. Due to residual backgrounds, the efficiency of the search was of 47% (79%) below (above) 34 MeV of lepton energy. The data (fig. 24) were analyzed by the SK collaboration in the dominant detection channel, inverse beta decay induced by electron antineutrinos (Table VII). The result was the strong constraint on diffuse $\bar{\nu}_e$'s (Eq. (2)) that already approaches theoretical predictions (Fig. 2).

A more detailed data analysis (Lunardini and Peres, 2008) has slightly relaxed this bound by using a more accurate detection cross section and varying the neutrino energy spectrum according to a variety of models. In the same analysis, subdominant detection channels were studied, resulting in the strongest limits so far on the ν_e component of the DSNB (from ν_e scattering on oxygen and on electrons, Tab. VII) and on the non-electron flavors components as well (from scattering on electrons). The ν_e limit from SK slightly improves on the result obtained by SNO (Aharmim *et al.*, 2006) using heavy water, but is still about one order of magnitude away from theoretical predictions. The

¹⁹ Backgrounds, of cosmogenic nature are present in scintillator, but reducible to low levels; see Wurm *et al.* (2007).

²⁰ Spallation products are expected in LAr detectors. Their presence is likely to be irrelevant for the DSNB detection, since they lie below 20 MeV of energy, which is anyway precluded by solar neutrinos.

²¹ For limits from various detectors see Aharmim *et al.* (2004, 2006); Eguchi *et al.* (2004); Malek *et al.* (2003).

bounds on the non-electron species are even looser, but still improve the older results by LSD (Aglietta *et al.*, 1992) by four orders of magnitude.

It is important to notice that all analyses of the SK data use only one fit parameter, the DSNB normalization, with fixed neutrino spectrum. Using fixed spectrum allows to place limits on the integrated flux in any energy interval, even below the physical threshold of the search. A multi-parameter fit is unrealistic due to the scarcity of data, but will be possible with more data available.

Complementary to water results, a limit on $\bar{\nu}_e$ s at lower energy was established by KamLAND, in a study originally designed mainly to constrain a possible $\bar{\nu}_e$ flux from the Sun. While limited by the small mass of KamLAND (1 kt), the result is an interesting test of the liquid scintillator technology, with its better signal discrimination, in anticipation of a next generation of $\mathcal{O}(10)$ kt mass experiments (Marrodan Undagoitia *et al.*, 2006).

An updated data analysis by the SK collaboration is in preparation (Iida, 2005). It includes the new 791 (500) days of data from the second (third) phase of SK, updated cross sections, and improved background analyses. The preliminary upper limit $\Phi_{\bar{\nu}_e}(E > 19.3 \text{ MeV}) < 1.08 \text{ cm}^{-2}\text{s}^{-1}$ (90% C.L.) has appeared at conferences (Iida, 2005, 2010). The SK collaboration is currently improving the spallation subtraction by muon track reconstruction, resulting in a lower threshold of 17.3 MeV in $\bar{\nu}_e$ energy (16 MeV positron energy) (Smy, 2009).

Aside from detailed data analyses, indirect upper bounds can be established on the basis of naturalness and theoretical considerations. In particular, a constraint on diffuse ν_e s follows from the constraint on the $\bar{\nu}_e$ component at SK by considering that the two components must be similar due to their common origin in the non-electron neutrino flavors inside the star through neutrino oscillations (Lunardini, 2006a). This is the “indirect” limit given in Table VIII, and, while considerably looser than the $\bar{\nu}_e$ bound, it is currently the strongest for the ν_e species.

2. Implications of the SK limit

As already observed (fig. 2) the SK limit touches the region of theoretical predictions of the DSNB, leaving most models unconstrained. This translates into loose constraints in the space of parameters that describe the flux, namely the neutrino spectra and luminosities and the normalization of the SNR. Only combinations of parameters giving the highest DSNB are excluded, and generally degeneracies imply only weak constraints on individual parameters.

Indicative (not statistical) constraints are shown in figs. 25 and 26 (from Lien *et al.* (2010); Yuksel *et al.* (2006)). Fig. 25 refers to fixed SNR ($R_{-4} = 3$) and shows the excluded region in the space of the luminosity and average energy of the $\bar{\nu}_e$ component of the DSNB. Parameters compatible with SN1987A are allowed, and for the theoretically natural luminosity of $L_{\bar{e}} = 5 \cdot 10^{52}$ ergs, a wide range of average energies (up to 20 MeV or so) is allowed. The range is expected to be even wider if uncertainties on the SNR are included.

Fig. 26 instead gives the exclusion of rates of neutron star-forming (successful) and direct black hole-forming (failed) supernovae depending on the neutrino spectra for these two supernova populations, compared with astrophysical limits on the same quantities from star formation rate measurements and supernova observations. Interestingly, the rate of failed supernovae alone is constrained to be below $\sim 0.8 \cdot 10^{-4} \text{ yr}^{-1} \text{ Mpc}^{-3}$, which is however well above the rate expected for a $\sim 20\%$ fraction of failed supernovae (sec. III.B).

While detailed analyses of parameter constraints from the SK limits have yet to be done, current results are sufficient to give a perspective of what can be expected from next generation searches (see sec. V). With a factor of 2-4 improvement in flux sensitivity, the parameter constraints from the DSNB will become competitive with those from astronomy and from SN1987A (Yuksel *et al.*, 2006).

D. Water Cherenkov detectors towards megaton scale

1. Number of events

After the very successful experience of the 50 kt mass of SK, water technology is now mature to expand to megaton scale. In this section I discuss the DSNB signal for a representative setup of a 0.4 Mt fiducial volume and 5 years running time, with energy resolution equal to that of SK (sec. IV.B). An efficiency of 93% (Bahcall *et al.*, 1997; Hirata *et al.*, 1988) is used as representative of a detector performance. However one must consider that the real efficiency depends on the details of the hardware and of the data analysis and therefore results will have to be rescaled once these details are known. I include only inverse beta decay events and neglect the subdominant channels (which contribute to less than $\sim 4\%$ (Volpe and Welzel, 2007)) and use backgrounds for the SK location, taken from Fogli *et al.* (2005). This setup is necessarily indicative; some technical details will be discussed in sec. IV.D.2. All results refer to the same flux parameters as in sec. III.E.4.

Fig. 27 shows the energy distribution of the signal and background events. It appears immediately that the signal to background ratio is always smaller than 0.2-0.3, and is maximum just above the threshold of 18 MeV. There the

signal is comparable to or larger than the atmospheric background but is exceeded by the invisible muon one. The atmospheric background starts to dominate at 25-30 MeV, thus closing the energy window (sec. IV.A). It appears that even for the most energetic neutrino spectrum, the peak of the event distribution is below the spallation cut, and would require a better background discrimination to be observed. The 2 MeV lowering of the threshold expected for the next SK analysis (sec. IV.C) could capture the peak at least in the most optimistic case.

Tables IX and X give the numbers of signal and background events in two intervals of positron energy. While the smaller bin ($18 < E_e < 28$ MeV) is realistic and reflects the region where the signal/background ratio is maximal, the wider interval ($10 < E_e < 28$ MeV) might be relevant to a possible upgrade (for example water plus Gadolinium, sec. IV.B) where spallation is effectively removed and only reactor neutrinos remain as background at low energy.

From the Tables it appears that the number of signal events above 18 MeV varies between tens and hundreds depending on the neutrino energy spectra and oscillation effects. An even larger variation should be expected in consideration of the uncertainty in the normalization of the core collapse rate (sec. III.A). The E^2 dependence of the cross section magnifies the differences due to different energy spectra of the neutrino flux, so that the event rate for the LL model can easily be twice as large as the other models.

To answer the question of statistical significance, one should consider the ~ 700 background events in the 18-28 MeV bin, corresponding to a 1σ statistical error of about 27 events. It follows that, for the exposure considered here, the signal should be statistically significant ($2.5 - 4.7 \sigma$) for the LL model. Instead, it may be below 3σ for the other models depending on the DSNB normalization, making a longer exposure necessary. In the worst case of 22 signal events, an exposure 16 times longer (for example, 20 years running time for a 0.8 Mt detector) would be required to reach a 3σ significance²².

For an upgraded configuration with subtracted spallation background, the number of events from the signal can exceed 200. If the invisible muon background is subtracted as well, the signal could be comparable to or larger than the background, thus ensuring excellent statistical significance even for the most unfavorable parameters. This is a very strong motivation for improvements in this direction. A discussion of possibilities is given in sec. IV.E.

For generality, I also give numbers of signal events above a range of thresholds, in fig. 28. They can be used to calculate the event rates in other energy bins of interest. For selected thresholds the figure also gives the 90% C.L. interval predicted by imposing compatibility with SN1987A and with direct measurements of the supernova rate (Lunardini, 2006b) (sec. III.A and III.D). One can see the substantial decline in the event rate with the increase of the threshold beyond the peak of the DSNB ($E \sim 6 - 7$ MeV, see sec. III.B). The diffuse flux, and therefore the event rate, could be substantially enhanced if failed supernovae are relatively numerous ($\sim 20\%$ or so) in the universe, as discussed in sec. III.B. Figure 29 gives the expected energy distribution and integrated rate of events expected in the best case scenario of fig. 18 (largest failed supernova flux, with S EoS, $\bar{p} = 0.68$ and $f_{NS} = 0.79$). It appears that above 18 MeV of positron energy the events due to failed supernovae could amount to about 2/3 of the total, enhancing the rate up to about 200 events for an exposure of 2 Mt·yr. This enhancement could allow an earlier detection at 3σ of the DSNB, already with half the exposure. Thanks to the more energetic spectrum of failed supernovae, lowering the energy threshold to 14 MeV or so would be sufficient to capture the bulk of the events from these objects and see the peak of the event distribution. With a 10 MeV threshold the number of signal events can exceed 300.

2. Technical considerations

Certainly the event rates given here are indicative, since they ultimately depend on the specific detector design. For example, the energy resolution and the fiducial volume (for a given total mass) are influenced by the detector's geometry, photocathode coverage, electronics, etc.. As discussed in sec. IV.A, location and depth influence the backgrounds importantly. Choosing the technical specifications of an experiment always involve balancing scientific, financial, technical and logistical requirements. Here I discuss some of the currently favored setups in their main physics aspects.

- geometry. The excavation of a cavern large enough to contain a single, undivided, 1 Mt mass of water is certainly challenging but possible. Considerations of rock stability suggest a cylindrical design for the detector, as envisioned for HyperKamiokande (Nakamura, 2003). For Mt masses, the same photocathode coverage of SK (40%) is unrealistic, and therefore a lower coverage (20-30%) is envisioned for at least part of the detector

²² Notice that these considerations on statistical significance assume that the normalization of the background is well known independently, which is not the case at this time. If poorly constrained, this normalization will be included in the data analysis as a fit parameter, as is currently done by the SK collaboration (Malek, 2003), and this weakens the sensitivity to the signal.

(Autiero *et al.*, 2007; Nakamura, 2003). This would result in a slight worsening of the low energy performance (~ 7 MeV rather than ~ 5 MeV threshold, which is however inconsequential for the energy window of the DSNB) as well as a somewhat poorer energy resolution (Autiero *et al.*, 2007), with consequent poorer background discrimination and ultimately higher energy threshold for DSNB searches. An alternative, currently proposed for DUSEL, is a modular design with ~ 0.1 Mt mass for each volume (fig. 30) (Diwan *et al.*, 2006). This would result in a smaller fiducial volume (for equal total mass), but is attractive because it breaks several challenges (excavation, instrumentation, maintenance, etc..) into more manageable parts that can be completed sequentially or in parallel depending on circumstances. The modular design also shortens the waiting time, since it can start to deliver data as soon as the first module is completed, similarly to what happened for another supermassive project, ICECUBE (Achterberg *et al.*, 2006).

- depth. Since the cosmic ray flux in a detector rapidly decreases with depth, even modest gains in depth result in substantially enhanced performance. This is especially true for the DSNB, for which detection is dramatically limited at low energy by spallation products of cosmic ray muons. A detailed study on depth requirements for a Mt Cherenkov detector (Bernstein *et al.*, 2009), gives the expected extension of the energy window with the increase of depth, relative to that of SK (3300 ft, equivalent to 1005 m and to 2900 m water-equivalent). Results are given in Table XI. For pure water, by going to 4850 ft depth the energy window can be pushed down to 15.5 MeV of positron energy, with an enhancement of the DSNB signal of about 40%. This depth is also required to observe the day-night asymmetry of solar neutrinos and is therefore recommended for the DUSEL design (Bernstein *et al.*, 2009).
- Location/latitude Even though latitude is important for the atmospheric neutrino background, considerations of depth always prevail in the choice of a particular underground location, together with considerations like access of people and technology to the site. Some sites that are currently being considered for a Mt water Cherenkov detector are South Dakota (Homestake mine), Japan, France (Frejus laboratory), Spain (Canfranc), and Finland (Phyäsalmi mine) (see Table VI).

E. Reducing backgrounds with liquid scintillator and Gadolinium

1. GADZOOKS

The idea of dissolving gadolinium in water was proposed by Beacom and Vagins (Beacom and Vagins, 2004), who discussed its cost-effectiveness and non-toxicity. They envisioned applying the idea to the SK detector, thus initiating a new phase of SK called GADZOOKS²³. This initiative is especially attractive for its relatively low cost and short timeline; it is now part of the R&D work of the SK collaboration.

It is estimated that, with Gd, the background due to spallation will be subtracted almost completely and the one due to invisible muons will be reduced by a factor of ~ 5 (Beacom and Vagins, 2004). As a result, the lower end of the energy window is determined by reactor neutrinos, and would typically be 11-12 MeV in neutrino energy. In the interval ~ 12 -22 MeV the signal dominates over the background. This is illustrated in fig. 31, where the enlarged energy window appears, possibly including (for the LL model) the peak of the event energy distribution.

The number of events expected at GADZOOKS can be evaluated by rescaling the event rates of Tables IX and X by the appropriate volume factor. Assuming 10 years running time and an indicative 22.5 kt fiducial volume one expects 9 - 28 signal events and 29 background events in the window of 10 - 28 MeV of positron energy. Thus, the excess due to the DSNB would be statistically significant for part of the parameter space, and the significance will likely be enhanced by the spectral analysis of the data. However, detailed studies of the signal properties would probably be beyond reach.

The intense R&D work on GADZOOKS aims at finding a Gd compound that meets four basic criteria: (i) solubility, (ii) limited impact on water transparency, (iii) negligible reactions with the detector materials (e.g., corrosion, etc.) and (iv) compatibility with a detector's filtration system²⁴. A 0.2% solution of GdCl_3 has been tested recently. A small volume of it has been deployed inside the SK detector and the effectiveness of neutron tagging has been demonstrated (Watanabe *et al.*, 2008). In other tests, the same solution was found to perform adequately in terms

²³ The acronym stands for "Gadolinium Antineutrino Detector Zealously Outperforming Old Kamiokande, Super!".

²⁴ A detector like SK requires constant purification of the water to avoid deterioration of its transparency. It is necessary to prove that a Gd compound can be effectively filtered and reinserted into the detector. Another requirement is the feasibility to completely remove the Gd compound from the water to restore the detector to a pure water phase.

of solubility but poorly in water transparency (Coleman *et al.*, 2008; Kibayashi *et al.*, 2009). Furthermore, concerns about corrosion effects in the SK tank disfavor this option, leading to the consideration of other compounds (GdCl_3 remains a possibility for other types of vessels, however, like the acrylic shell of SNO).

Tests indicate Gd sulfate ($\text{Gd}_2(\text{SO}_4)_4$) as best candidate so far, as it meets the criteria outlined above and seems safe for stainless steel tanks (Kibayashi *et al.*, 2009).

More research on GADZOOKS will be done at a dedicated 200 t prototype at Kamioka, which is currently under construction (Kibayashi *et al.*, 2009)²⁵

2. Liquid scintillator at the 50 kt scale

As a representative example of future liquid scintillator detectors, here I discuss the largest, the european LENA (Marrodan Undagoitia *et al.*, 2006; Wurm *et al.*, 2007). With a mass of 50 kt, LENA will have event rates comparable with those of SK, with the advantages of liquid scintillator, namely the better background discrimination and better energy resolution (sec. IV.B).

Thanks to the detection in coincidence of the positron and neutron capture (sec. IV.B), the detection of diffuse $\bar{\nu}_e$ s at LENA will be similar to that at GADZOOKS: the spallation and invisible muon backgrounds are effectively subtracted, so the energy window is determined by reactor and atmospheric neutrinos and is about 10-28 MeV wide. To calculate the signal event rate, one should consider that LENA will have $N_p = 2.9 \cdot 10^{33}$ protons in the fiducial volume, nearly twice the number of SK ($N_p = 1.5 \cdot 10^{33}$). This results in a doubled event rate compared to GADZOOKS: about 18-56 events in 10 years. The background events expected for the same exposure are about 11-13, due to atmospheric neutrinos, to reactor neutrinos, and to a residual spallation product, fast neutrons (Wurm *et al.*, 2007). Thus, the signal exceeds the background by a factor of 2-5, resulting in a statistical significance of more than 4σ . Table XII gives a further illustration of the number of signal and background events expected at LENA in different energy windows (relevant to different locations, see sec. IV.B) for $\bar{p} = 0.68$.

The current design of LENA is shown in fig. 32 (Lachenmaier, 2009). It is characterized by a vertical geometry, with the inner detector surrounded by a water Cherenkov volume acting as muon veto. A 30% wall coverage of photomultipliers is envisioned. Several locations are currently considered for LENA; detailed engineering studies exist for the Pyhäsalmi mine (Nuijten, 2008).

F. Liquid argon for ν_e detection

1. Numbers of events

From the intense scoping work of the past years it has been recognized that a minimum mass of about 100 kt is necessary for non-beam physics with liquid argon. A detector of this scale represents a daunting challenge, and is likely to become reality in more than a decade from now, after several intermediate mass solutions. Still, 100 kt is the ultimate goal, and therefore here I discuss such case as a way to further motivate it. A running time of 5 years is considered for illustration. Here I include only the dominant process, charged current ν_e interaction with argon, (Table VII). For this, the energy of the emitted electron differs from that of the incoming neutrino by ~ 3 -4 MeV depending on the nuclear transition taking place (Cocco *et al.*, 2004). Since detailed information on the spectrum of these transitions is not available, however, here event rates will be discussed in terms of neutrino energy. All results refer to the diffuse flux as in fig. 16.

Fig. 33 shows the distribution of signal and backgrounds in neutrino energy, for the extreme values of the survival probability p . The signal peaks between 12 and 22 MeV depending on the oscillation scenario and on the original neutrino spectra. At the peak, $\sim 0.8 - 1.8$ events/MeV are expected. Backgrounds dominate below ~ 19 MeV and above 29-39 MeV depending on the parameters. This energy window is similar to that of a water detector (fig. 27). Unlike the case of water, however, here it may happen (for the most energetic neutrino spectrum, from the LL model) that the peak of the signal is *inside* the energy window. This is thanks to the faster rise of the cross section with energy, compared to inverse beta decay.

Another interesting comparison with water is in how the various detector specifics influence the number of events. The number of nuclei in 100 kt of argon ($N_{Ar} = 1.5 \cdot 10^{33}$) happens to be the same as the number of hydrogen nuclei

²⁵ Other important questions have to be addressed before GADZOOKS can be realized: one of them is environmental concerns (real or perceived by the public opinion), related to the existence of a leak in the SK tank. I leave this aspect to more specialized literature (e.g., Vagins (2009)).

inside the fiducial volume of SK. However, in the energy window the cross section for argon is higher by a factor between 1.7 and 3.5. Therefore, if the two detectors receive equal fluxes of ν_e and $\bar{\nu}_e$ (e.g., if $p = \bar{p} = 0$, which is the case for inverted hierarchy and $\sin^2 \theta_{13} \lesssim 3 \cdot 10^{-6}$, see sec. III.C), the number of events in argon will be significantly larger. This can be seen by comparing figs. 33 and 31.

Tables XIII and XIV give the number of events from the signal and from the atmospheric background in energy intervals of interest. In the 19 - 39 MeV window the detector may register between 6 and 28 events of signal and 9 events of atmospheric background. The signal increases with the average energy of the ν_e flux entering the detector, and therefore is higher for the LL model and for $p = 0$ (complete swap between the original ν_e and ν_x fluxes). Only for the LL model the signal would be statistically significant for the exposure considered, while the lowest signal would require about 1200 kt·yr to have a 3σ statistical significance. One should remember, however, that the overall normalizations of the DSNB and of the atmospheric neutrino flux are highly uncertain, and therefore the signal to background ratio could very well be a factor of a few larger for all models, in which case a statistically significant observation might be more likely. Restricting the energy window down to 29 MeV lowers the number of events, but increases the signal to background ratio, and therefore might be useful. Tables XIII and XIV also give numbers of events in a larger energy window, 5 - 39 MeV, which might be applicable if a method is found to subtract events from solar neutrinos, probably on the basis of directional information from kinematics reconstruction. This possibility has not been investigated so far, and so, while speculative, it remains open. The Tables show that accessing lower energies might enhance the event rate by up to a factor of 3 for the models with lower neutrino average energy.

For completeness, fig. 34 gives the numbers of DSNB events above a certain neutrino energy E_{th} , as a function of E_{th} .

Similarly to water detectors, also for LAr the event rate could be enhanced by failed supernovae. Fig. 35 illustrates this, by showing the number and energy distribution of events from normal and failed supernovae for the best case scenario in fig. 19 (largest failed supernova flux, with the S EoS, $p = 0.32$ and $f_{NS} = 0.78$). It appears that the contribution of failed supernovae peaks in the energy window and enhances the event rate by a factor of ~ 2 in the same energy interval. This implies a higher chance that a LAr experiment might see an indication of signal in its earliest phase of operation.

2. technical considerations

The technical realization of the liquid argon concept at 100 kt scale is still a subject of discussion. Current research is focused on testing the performance of liquid argon in lower mass projects, on designing the necessary electronics, and on the engineering of the final 100 kt structure and its accommodation in underground laboratories. Essential criteria are the scalability (in mass) of the design and safety in operations of handling and containing the argon under pressure. Current low mass efforts that are specific for neutrino physics include the approved MicroBOONE (Anderson *et al.*, 2010a), the almost functioning ArgoNEUT (Anderson *et al.*, 2010b) and a 100 ton LAr TPC proposed as an extension of T2K (Meregaglia and Rubbia, 2006).

Larger structures of 100 kt mass are already being planned. Fig. 36 illustrates two designs: the US-based Liquid Argon Neutrino and Nucleon Decay Detector (LANNDD) (Cline *et al.*, 2006) and the european Giant Liquid Argon Charge Imaging Experiment (GLACIER) (Ereditato and Rubbia, 2006; Rubbia, 2009b). LANNDD is characterized by a cellular structure: 512 cubic cells, each of 0.1844 kt mass. GLACIER instead has a single volume structure, made of a cylindric tank of stainless steel, of 70 m radius, with a domed roof. Later these technical features may be adapted to the characteristics of the underground laboratory that will house them.

V. PERSPECTIVES: WHAT CAN BE LEARNED AND HOW?

A. What can and can not be learned

The question of what can be learned from data on the DSNB has been explored only partially so far. It is reasonable to expect that, as data start to appear, there will be a first phase of analysis that will constrain the basic ingredients of the DSNB at the coarse level, with errors of the order of 50-100% due to backgrounds and parameter degeneracies. What these basic ingredients are emerges from the previous sections: the neutrino spectra in the different flavors, conversion/survival probabilities, and normalization parameters like the total neutrino luminosity.

Many other important phenomena could be accessible only with an advanced precision phase of the DSNB, or, more likely, with high statistics data from a nearby supernova. Here I do not discuss them, but briefly list them for completeness.

- regeneration of ν_e and $\bar{\nu}_e$ due to oscillations inside the Earth. In the DSNB these effects are below $\sim 5\%$ (Lunardini, 2006a) and therefore statistically insignificant.
- the swap in the neutrino energy spectrum due to neutrino-neutrino refraction (sec. III.B). The spectral step caused by the swap for a single supernova will be smoothed out by the integration over the redshift and by the presence of individual differences between supernova progenitors (Chakraborty *et al.*, 2010). Besides, the swap typically occurs below 10 MeV of energy, and thus is likely to fall outside the energy window for DSNB detection.
- the SNR at large redshift, $z \gtrsim 1$. This is because neutrino produced at large redshifts accumulate at low energy, where backgrounds dominate.
- the normalization of the supernova rate. Such normalization is degenerate with the total luminosity of emitted neutrinos. Probably, it will be better constrained by astronomical surveys of supernovae.
- shockwave effects on the neutrino spectrum due to oscillations. First pointed out in Schirato and Fuller (2002), these effects are very interesting probes of oscillation parameters as well as of the physics of the shock. Once integrated over the duration of a neutrino burst, and over a diverse population of stars at different redshifts, they reduce to a $\sim 10\%$ size or less (Ando and Sato, 2003; Galais *et al.*, 2009), with no distinctive spectral features in the DSNB. Therefore, they are likely to be indistinguishable from many other effects of similar magnitude.
- the time structure of neutrino emission from a supernova, including the neutronization burst, the accretion phase and the cooling phase, with their characteristic time scales. The DSNB is a sum of many time-integrated supernova bursts, which causes loss of information.

B. Testing the physics of supernovae: neutrino spectra

Naturally, the sensitivity of an experiment to the DSNB spectrum depends critically on its energy window. Limited sensitivity is expected for pure water and LAr, where the window is only 10-15 MeV wide, while liquid scintillator and GADZOOKS-type (water+Gd) designs should perform better thanks to the larger window. Detailed studies have been done for water, water+Gd, and liquid scintillator, most of them discussing the dependence of event rates on the neutrino spectra (e.g, Chakraborty *et al.* (2008); Fogli *et al.* (2005); Volpe and Welzel (2007)), while the question of parameter degeneracy has been addressed only in part (Lunardini, 2007a).

One way to eliminate the degeneracy with normalization parameters (neutrino luminosities and R_{-4}), is to study ratios of events, for example the ratio r of the number of events in the first and second energy bin (Lunardini, 2007a)²⁶. Taking bins of 5 MeV width, this ratio is:

$$r \equiv \frac{N(18 \leq E_e/\text{MeV} < 23)}{N(23 \leq E_e/\text{MeV} < 28)}, \quad (23)$$

for the water only case, and

$$r \equiv \frac{N(10 \leq E_e/\text{MeV} < 15)}{N(15 \leq E_e/\text{MeV} < 20)}, \quad (24)$$

for water+Gd, in terms of the positron energy E_e .

In Lunardini (2007a) values of r were calculated for a wide region in the space of the spectral parameters $\alpha_w - E_{0w}$, for fixed SNR and in the assumption that the spectral form in Eq. (6) applies to the $\bar{\nu}_e$ flux at Earth. The resulting isocontours of r are shown in fig. 37 as long dashed lines. For pure water r varies in the range $r \simeq 1.5 - 4.3$. For a 2 Mt \times yr exposure, the error on r is larger than $\sim 100\%$ due to the high background rate (Lunardini, 2007a); this confirms the conclusion that the sensitivity to the neutrino spectrum is limited for pure water. For the configuration with extended energy window (water+Gd) one gets $r \simeq 1 - 2.5$. Thanks to the better background reduction, the error is down to $\sim 20 - 30\%$, meaning that at least the extreme cases should be distinguishable for the typical luminosity of the DSNB.

²⁶ Including higher energy bins enhances the backgrounds more than the signal and therefore it worsens the sensitivity to the neutrino spectrum (Lunardini, 2007a).

If in the future the neutrino luminosity, the normalization of the SNR, and background fluxes become known precisely, the number of signal events N in the energy window (e.g. in the first three (four) energy bins for pure water (water+Gd)) can be used jointly with the ratio r to constrain the spectral parameters. Isocontours of N are given in fig. 37 as solid lines. These lines intersect the isocontours of r , suggesting that a joint measurement of N and r could be more constraining than the two separately. An example of such joint measurement is shown in the figure, with central values and 1σ statistical errors on the two quantities. Notice that the region allowed by the measurement of N is contained inside the one allowed by the measurement of r , meaning that the number of events alone is sufficient to constrain the original neutrino spectrum, if normalizations are known very well. In presence of errors on these quantities the ratio r will be more constraining instead.

In essence, the results in fig. 37 tell us that data will allow us to reconstruct the spectrum of the neutrino emitted by a supernova in terms of two effective parameters, an average energy and a shape parameter. The next step of the analysis would be to reconstruct the more fundamental quantities that determine the effective ones, such as the neutrino spectra in the different flavors at the production point, and the neutrino mixings and mass hierarchy. This second level of detail is certainly more challenging, and is likely to require a combination of precision-phase experiments and improved theoretical modeling.

The study by the LENA collaboration (Wurm *et al.*, 2007) gives an example of this, by illustrating the potential of an advanced phase of LENA (sec. IV.E.2) for the reconstruction of the neutrino spectra at production. Monte Carlo spectra of events at LENA were created according to one of the flux models in Table I, with fixed SNR and fixed \bar{p} , and then compared to all possible combinations of event numbers in two energy bins using a χ^2 analysis. The result of the analysis is a probability that a Monte Carlo spectrum created according to a given model is wrongly assigned to a different combination of event numbers and therefore to an alternative SN model. Fig. 38 shows the 1 and 2 σ exclusion areas, which are those outside the colored curves. It emerges that, for $\bar{p} = 0.68$, the LL and TBP models can be distinguished with more more than 2.6 σ significance. However, distinguishing the KRJ and the LL models with similar significance would require more than 30 years of running time (Wurm *et al.*, 2007). Instead, the very energetic spectrum of the LL model with $\bar{p} = 0$ could be excluded with only 15 years of data taking (Wurm *et al.*, 2007).

C. Testing neutrino flavor conversion

The sensitivity of the DSNB to neutrino oscillation effects, and therefore to the oscillation parameters θ_{13} and the mass hierarchy (sec. III.C), remains an open question. Many studies have included conversion effects in predictions of the DSNB, examining their impact on the rates and energy distributions of events at detectors (sec. IV). Effects are strong for both quantities, however, what exactly can be concluded on oscillation parameters is not clear, in consideration of the many degeneracies. Specifically, event rates have a degeneracy with the the SNR and with the total neutrino luminosity, while energy distributions are meaningful only with priors (or a measurement from a galactic supernova) on the originally emitted neutrino fluxes in the different flavors. A detailed reconstruction of spectral shapes might resolve this degeneracy to some extent, but only for the larger energy windows of GADZOOKS and of a liquid scintillator detector, provided that they run for at least a decade to accumulate sufficient statistics.

Some of the degeneracies can be resolved by the *combination of several complementary datasets*. For example, a set of data from ν_e and another from $\bar{\nu}_e$ would help to eliminate degeneracies with the normalization parameters and would allow to probe both p and \bar{p} . This can lead to the discrimination of θ_{13} and mass hierarchy, as already observed for an individual supernova (e.g., Lunardini and Smirnov (2003); Minakata *et al.* (2008); Skadhauge and Zukanovich Funchal (2007)). For the DSNB, this step of connecting measured probabilities with the fundamental oscillation parameters might be complicated by the integration over the diverse supernova population; therefore here I focus on probability determination, and make only basic statements on oscillation parameters, for the case in which the formulae in Table II for $p(\theta_{13}, \Delta m_{32}^2)$ and $\bar{p}(\theta_{13}, \Delta m_{32}^2)$ are valid.

Let us consider $\bar{\nu}_e$ data from a 0.4 Mt water detector and ν_e ones from 100 kt LAr. Take the ratio of numbers of events in the energy window at the two detectors:

$$r_N = \frac{N_{wa}}{N_{Ar}}, \quad (25)$$

where normalization parameters (R_{-4} and total neutrino luminosity) cancel. For given SNR parameters and a given model of neutrino spectra, r_N is larger for smaller \bar{p} (more $\bar{\nu}_e$ permutation, i.e. more energetic $\bar{\nu}_e$ spectrum at Earth, and thus higher event rate in water). It also grows with increasing p (less ν_e permutation, i.e. less energetic ν_e spectrum at Earth and thus lower event rate in LAr).

Table XV gives the value of r_N for the three models of neutrino emission (LL, TBP, KRJ) of Table I, and for four combinations of \bar{p}, p . The intervals $E = 19.3 - 31$ MeV and $E = 19 - 39$ MeV were taken as windows in neutrino energy

for water and LAr respectively. Note that, for generality, the table includes the case $(\bar{p}, p) = (0, 0.32)$, which can be realized only in absence of neutrino self-interactions (see Table II). From the table it appears that r_N varies between 2.7 and 8.9. Values below 3.8 would indicate large $\bar{\nu}_e$ survival, $\bar{p} \sim 0.68$, and disfavor a small θ_{13} ($\sin^2 \theta_{13} \lesssim 10^{-5}$ or so, see sec. III.C). Instead, $r_N > 6$ would indicate a complete $\bar{\nu}_e$ permutation with only partial ν_e conversion, revealing that oscillations induced by self-interactions were not active for at least part of the neutrino flux. $4 \lesssim r_N \lesssim 6$ would point towards a small θ_{13} .

How well can r_N be measured, considering the large errors involved? Fig. 39 shows the regions in the $N_{wa} - N_{Ar}$ plane that correspond to the values of r_N in Table XV, compared with two possible measurements of N_{wa} and N_{Ar} obtained with 5 years exposure of both detectors. The dots show the hypothetical measurement, and the ovals represent the 90% C.L. allowed region for the “true” numbers of events. This region is calculated using the gaussian errors on the total numbers of events of signals and backgrounds together, e.g., $\sigma_{wa} = \sqrt{N_{wa} + N_{bckg}}$. For the water detector, the background is made of 647 events from invisible muons and 83 events from atmospheric neutrinos. For LAr about 8 events are expected from atmospheric neutrinos in the energy window. The 90% C.L. contours in fig. 39 are quite extended, spanning tens of events for LAr and about 100 events for water. Still, the figure shows that if the measured ratio of event rates is near one of the extreme values (e.g., $r_N \sim 3.8$ or $r_N \sim 9$), the opposite extreme can be excluded. Thus, there is some sensitivity to the oscillation probabilities and therefore to the neutrino mass hierarchy and to θ_{13} , although indirectly. Such sensitivity might be precious especially if θ_{13} is small and therefore beyond the reach of terrestrial experiments. One should also consider that, in view of the large uncertainties in the normalization of the DSNB, the signal for a given detector exposure might very well be higher by a factor of 2 or so than what shown here, resulting in higher statistics and therefore better discrimination power.

The results given here have the character of illustration only, because the neutrino spectra could be outside the range of models considered here. One should also keep in mind that, while results were given only for the extreme values of p, \bar{p} , the allowed region for these parameters is truly a continuum between such extremes. From fig. 39 one expects that most of this continuum will remain allowed after the first phase of data from the DSNB.

D. Sensitivity to neutrino exotica

Analogously to what happened with SN1987A, the data from the diffuse supernova neutrinos will test innumerable new physics hypotheses –typically the existence of new particles and/or new forces – from searches of unexpected features in the neutrino signal.

The sensitivity of the DSNB to these exotica has been studied only minimally. In view of the substantial cosmological contribution to it (see sec. III.E.3), one expects the DSNB to be particularly constraining, compared to SN1987A, of phenomena that require large propagation distances, such as effects of decay or absorption of the neutrinos during their propagation across the universe.

Effects of neutrino decay on the DSNB were studied by Ando (2003); Fogli *et al.* (2004). Depending on the neutrino mass spectrum, the decay can enhance or suppress the electron flavor component, in a way that could be observable for ratios of the neutrino lifetime over mass as high as $\tau/m \simeq 10^{10}$ s/eV (fig. 40). One should be mindful, however, of the possible degeneracy with the luminosity of the neutrino flux and with the SNR normalization.

An example of exotic absorption is the possibility of depletion of the DSNB due to a high rate of neutrino-antineutrino annihilation in the cosmological relic neutrino background, mediated by new light gauge bosons (Goldberg *et al.*, 2005).

About non-propagation (between source and detector) effects, it has been shown that resonant spin flavor conversion influences the expected event rates (Volpe and Welzel, 2007). It has also been observed that the DSNB could in principle provide a test of dark energy, complementary to astrophysical measurements (Hall *et al.*, 2006).

Besides affecting the DSNB, physics beyond the Standard Model could also mimic it under certain circumstances. These could be the annihilation or decay of light dark matter into neutrinos of energy comparable to the DSNB (see e.g. Palomares-Ruiz (2008); Palomares-Ruiz and Pascoli (2008)). A flux similar to the DSNB could be made of solar antineutrinos, if their production is enhanced by resonant spin-flavor conversion (Raffelt and Rashba, 2009). Ultimately, when detectors reach the precision phase, it will be possible to distinguish the DSNB from other, non-supernova fluxes, on the basis of spectral and/or directional information. For the first detection phase, however, it is likely that a complete disambiguation might not be possible, so that a first detection of a diffuse flux will have multiple interpretations.

E. Directions for improvement

1. Phenomenology of the DSNB

The directions in which phenomenology can develop are many. Here I outline some that I consider most important to advance the field.

- *Contribution of different supernova types.* Perhaps, the truly unique value of the DSNB – in comparison to neutrinos from individual supernovae – is its sensitivity to the diverse stellar population that contributes to it, which spans decades of progenitor masses and different stellar properties (magnetic fields, metallicities, etc.). A comprehensive study of how this diversity is reflected in the DSNB would be extremely important to fully explore the physics potential of this flux. It would require a systematic modeling of the neutrino emission for a large variety of supernova progenitors, a goal that is certainly ambitious but realistic, in principle.
- *from one supernova to many: what does really matter?* As commented previously, when summing over many sources and including redshift effects, a certain loss of information is unavoidable. It would be desirable to have a systematic study of the features and size of each different effect (e.g., oscillations, propagation effects, time structures, etc.). Like most complex phenomena, it is possible that several small effects might sum to a sizable contribution. Such level of detail might be premature at this time, but will be needed when the precision phase begins.
- *What fundamental physics will we learn?* Related to the previous point is the question of how much information will be possible to extract from the DSNB data on specific quantities of interest, like the SNR, neutrino spectra, oscillation parameters, etc. This question is closely connected to that of experimental capability, and requires a careful study of how data can be processed for best parameter extraction. It will be of immediate relevance after the DSNB is first detected.

In addition to these directions, it is expected that studies of the DSNB will be updated over time, following the developments in the physics of neutrinos and of supernovae. New, more precise determinations of the SNR will be used after a new phase of supernova surveys, some of which are already taking data (Astier *et al.*, 2010; Perlmutter *et al.*, 2004). A more detailed description of oscillation effects will have to be adopted once the phenomenology of neutrino self-interactions (sec. III.C) is completely understood. Progress in the determination of oscillation parameters – especially if θ_{13} and the mass hierarchy are measured – will help to converge towards a uniquely determined oscillation scenario. Finally, as the modeling of neutrino emission and transport in supernovae progresses, updated neutrino fluxes will be available with a reduced uncertainty on the neutrino spectra and luminosities.

If a galactic supernova is observed in the next decade or so, the study of the DSNB will take a different turn. The abundance of data from the single nearby supernova will eliminate or greatly reduce the uncertainty on the original neutrino fluxes and on oscillations. This will allow more precise predictions for the DSNB, with more focus on its sensitivity to the supernova population of the universe and a number of cosmological and astrophysical effects.

2. Experimental searches

From what was discussed so far, one can see that the experimental study of the DSNB has two strong limiting factors: the detector mass and the backgrounds.

Increasing the mass of a detector is of course desirable for a higher statistical significance of a DSNB signal. At the moment, any expansion beyond Mt (0.1 Mt) mass for water Cherenkov (LAr) seems speculative. However, there are initial studies for a 5 Mt mass water Cherenkov detector to be built under sea, off the coast of Japan (Suzuki *et al.*, 2001). The sensitivity of this design to supernova neutrinos has been studied at a basic level (Kistler *et al.*, 2008a), but many questions of technical nature remain open. In particular, the larger volume is likely to come at the price of worse performance in terms of energy threshold, depth, etc., in a way that remains to be assessed.

For currently planned detectors, efforts to better discriminate the backgrounds at low energy, and therefore expand the energy window, are in progress (sec. IV). Even though it might be possible to gain 2-3 MeV by purely technical upgrades, a new approach might be needed to discriminate backgrounds that are orders of magnitude larger than the signal, like solar neutrinos for LAr detectors or reactor antineutrinos for water and liquid scintillator. In the absence of concrete ideas, here I outline some possible directions for further thinking, some of which are purely speculative at the moment.

- *directional detection.* Reconstructing the direction of arrival of neutrinos and antineutrinos in a detector would be a very effective way to discriminate the solar and reactor backgrounds. Unfortunately, the relevant detection

processes have weak correlation between the direction of the neutrino and that of the daughter lepton at the energies of interest (see e.g., Strumia and Vissani (2003)). Therefore the complete kinematics of the process would need to be reconstructed for directional sensitivity. This seems unrealistic for water and LAr detectors (Rubbia, 2009a). Studies in the context of geoneutrinos show that some directional information can be extracted by adding ^6Li , ^{10}B or Gadolinium to liquid scintillator (Hochmuth *et al.*, 2007; Terashima *et al.*, 2008), with ^6Li emerging as the best candidate (Terashima *et al.*, 2008). It is not clear, however, if the improvement in directionality would be sufficient to separate reactor neutrinos at the level needed to study the DSNB.

- *turning off or optimizing nuclear reactors.* Considering the current efforts in developing renewable energy, it is conceivable that in the far future fission reactors will be abandoned. The absence of reactor neutrinos would allow a sensitivity to the $\bar{\nu}_e$ component of the DSNB down to at least 4.5 MeV, where the flux of geoneutrinos terminates (Krauss *et al.*, 1984). This implies the possibility to study the peak of the DSNB, which would allow a detailed reconstruction of the neutrino spectrum and would provide precious information on supernovae at large redshift ($z > 1$, see sec. III.E.3). If a new generation of fission reactors is built, instead, its flux might be reduced by negotiating down times with the reactor managements, or even by negotiating a reactor-free zone within a certain distance from major detectors. Negotiations could prove unreliable, however. Interestingly, one could minimize the reactor flux also by arranging the detector-reactor distance to maximize the suppression effect of oscillations, which can be as large as $(1 - \sin^2 2\theta_{12}) \simeq 0.13$. This could be done either by planned construction of detectors and reactors, or with a movable detector like Hanohano (Learned *et al.*, 2007).
- *extraterrestrial detectors.* In the light of a renewed interest in manned exploration of space, one can dream that a few centuries from now underground laboratories might exist on the moon and/or on Mars or other planets of the solar system. Even without a colonization of them, scientific labs may flourish there the same way they do in Antarctica today, even though with the new challenges of extraterrestrial conditions. A large neutrino detector on Mars, for example, would benefit from the lower solar flux and from the suppressed atmospheric neutrino flux reflecting the thinner atmosphere. Reactor neutrinos might be absent there if power is provided by alternative forms of energy (fusion, solar, etc.). Of course, investing in such detector would require a strongly motivated and diverse scientific agenda, which might include studying the radioactivity of the planet with geoneutrinos.

F. Final considerations

At the opening of a new phase of neutrino telescopes, the possibility to observe diffuse supernova neutrinos has a quiet appeal of its own, that well complements the thrill of playing the lottery of galactic supernovae. As new detectors turn on, the DSNB could be the first new signal to emerge, nicely sandwiched between higher precision data from known sources at low and high energy. This is a guaranteed flux that must be there – even though with a large normalization uncertainty – and once detected, it will mark the transition of supernova neutrinos from rare events (SN1987A) to everyday physics, like solar and atmospheric neutrino have been in the past several years.

Over decades, the DSNB will go through the phases of discovery, maturity and precision, delivering unique information on the population of core collapse supernovae all the way to cosmological distances, and thus complementing information from individual supernovae on the physics of core collapse and on the properties of the neutrino as a particle. In addition, there might be surprises: unexpected turns of which neutrino physics has been rich so far.

Acknowledgments

I am indebted to Michael Smy for important comments and feedback; many thanks to Shunsaku Horiuchi, James Keehn and Orlando L. G. Peres for useful discussions. I acknowledge the support of the NSF under Grant No. PHY-0854827.

References

- Achterberg, A., *et al.* (IceCube), 2006, *Astropart. Phys.* **26**, 155.
 Agafonova, N. Y., *et al.*, 2007, *Astropart. Phys.* **27**, 254.
 Aglietta, M., *et al.*, 1992, *Astropart. Phys.* **1**, 1.
 Aharmim, B., *et al.* (SNO), 2004, *Phys. Rev.* **D70**, 093014.
 Aharmim, B., *et al.* (SNO), 2006, *hep-ex/0607010* .
 Ahmad, Q. R., *et al.* (SNO), 2001, *Phys. Rev. Lett.* **87**, 071301.
 Akhmedov, E. K., C. Lunardini, and A. Y. Smirnov, 2002, *Nucl. Phys.* **B643**, 339.

- Alekseev, E. N., L. N. Alekseeva, V. I. Volchenko, and I. V. Krivosheina, 1987, JETP Lett. **45**, 589.
- Amerio, S., *et al.* (ICARUS), 2004, Nucl. Instrum. Meth. **A527**, 329.
- Anderson, C., *et al.*, 2010a, microBOONE collaboration, see <http://www-microboone.fnal.gov/index.html>.
- Anderson, C., *et al.*, 2010b, argoNeuT collaboration, see <http://t962.fnal.gov>.
- Ando, S., 2003, Phys. Lett. **B570**, 11.
- Ando, S., 2004, Astrophys. J. **607**, 20.
- Ando, S., J. F. Beacom, and H. Yuksel, 2005, eprint astro-ph/0503321.
- Ando, S., and K. Sato, 2003, Phys. Lett. **B559**, 113.
- Ando, S., and K. Sato, 2004, New J. Phys. **6**, 170.
- Ando, S., K. Sato, and T. Totani, 2003, Astropart. Phys. **18**, 307.
- Apollonio, M., *et al.* (CHOOZ), 1999, Phys. Lett. **B466**, 415.
- Araki, T., *et al.*, 2005a, Nature **436**, 499.
- Araki, T., *et al.* (KamLAND), 2005b, Phys. Rev. Lett. **94**, 081801.
- Arnaud, N., *et al.*, 2004, Astropart. Phys. **21**, 201.
- Astier, P., *et al.*, 2010, sNLS collaboration, <http://www.cfht.hawaii.edu/SNLS/>.
- various authors, 2008, homestake April meeting, http://homestake.sdsmt.edu/April_20-26/meeting.htm.
- Autiero, D., *et al.*, 2007, JCAP **0711**, 011.
- Bahcall, J. N., P. I. Krastev, and E. Lisi, 1997, Phys. Rev. **C55**, 494.
- Bahcall, J. N., A. M. Serenelli, and S. Basu, 2005, Astrophys. J. **621**, L85.
- Barger, V., *et al.*, 2007, eprint 0705.4396.
- Battistoni, G., A. Ferrari, T. Montaruli, and P. R. Sala, 2005, Astropart. Phys. **23**, 526.
- Beacom, J. F., and M. R. Vagins, 2004, Phys. Rev. Lett. **93**, 171101.
- de Bellefon, A., *et al.*, 2006, eprint hep-ex/0607026.
- Bellini, G., *et al.*, 2010, Phys. Lett. **B687**, 299.
- Bernstein, A., *et al.*, 2009, eprint 0907.4183.
- Bionta, R. M., *et al.*, 1987, Phys. Rev. Lett. **58**, 1494.
- Bisnovatyi-Kogan, G. S., and Z. F. Seidov, 1982, Soviet Astronomy (Tr: A. Zhurn.) **26**, 132.
- Boehm, F., *et al.*, 2000, Phys. Rev. **D62**, 072002.
- Botticella, M. T., *et al.*, 2008, Astron. Astrophys. **479**, 49.
- Cappellaro, E., R. Evans, and M. Turatto, 1999, Astron. Astrophys. **351**, 459.
- Cappellaro, E., *et al.*, 2005, Astron. Astrophys. **430**, 83.
- Cardall, C. Y., A. O. Razoumov, E. Endeve, and A. Mezzacappa, 2005, eprint astro-ph/0510704.
- Chakraborty, S., S. Choubey, B. Dasgupta, and K. Kar, 2008, eprint 0805.3131.
- Chakraborty, S., S. Choubey, and K. Kar, 2010, eprint 1006.3756.
- Cline, D. B., F. Raffaelli, and F. Sergiampietri, 2006, JINST **1**, T09001.
- Cocco, A. G., A. Ereditato, G. Fiorillo, G. Mangano, and V. Pettorino, 2004, JCAP **0412**, 002.
- Cole, S., *et al.* (The 2dFGRS), 2001, Mon. Not. Roy. Astron. Soc. **326**, 255.
- Coleman, W., A. Bernstein, S. Dazeley, and R. Svoboda, 2008, Nucl. Instrum. Meth. **A595**, 339.
- Dadykin, V. L., *et al.*, 1987, JETP Lett. **45**, 593.
- Dahlen, T., L. Strolger, and A. G. Riess, 2010, in *Bulletin of the American Astronomical Society*, volume 41 of *Bulletin of the American Astronomical Society*, pp. 360–+.
- Dahlen, T., *et al.*, 2004, Astrophys. J. **613**, 189.
- Daigne, F., K. A. Olive, P. Sandick, and E. Vangioni, 2005, Phys. Rev. **D72**, 103007.
- Dasgupta, B., and A. Dighe, 2008, Phys. Rev. **D77**, 113002.
- Dasgupta, B., A. Dighe, A. Mirizzi, and G. G. Raffelt, 2008, Phys. Rev. **D77**, 113007.
- Dasgupta, B., A. Dighe, G. G. Raffelt, and A. Y. Smirnov, 2009, Phys. Rev. Lett. **103**, 051105.
- Dighe, A. S., and A. Y. Smirnov, 2000, Phys. Rev. **D62**, 033007.
- Diwan, M., *et al.*, 2006, eprint hep-ex/0608023.
- Duan, H., G. M. Fuller, J. Carlson, and Y.-Z. Qian, 2006a, Phys. Rev. Lett. **97**, 241101.
- Duan, H., G. M. Fuller, J. Carlson, and Y.-Z. Qian, 2006b, Phys. Rev. **D74**, 105014.
- Duan, H., G. M. Fuller, J. Carlson, and Y.-Z. Qian, 2007a, Phys. Rev. **D75**, 125005.
- Duan, H., G. M. Fuller, J. Carlson, and Y.-Q. Zhong, 2007b, Phys. Rev. Lett. **99**, 241802.
- Duan, H., G. M. Fuller, and Y.-Z. Qian, 2006c, Phys. Rev. **D74**, 123004.
- Duan, H., G. M. Fuller, and Y.-Z. Qian, 2007c, Phys. Rev. **D76**, 085013.
- Eguchi, K., *et al.* (KamLAND), 2003, Phys. Rev. Lett. **90**, 021802.
- Eguchi, K., *et al.* (KamLAND), 2004, Phys. Rev. Lett. **92**, 071301.
- Ereditato, A., and A. Rubbia, 2006, Nucl. Phys. Proc. Suppl. **155**, 233.
- Esteban-Pretel, A., S. Pastor, R. Tomas, G. G. Raffelt, and G. Sigl, 2007, eprint arXiv:0706.2498 [astro-ph].
- Esteban-Pretel, A., *et al.*, 2008, eprint 0807.0659.
- Fischer, T., S. C. Whitehouse, A. Mezzacappa, F. K. Thielemann, and M. Liebendorfer, 2008, eprint 0809.5129.
- Fischer, T., S. C. Whitehouse, A. Mezzacappa, F. K. Thielemann, and M. Liebendorfer, 2009, eprint 0908.1871.
- Fogli, G. L., E. Lisi, A. Marrone, and A. Mirizzi, 2007, eprint arXiv:0707.1998 [hep-ph].
- Fogli, G. L., E. Lisi, A. Mirizzi, and D. Montanino, 2004, Phys. Rev. **D70**, 013001.
- Fogli, G. L., E. Lisi, A. Mirizzi, and D. Montanino, 2005, JCAP **0504**, 002.

- Fukugita, M., and M. Kawasaki, 2003, Mon. Not. Roy. Astron. Soc. **340**, L7.
- Galais, S., J. Kneller, C. Volpe, and J. Gava, 2009, eprint 0906.5294.
- Goldberg, H., G. Perez, and I. Sarcevic, 2005, eprint hep-ph/0505221.
- Hall, L. J., H. Murayama, M. Papucci, and G. Perez, 2006, eprint hep-ph/0607109.
- Hannestad, S., G. G. Raffelt, G. Sigl, and Y. Y. Y. Wong, 2006, Phys. Rev. **D74**, 105010.
- Hartmann, D. H., and S. E. Woosley, 1997, Astropart. Phys. **7**, 137.
- Hirata, K., *et al.* (KAMIOKANDE-II), 1987, Phys. Rev. Lett. **58**, 1490.
- Hirata, K. S., *et al.*, 1988, Phys. Rev. **D38**, 448.
- Hochmuth, K. A., *et al.*, 2007, Astropart. Phys. **27**, 21.
- Hopkins, A. M., 2006, eprint astro-ph/0611283.
- Hopkins, A. M., and J. F. Beacom, 2006, Astrophys. J. **651**, 142.
- Horiuchi, S., J. F. Beacom, and E. Dwek, 2009, Phys. Rev. **D79**, 083013.
- Horowitz, C. J., 2002, Phys. Rev. **D65**, 043001.
- Huedepohl, L., B. Mueller, H. T. Janka, A. Marek, and G. G. Raffelt, 2009, eprint 0912.0260.
- Iida, T., 2005, J. Phys.: Conf. Ser. **136**, 042075.
- Iida, T., 2010, PhD thesis, U. of Tokyo, 2010. Available at <http://www-sk.icrr.u-tokyo.ac.jp/sk/pub/>.
- Iocco, F., G. Mangano, G. Miele, G. G. Raffelt, and P. D. Serpico, 2005, Astropart. Phys. **23**, 303.
- Jung, C. K., 1999, eprint hep-ex/0005046.
- Kaplinghat, M., G. Steigman, and T. P. Walker, 2000, Phys. Rev. **D62**, 043001.
- Keehn, J. G., and C. Lunardini, 2010, in preparation.
- Keil, M. T., G. G. Raffelt, and H.-T. Janka, 2003, Astrophys. J. **590**, 971.
- Kibayashi, A., *et al.*, 2009, eprint 0909.5528.
- Kistler, M. D., H. Yuksel, S. Ando, J. F. Beacom, and Y. Suzuki, 2008a, eprint 0810.1959.
- Kistler, M. D., H. Yuksel, J. F. Beacom, and K. Z. Stanek, 2008b, Astrophys. J. **673**, L119.
- Kneller, J. P., and C. Volpe, 2010, eprint 1006.0913.
- Krastev, P. I., and S. T. Petcov, 1988, Phys. Lett. **B205**, 84.
- Krauss, L. M., S. L. Glashow, and D. N. Schramm, 1984, Nature **310**, 191.
- Lachenmaier, T., 2009, talk at NNN09, available at <http://nnn09.colostate.edu/>.
- Lattimer, J. M., and F. D. Swesty, 1991, Nucl. Phys. A **535**, 331.
- Learned, J. G., S. T. Dye, and S. Pakvasa, 2007, eprint 0810.4975.
- Liebendoerfer, M., *et al.*, 2004, Astrophys. J. Suppl. **150**, 263.
- Lien, A., B. D. Fields, and J. F. Beacom, 2010, eprint 1001.3678.
- Lunardini, C., 2006a, Phys. Rev. **D73**, 083009.
- Lunardini, C., 2006b, Astropart. Phys. **26**, 190.
- Lunardini, C., 2007a, Phys. Rev. **D75**, 073022.
- Lunardini, C., 2007b, Nucl. Phys. Proc. Suppl. **168**, 131.
- Lunardini, C., 2009, Phys. Rev. Lett. **102**, 231101.
- Lunardini, C., and O. L. G. Peres, 2008, eprint 0805.4225.
- Lunardini, C., and A. Y. Smirnov, 2003, JCAP **0306**, 009.
- Malaney, R. A., 1997, Astropart. Phys. **7**, 125.
- Malek, M., *et al.* (Super-Kamiokande), 2003, Phys. Rev. Lett. **90**, 061101.
- Malek, M. S., 2003, uMI-31-06530.
- Marek, A., and H. T. Janka, 2009, Astrophys. J. **694**, 664.
- Marrodan Undagoitia, T., *et al.*, 2006, Prog. Part. Nucl. Phys. **57**, 283.
- Meregaglia, A., and A. Rubbia, 2006, Acta Phys. Polon. **B37**, 2387.
- Mikheev, S. P., and A. Y. Smirnov, 1985, Sov. J. Nucl. Phys. **42**, 913.
- Mikheev, S. P., and A. Y. Smirnov, 1986, Sov. Phys. JETP **64**, 4.
- Minakata, H., H. Nunokawa, R. Tomas, and J. W. F. Valle, 2008, JCAP **0812**, 006.
- Nakamura, K., 2003, Int. J. Mod. Phys. **A18**, 4053.
- Nakazato, K., K. Sumiyoshi, H. Suzuki, and S. Yamada, 2008, Phys. Rev. **D78**, 083014.
- Nuijten, G., 2008, talk at NNN08, 2008, available at <http://indico.in2p3.fr/conferenceDisplay.py?confId=402>.
- Ott, C. D., A. Burrows, L. Dessart, and E. Livne, 2008, Astrophys. J. **685**, 1069.
- Palomares-Ruiz, S., 2008, Phys. Lett. **B665**, 50.
- Palomares-Ruiz, S., and S. Pascoli, 2008, Phys. Rev. **D77**, 025025.
- Peres, O. L. G., and A. Y. Smirnov, 2009, Phys. Rev. **D79**, 113002.
- Perlmutter, S., *et al.*, 2004, sNAP letter of intent, at <http://snap.lbl.gov/>.
- Raffelt, G., and T. Rashba, 2009, eprint 0902.4832.
- Raffelt, G. G., and A. Y. Smirnov, 2007, eprint arXiv:0705.1830 [hep-ph].
- Rubbia, A., 2009a, private communication.
- Rubbia, A., 2009b, J. Phys. Conf. Ser. **171**, 012020.
- Salpeter, E. E., 1955, Astrophys. J. **121**, 161.
- Schirato, R. C., and G. M. Fuller, 2002, eprint astro-ph/0205390.
- Schwetz, T., M. A. Tortola, and J. W. F. Valle, 2008, New J. Phys. **10**, 113011.
- Selvi, M. (LVD), 2007, AIP Conf. Proc. **944**, 16.

- Shen, H., H. Toki, K. Oyamatsu, and K. Sumiyoshi, 1998, Nucl. Phys. A **637**, 435.
- Skadhauge, S., and R. Zukanovich Funchal, 2007, JCAP **0704**, 014.
- Smartt, S. J., J. J. Eldridge, R. M. Crockett, and J. R. Maund, 2008, eprint 0809.0403.
- Smy, M., 2009, talk at the workshop “Supernova Physics and DUSEL.
- Smy, M., 2010, private communication.
- Strigari, L. E., J. F. Beacom, T. P. Walker, and P. Zhang, 2005, JCAP **0504**, 017.
- Strigari, L. E., M. Kaplinghat, G. Steigman, and T. P. Walker, 2004, JCAP **0403**, 007.
- Strumia, A., and F. Vissani, 2003, Phys. Lett. **B564**, 42.
- Sumiyoshi, K., S. Yamada, and H. Suzuki, 2007, eprint 0706.3762.
- Sumiyoshi, K., S. Yamada, and H. Suzuki, 2008, eprint 0808.0384.
- Sumiyoshi, K., S. Yamada, H. Suzuki, and S. Chiba, 2006, Phys. Rev. Lett. **97**, 091101.
- Suzuki, Y., 2004, talk at the 2004 Nobel Symposium on Neutrino Physics, Enkoping, Sweden, published in L. Bergstrom, O. Botner, P. Carlson, P. O. Hulth, T. Ohlsson: Neutrino Physics, Physica Scripta, vol. T121, 2005.
- Suzuki, Y., *et al.* (TITAND Working Group), 2001, eprint hep-ex/0110005.
- Svoboda, R., 2008, summary talk at the DUSEL meeting of Lead, SD. Available at: <http://neutrino.lbl.gov/dusel/HomestakeWorkshopApril2008/Physics/>.
- Terashima, A., *et al.* (KamLAND), 2008, J. Phys. Conf. Ser. **120**, 052029.
- Thompson, T. A., A. Burrows, and P. A. Pinto, 2003, Astrophys. J. **592**, 434.
- Totani, T., and K. Sato, 1995, Astropart. Phys. **3**, 367.
- Totani, T., K. Sato, H. E. Dalhed, and J. R. Wilson, 1998, Astrophys. J. **496**, 216.
- Totani, T., K. Sato, and Y. Yoshii, 1996, Astrophys. J. **460**, 303.
- Vagins, M., 2009, talk at TeV particle astrophysics 2009, available at <http://www-conf.slac.stanford.edu/tevpa09/>.
- Volpe, C., and J. Welzel, 2007, eprint 0711.3237.
- Watanabe, H., *et al.* (Super-Kamiokande), 2008, eprint 0811.0735.
- Wolfenstein, L., 1978, Phys. Rev. **D17**, 2369.
- Woosley, S. E., and T. A. Weaver, 1995, astrophys. J. Suppl. 101, 181.
- Woosley, S. E., J. R. Wilson, and R. Mayle, 1986, Astrophys. Jour., Part 1 **302**, 19.
- Wurm, M., *et al.*, 2007, Phys. Rev. **D75**, 023007.
- Yuksel, H., S. Ando, and J. F. Beacom, 2006, Phys. Rev. **C74**, 015803.
- Yuksel, H., and J. F. Beacom, 2007, eprint astro-ph/0702613.
- Zhang, W., *et al.*, 1988, Phys. Rev. Lett. **61**, 385.

Figures

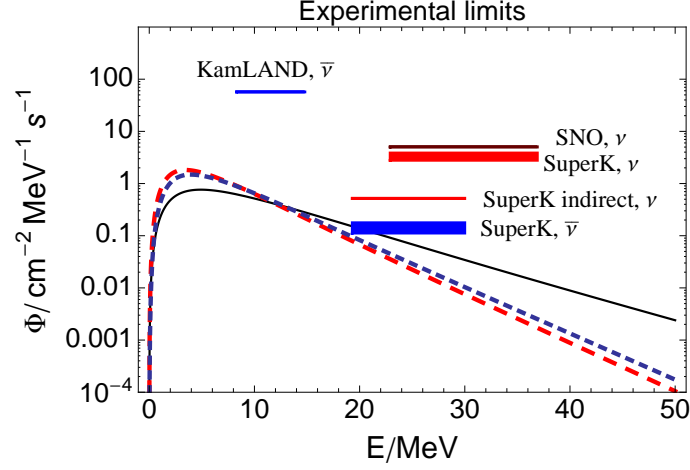


FIG. 1 Experimental limits for the ν_e and $\bar{\nu}_e$ components of the DSNB, (Table VIII) compared with theoretical predictions for three different models of neutrino spectra (Table I); the upper to lower curves at 20 MeV refer to the Lawrence Livermore (LL), Garching (KRJ), and Arizona (TBP) and models, and complete flavor permutation ($p = \bar{p} = 0$), for which fluxes are maximal for the energies of interest. To make the comparison meaningful, limits on the energy-integrated fluxes have been divided by the size of the energy window of sensitivity of the experiment (see sec. IV.A). For the SK limits, the widths of the lines represent how each bound varies with the variation of the neutrino energy spectrum. See sec. IV.C for details.

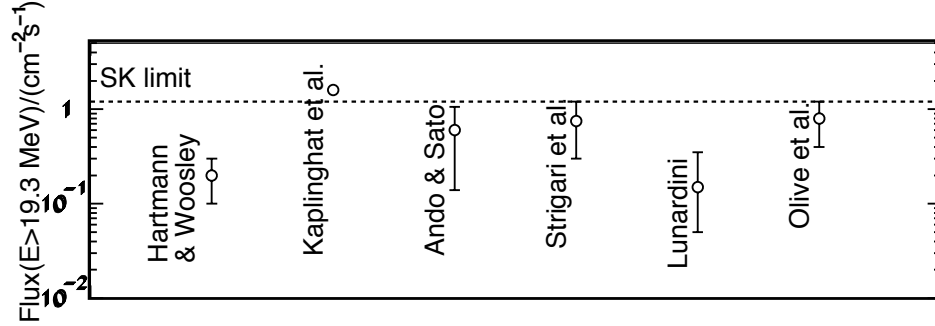


FIG. 2 A sample of theoretical predictions (Ando, 2004; Ando and Sato, 2004; Daigne *et al.*, 2005; Hartmann and Woosley, 1997; Kaplinghat *et al.*, 2000; Lunardini, 2006b; Strigari *et al.*, 2004) for the $\bar{\nu}_e$ component of the DSNB above the SK energy threshold (figure adapted from Lunardini (2006b)). The result of Lunardini (2006b) is quoted with a 99% C.L. error bar; for the others, the error bars are an indicative description of the uncertainty due to uncertain input parameters. The SK limit (Eq. (2)) is shown for comparison.

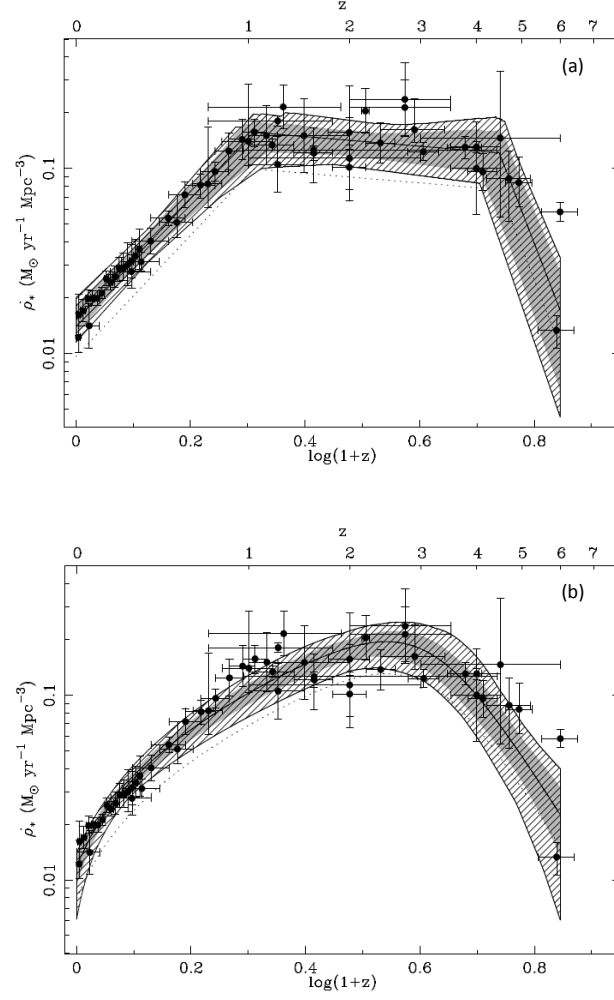


FIG. 3 Measurements of the cosmological star formation rate and functional fits, from Hopkins (2006). The grey shaded and hatched regions are the 1σ and 3σ confidence regions obtained with (a) the piecewise parameterization and (b) the Cole et al. parameterization, Eq. (4). The SK limit on the DSNB, Eq. (2), constrains the normalization to values lower by a factor 0.74 - 1 depending on the neutrino spectrum; the rescaled SFR is indicated by the dotted curves, see Hopkins (2006) for details.

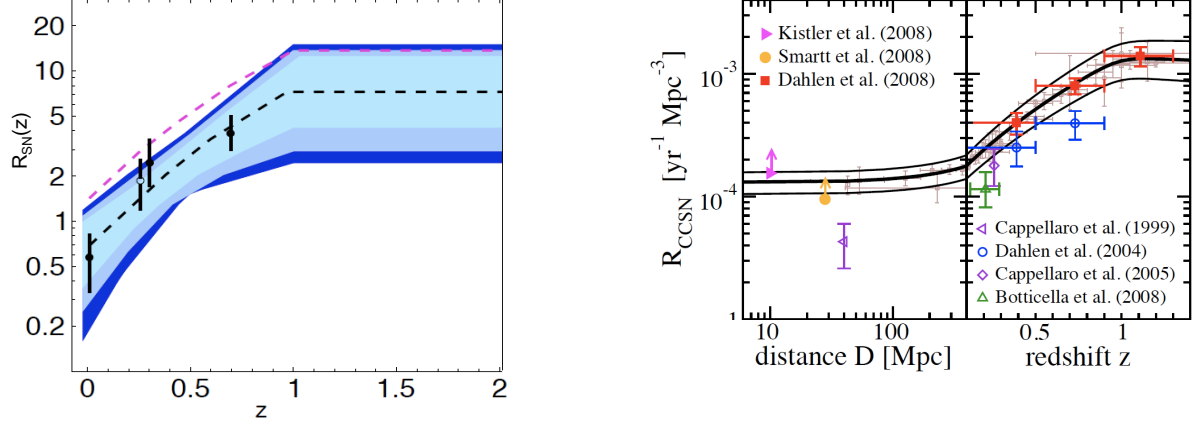


FIG. 4 Left: Direct supernova rate measurements as of 2005, in units of $10^{-4} \text{ yr}^{-1} \text{ Mpc}^{-3}$ (Cappellaro *et al.*, 1999, 2005; Dahlen *et al.*, 2004) and their piecewise fit (Lunardini, 2006b). Shaded areas correspond to 68.3, 90, 95.4% C.L.. The flattening of the curve at $z \simeq 1$ is motivated by SFR observations (fig. 3) and not by the supernova data themselves. The upper dashed line represents Eq. (5) and is the SNR obtained from a SFR data fit via Eq. (3) (Hopkins, 2006). Right: direct supernova rate measurements updated with 2008 data (Botticella *et al.*, 2008; Dahlen *et al.*, 2010; Kistler *et al.*, 2008b; Smartt *et al.*, 2008); from Horiuchi *et al.* (2009).

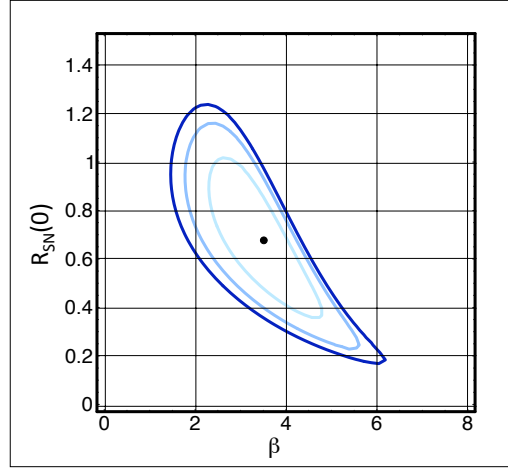


FIG. 5 Best fit point and isocontours of χ^2 in the space of the parameters describing the SNR function, $R_{SN}(z)$, from a 2005 analysis (Lunardini, 2006b). These are the intercept, $R_{SN}(0)$ (in units of $10^{-4} \text{ yr}^{-1} \text{ Mpc}^{-3}$) and the power, β (for the piecewise parameterization in Eq. (4)). The contours refer to 68.3, 90, 95.4% C.L..

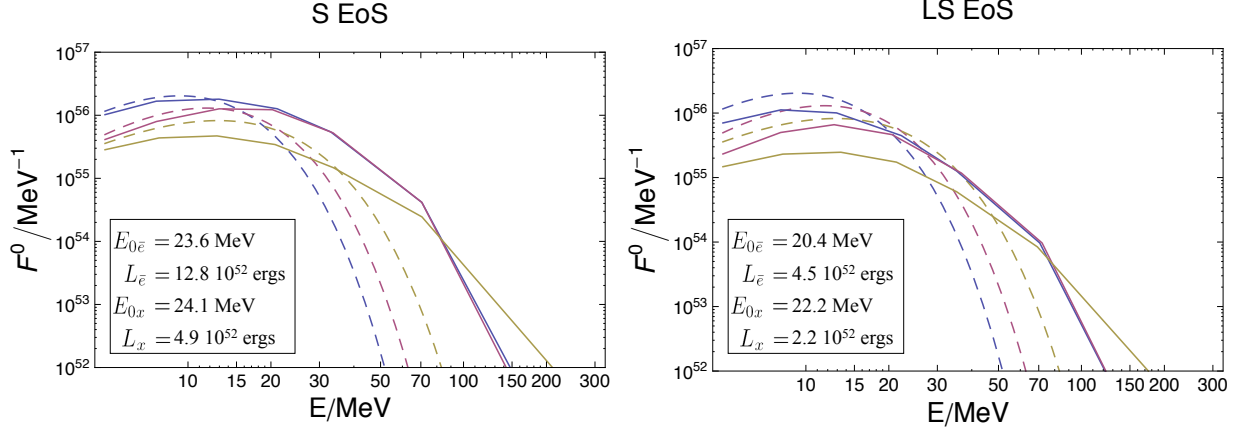


FIG. 6 Neutrino fluxes at production inside the star for direct black hole-forming collapse (solid lines), from Nakazato *et al.* (2008). Curves from upper to lower at 5 MeV correspond to ν_e , $\bar{\nu}_e$, ν_x . Spectra are shown for the Shen et al. (left panel) and Lattimer-Swesty (right) equation of state. For each, the neutrino luminosities and average energies are given (inserts). See text for details. The dashed lines represent typical spectra for neutron star-forming collapse (Eq. (1)), with the parameters $E_{0\bar{e}} = 15$ MeV, $E_{0x} = 18$ MeV, $L_{\bar{e}} = L_x = 5 \cdot 10^{52}$ ergs, $\alpha_{\bar{e}} = 3.5$ and $\alpha_x = 2.5$.

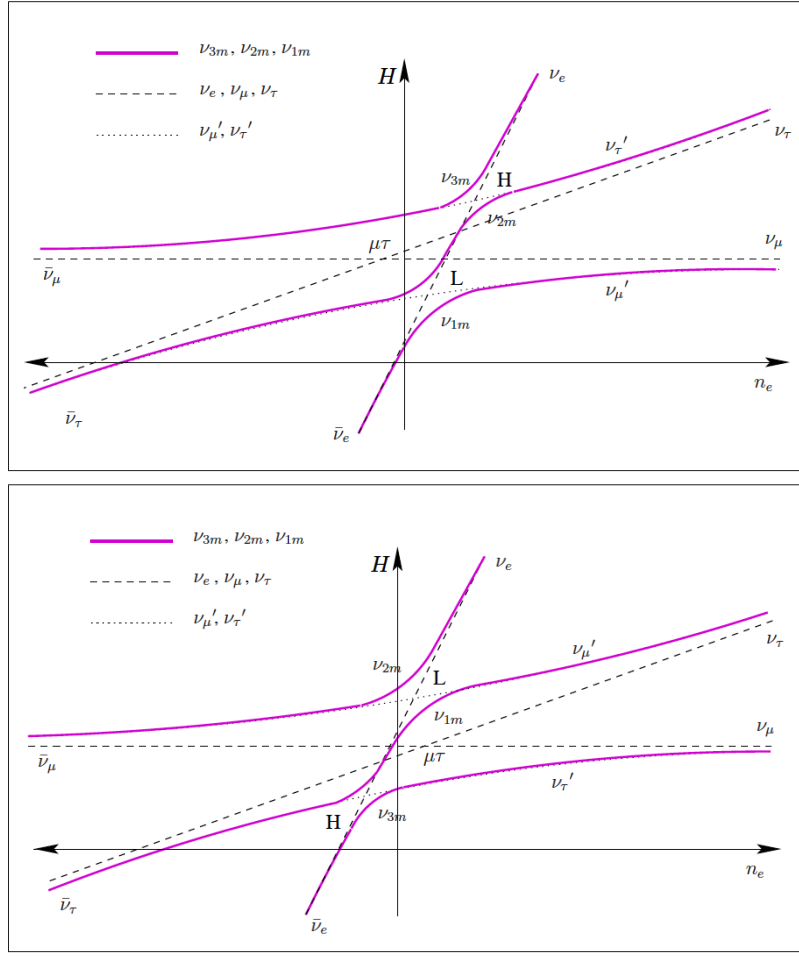


FIG. 7 Schematic representation of the neutrino energy levels in matter vs electron number density, n_e , for normal (upper pane) and inverted (lower pane) mass hierarchy, from Akhmedov *et al.* (2002). Dashed line: in the absence of mixing (unphysical), solid line: with mixing (physical case). The semi-plane with positive (negative) density, $n_e > 0$ ($n_e < 0$), describes the conversion of neutrinos (antineutrinos), to account for the fact that the refraction potential has opposite sign for neutrinos and antineutrinos. The positions of the high (H) and low (L) density MSW resonances are marked. See Akhmedov *et al.* (2002); Lunardini and Smirnov (2003) for details.

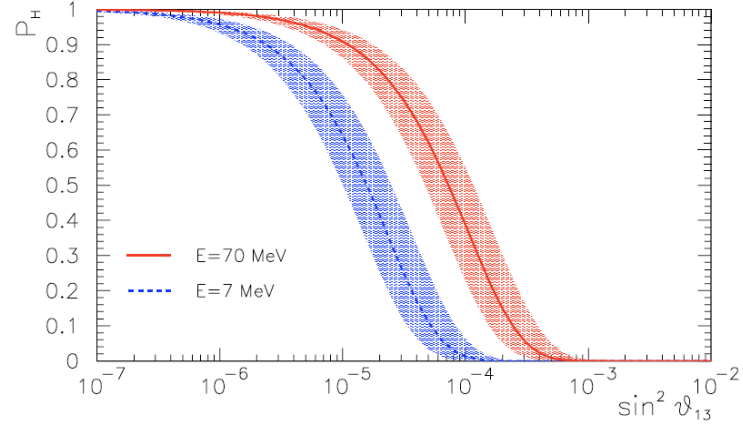


FIG. 8 The transition probability in the H resonance, P_H (eq. 12), as a function of θ_{13} for two values of the neutrino energy for $C = 4$ and $|\Delta m_{32}^2| = 3 \cdot 10^{-3} \text{ eV}^2$. The shaded regions represent the uncertainty associated to $C = 1 - 15$.

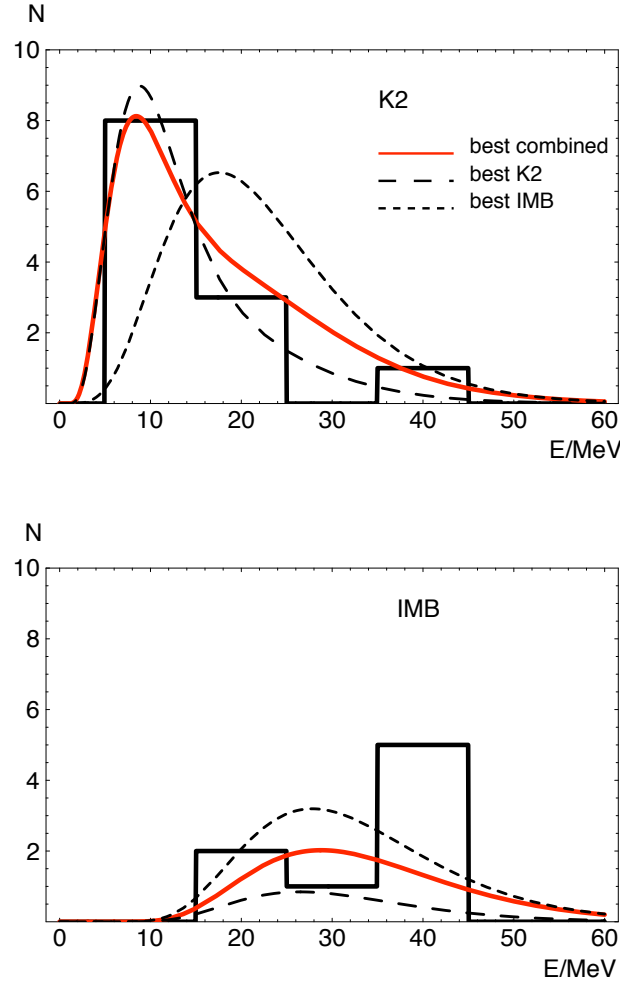


FIG. 9 The observed positron energy spectra of events at Kamiokande II (K2) and IMB, compared with the predicted spectra in the points of minimum χ^2 for the two data sets separately and combined (Lunardini, 2006b).

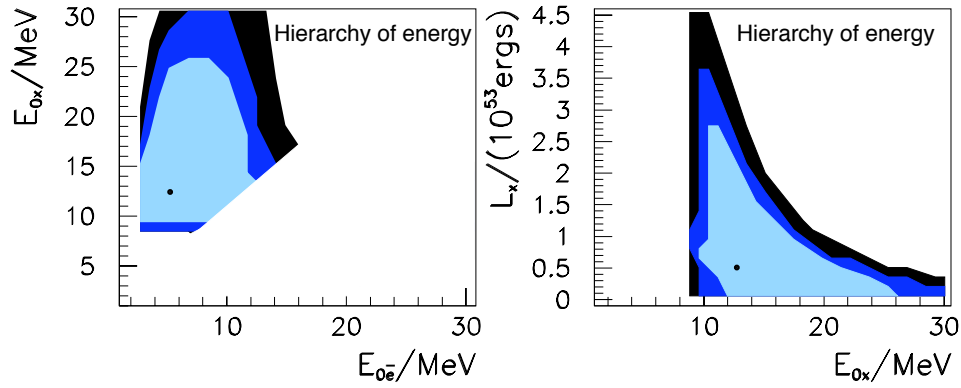


FIG. 10 From Lunardini (2006b): projections of the 68%,90%,99% C.L. regions allowed by the SN1987A data on the planes $E_{0\bar{e}} - E_{0x}$ and $E_{0x} - L_x$, with the hierarchy $E_{0\bar{e}} < E_{0x}$ imposed as a prior. The dots in each panel mark the projections of the points of maximum likelihood. The entire plane $E_{0\bar{e}} - L_{\bar{e}}$ (not shown) is allowed at 68% C.L..

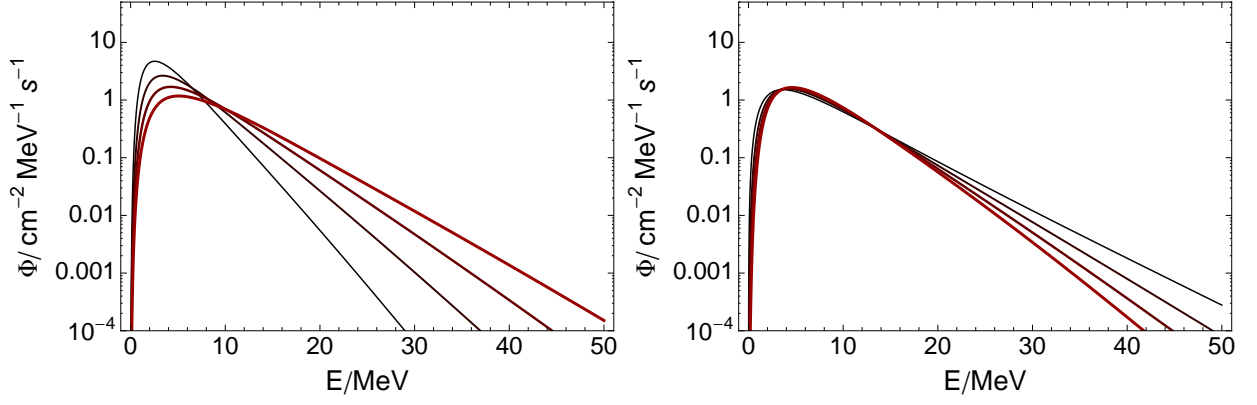


FIG. 11 Examples of unoscillated flux, Φ_w^0 ($w = e, \bar{e}, x$) (Eq. (18)), for different spectral parameters E_{0w}, α_w . Left: the curves of increasing thickness (increasing color intensity) correspond to $E_{0w} = 9, 12, 15, 18$ MeV, with $\alpha_w = 3.8$. Right: the curves of increasing thickness (increasing color intensity) correspond to $\alpha_w = 2, 3, 4, 5$ with $E_{0w} = 15.4$ MeV.

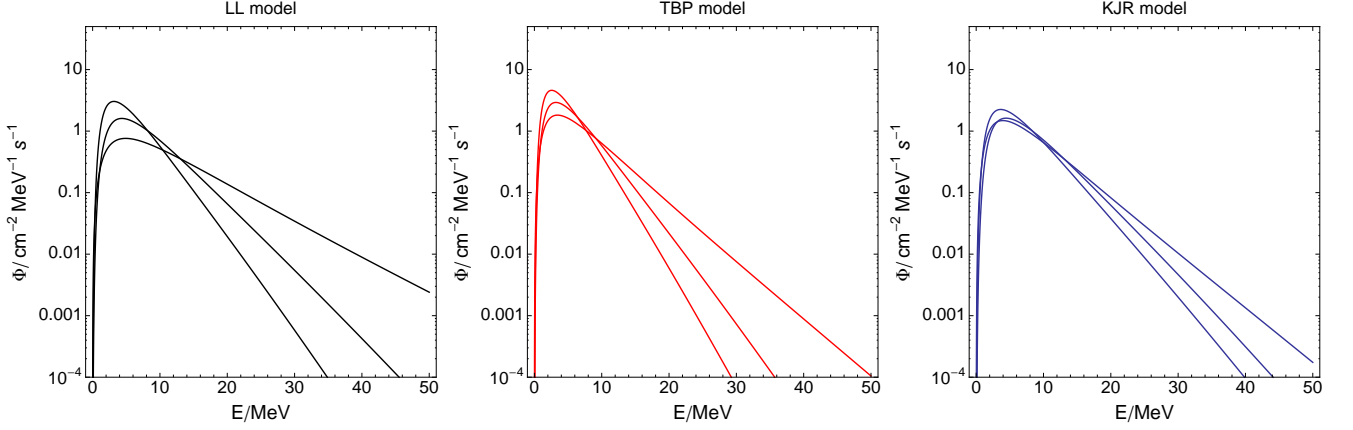


FIG. 12 The fluxes $\Phi_e^0, \Phi_{\bar{e}}^0, \Phi_x^0$, defined in Eq. (18), for the three models in Table I. For each model, the colder to hotter spectra refer to $\nu_e, \bar{\nu}_e, \nu_x$.

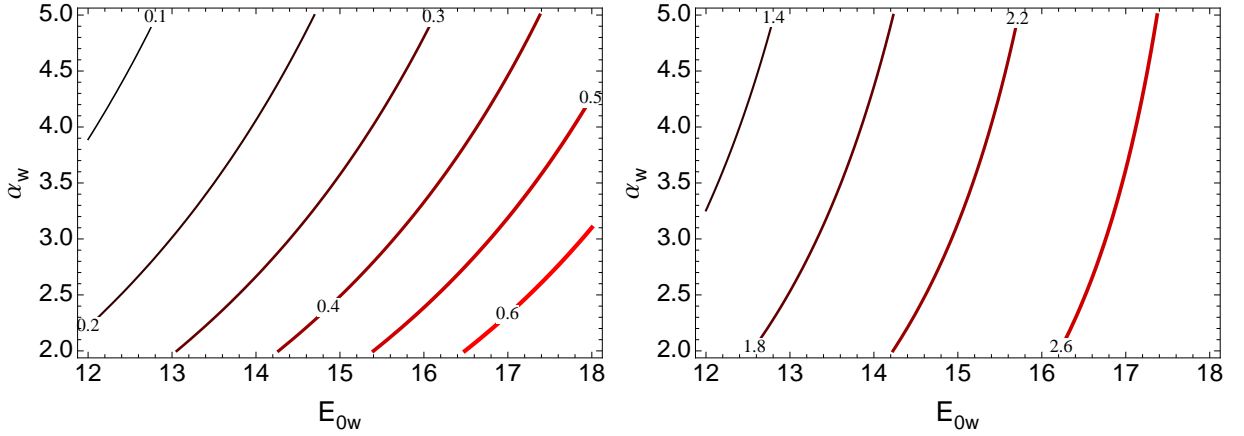


FIG. 13 Isocontours of the total (unoscillated) flux, ϕ_w^0 , above the threshold energy E_{th} , in $\text{cm}^{-2}\text{s}^{-1}$, in the E_{0w}, α_w plane. Left: $E_{th} = 19.3$ MeV. Right: $E_{th} = 11.3$ MeV.

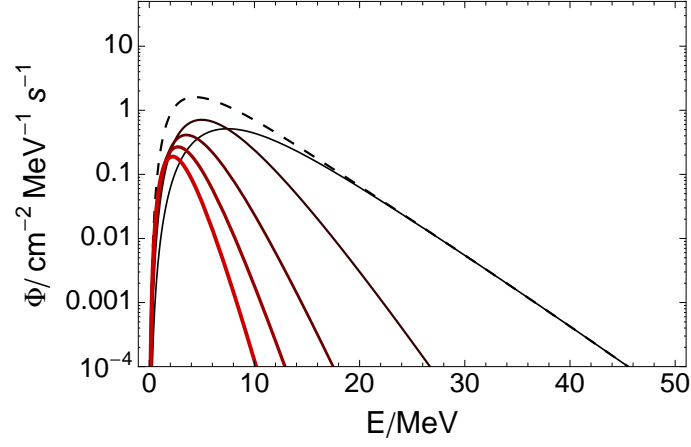


FIG. 14 The contribution to the *unoscillated* $\bar{\nu}_e$ flux of sources in bins of increasing redshift, for the best fit SNR parameter $\beta = 3.28$ (Hopkins and Beacom, 2006). The solid curves from thinner to thicker (darker to lighter color) refer to the intervals: $z = 0 - 1$, $z = 1 - 2$, $z = 2 - 3$, $z = 3 - 4$ and $z = 4 - 5$. The dashed line is the total flux integrated over all redshifts. The parameters of the LL model were used (Table I).

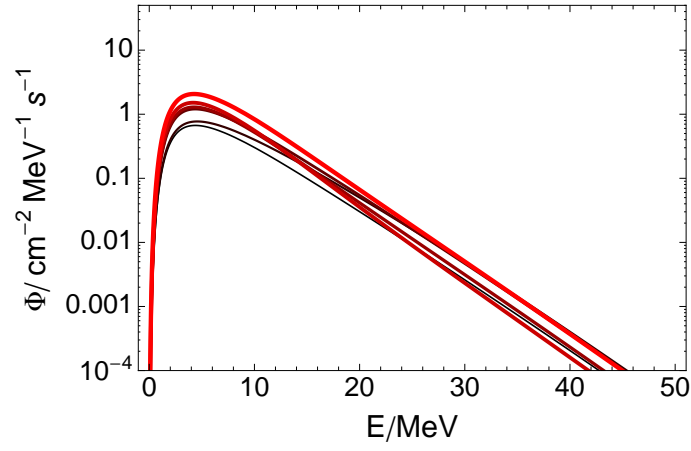


FIG. 15 The *unoscillated* $\bar{\nu}_e$ flux calculated for different points in the allowed region of the parameters $\beta, R_{SN}(0)$ (fig. 5). The curves from thinner to thicker (darker to lighter color) refer to the points: $(\beta, R_{SN}(0)) = (3, 0.5), (2, 1.1), (3, 0.9), (4, 0.5), (5, 0.3), (4, 0.8)$, where $R_{SN}(0)$ is in units of $10^{-4} \text{ yr}^{-1} \text{ Mpc}^{-3}$. The parameters of the LL model were used (Table I).

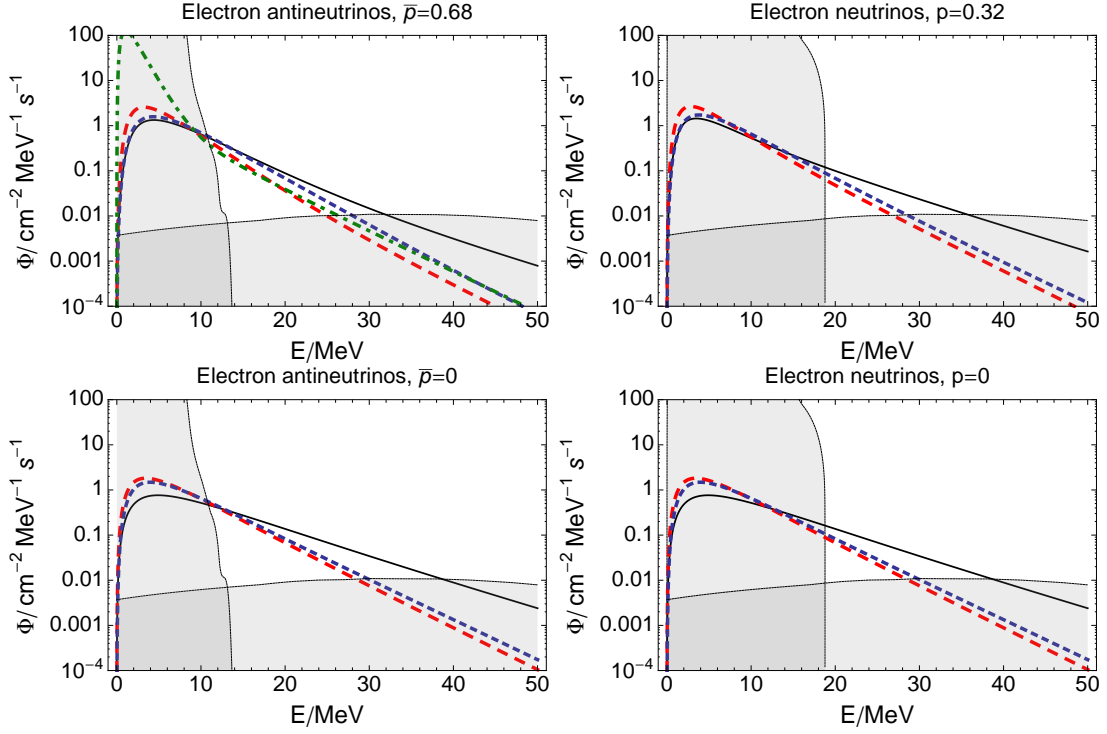


FIG. 16 Examples of energy spectra of the ν_e and $\bar{\nu}_e$ components of the DSNB from the literature for the two extreme values of p and \bar{p} . The solid, long dashed and short dashed curves are from the Lawrence Livermore (LL), Arizona (TBP) and Garching (KRJ) models (Table I). The dashed-dotted line corresponds to the best fit of a multi-parameter statistical analysis of SN1987A data (Lunardini, 2006b) (Eq. 17). All the curves were obtained for the piecewise SNR function (Eq. 5) with $R_{-4} = 1$. The four panels also show backgrounds due to other neutrino sources (see sec. IV.A): $\bar{\nu}_e$ s from the atmosphere (Battistoni *et al.*, 2005) and from reactors (below ~ 11 MeV, inclusive of oscillation effects, from Wurm *et al.* (2007)), and ν_e s from the atmosphere (Battistoni *et al.*, 2005) and from the Sun (below ~ 19 MeV) (Bahcall *et al.*, 2005). All these background fluxes are for the Kamioka site.

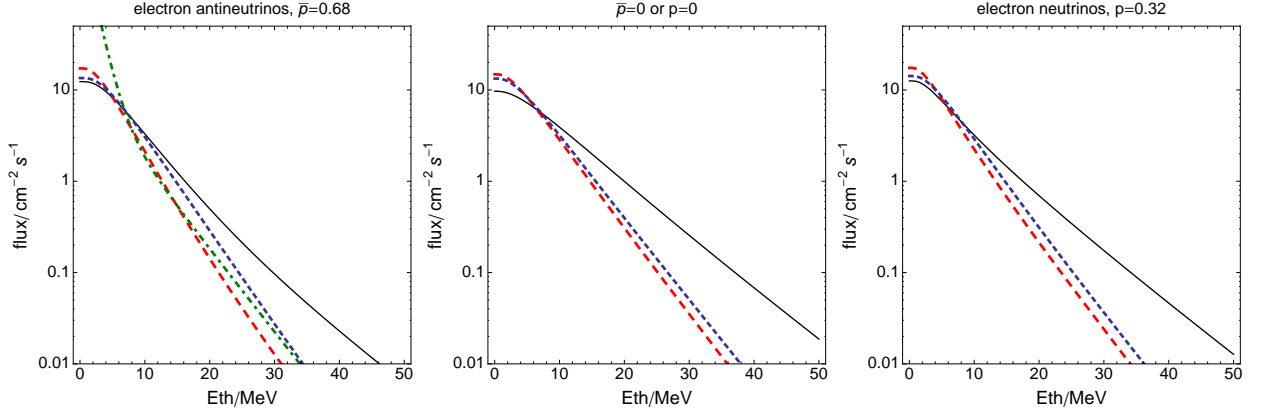


FIG. 17 Diffuse ν_e and $\bar{\nu}_e$ fluxes integrated above a threshold energy E_{th} , as a function of E_{th} for selected values of p, \bar{p} . The middle panel refers to the case in which the $\bar{\nu}_e$ and ν_e fluxes both undergo complete flavor permutation into ν_x , and therefore are equal. The solid, long dashed and short dashed curves are from the Lawrence Livermore (LL), Arizona (TBP) and Garching (KRJ) models (Table I). The dashed-dotted line corresponds to the best fit of a multi-parameter statistical analysis of SN1987A data (Lunardini, 2006b) (Eq. (17)). All other parameters are as in fig. 16.

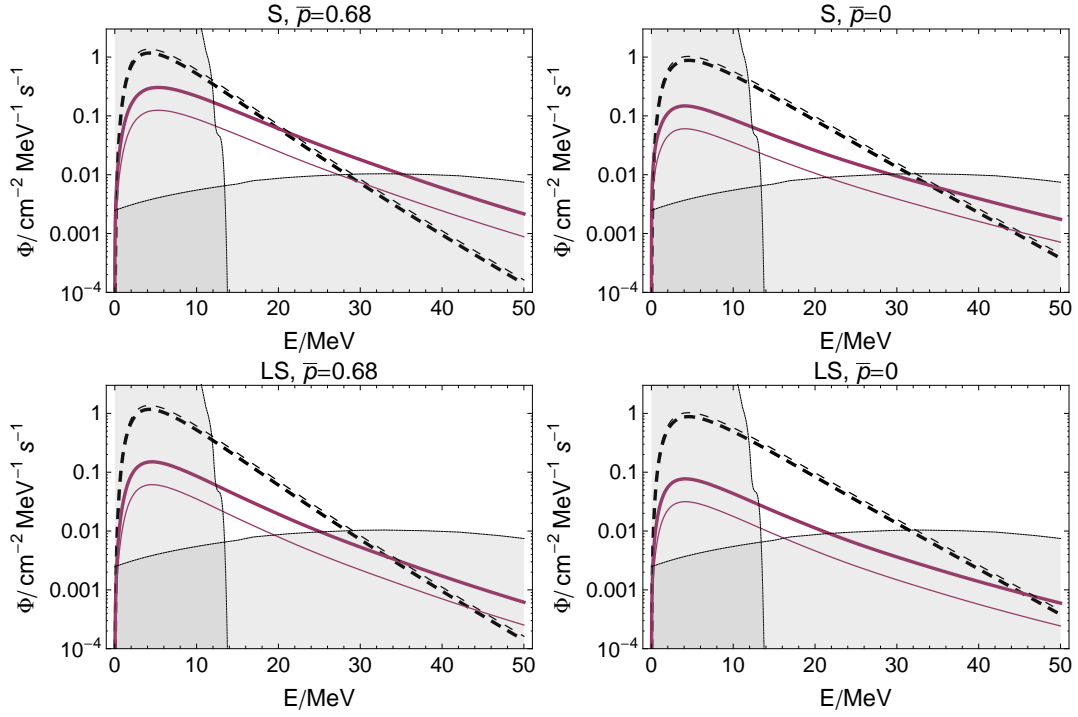


FIG. 18 From Keehn and Lunardini (2010); Lunardini (2009): the diffuse flux of $\bar{\nu}_e$ at Earth from direct black hole-forming collapses, i.e. failed supernovae (solid lines), for the Shen et al. (S) and Lattimer-Swesty (LS) equation of state and different values of the survival probability \bar{p} . The flux from neutron star-forming collapses is also plotted (dashed curves). Direct black hole-forming collapses are assumed to be 22% (thick curves) or 9% (thin curves) of the total. The $\bar{\nu}_e$ atmospheric and reactor backgrounds are shown for comparison.

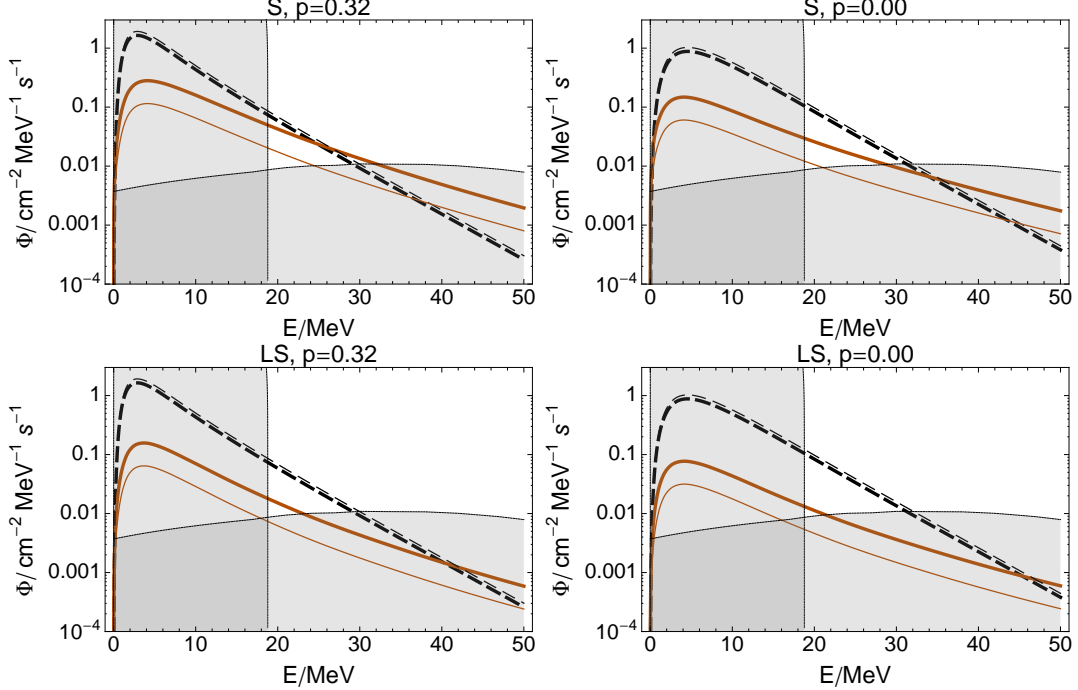


FIG. 19 From Keehn and Lunardini (2010): the same as fig. 18 for ν_e . The backgrounds from solar and atmospheric neutrinos are shown for comparison.

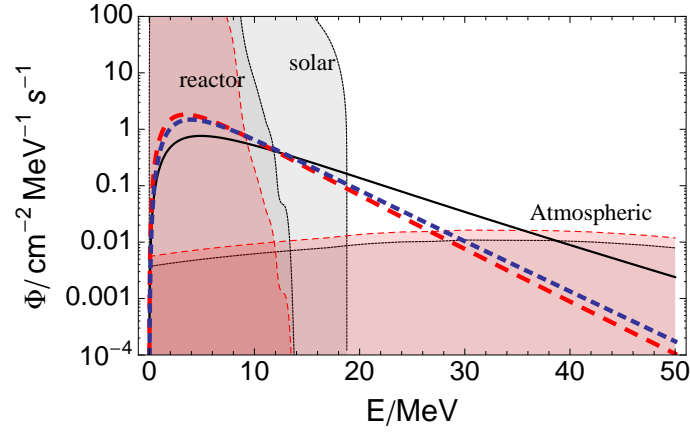


FIG. 20 Backgrounds fluxes: $\bar{\nu}_e$ s from reactors (taken from Wurm *et al.* (2007)) and from the atmosphere (Battistoni *et al.*, 2005), and ν_e from the Sun (Bahcall *et al.*, 2005) and from the atmosphere (Battistoni *et al.*, 2005). These backgrounds are compared with the signal from the DSNB with $p = \bar{p} = 0$ for different models, as in fig. 16. The atmospheric and reactor fluxes are shown for the Kamioka (solid, gray) and Homestake (dashed, red) sites. The atmospheric fluxes of ν_e and $\bar{\nu}_e$ are very similar, so only one of them is plotted. The calculations of the background fluxes include oscillation effects, which are responsible for the visible modulation of the reactor spectrum.

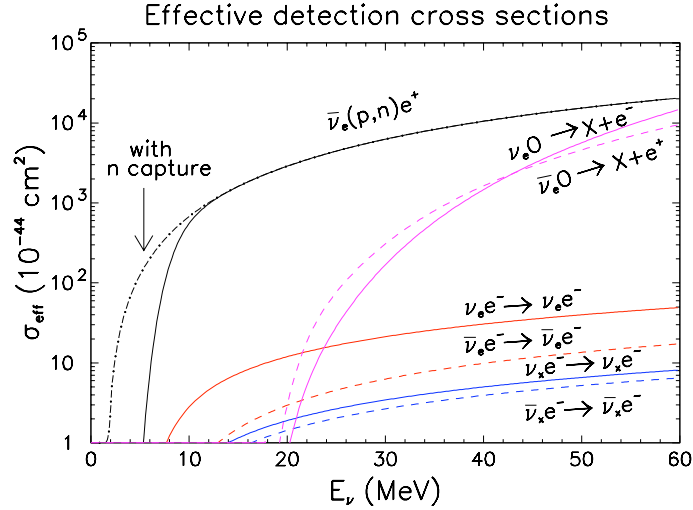


FIG. 21 Effective cross sections for neutrinos in water (Strumia and Vissani, 2003), including the SK energy resolution and threshold effects. Figure from Fogli *et al.* (2005).

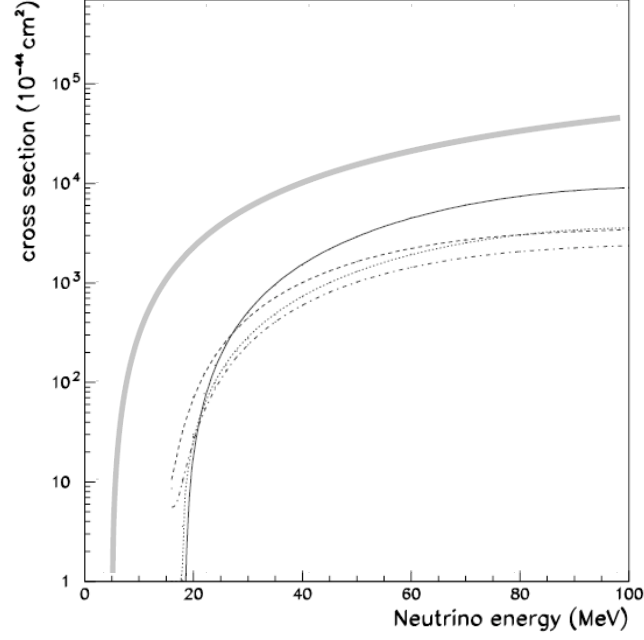


FIG. 22 Cross sections for neutrino scattering on nuclei relevant to a liquid scintillator experiment: inverse beta decay (thick solid), ν_e and $\bar{\nu}_e$ charged current scattering on ^{12}C (thin solid and dashed), ν_e and $\bar{\nu}_e$ neutral current scattering on ^{12}C (dotted and dot-dashed). Figure adapted from Agafonova *et al.* (2007).

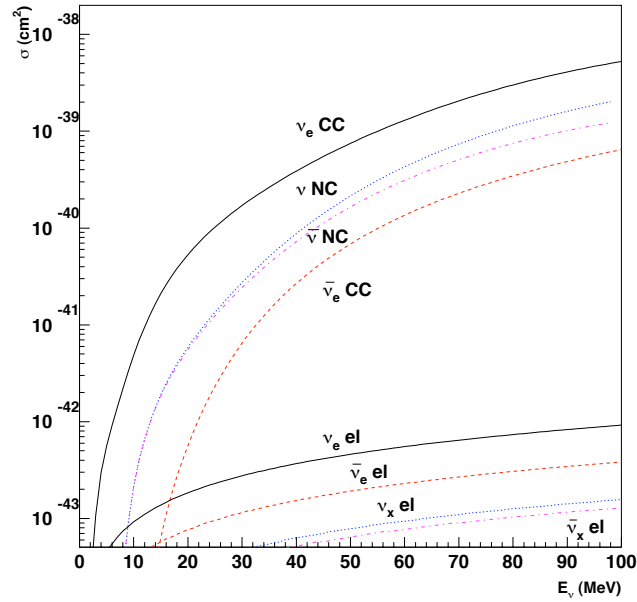


FIG. 23 Cross sections for neutrinos in liquid argon, from Cocco *et al.* (2004). CC (el) stands for Charged Current (elastic scattering).

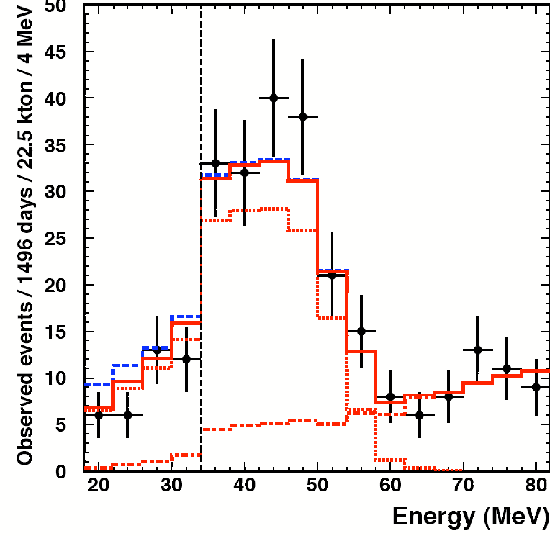


FIG. 24 The distribution in lepton energy of the SK events from diffuse $\bar{\nu}_e$ s and of the fitted backgrounds. The dotted and dashed histograms below the solid one are the fitted backgrounds from invisible muons and atmospheric neutrinos (ν_e and $\bar{\nu}_e$) respectively. The solid histogram is the sum of these two backgrounds. The dashed line above the solid one shows the sum of the total background and of the largest signal allowed (at 90% C.L.) by the analysis in Malek *et al.* (2003). The figure is taken from Malek (2003), with permission, and includes the SK step-like efficiency function (in contrast with the analogous figure in Malek *et al.* (2003), which is corrected for efficiency).

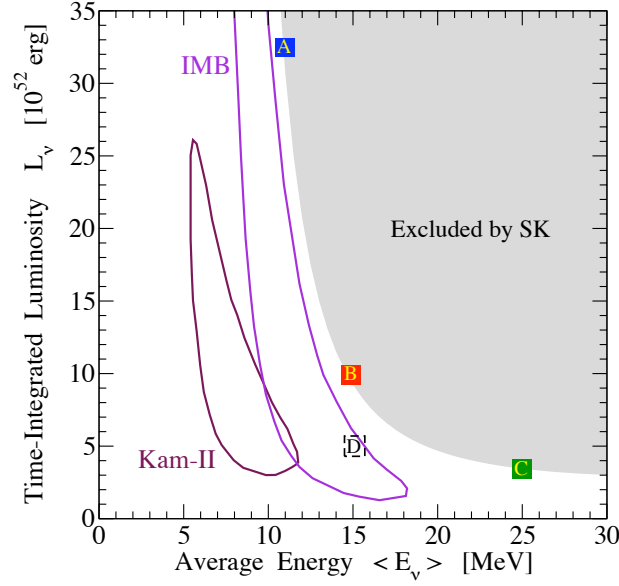


FIG. 25 From Yuksel *et al.* (2006): exclusion region from the SK limit (shaded area) in the space of luminosity and average energy of the neutrino flux. A thermal neutrino spectrum is assumed, and the parameters $R_{-4} = 3$, and $\beta = 2.5$ were used to describe the SNR (Eq. (4)). Regions allowed by SN1987A data are shown as well (contours).

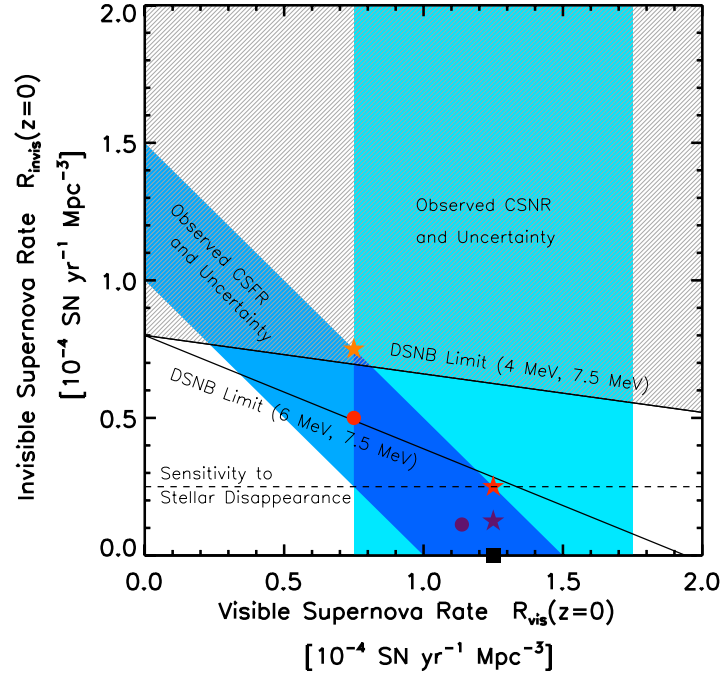


FIG. 26 From Lien *et al.* (2010): exclusion region (shaded grey) from the SK limit in the space of the cosmic rates (at $z = 0$) of neutron star-forming (successful) and black hole-forming (failed) supernovae. For these two stellar populations, thermal neutrino spectra were used with temperatures of 4 and 7.5 MeV respectively. A second contour gives the constraint for a different set of temperatures (6 and 7.5 MeV). The remaining shaded regions are those allowed by current measurements of the star formation rate (dark blue, diagonal) and of the supernova rate (light blue, vertical). The dashed line represents the projected sensitivity of future searches for failed supernovae. Stars, circles and squares refer to the parameters used in Lien *et al.* (2010) for flux predictions.

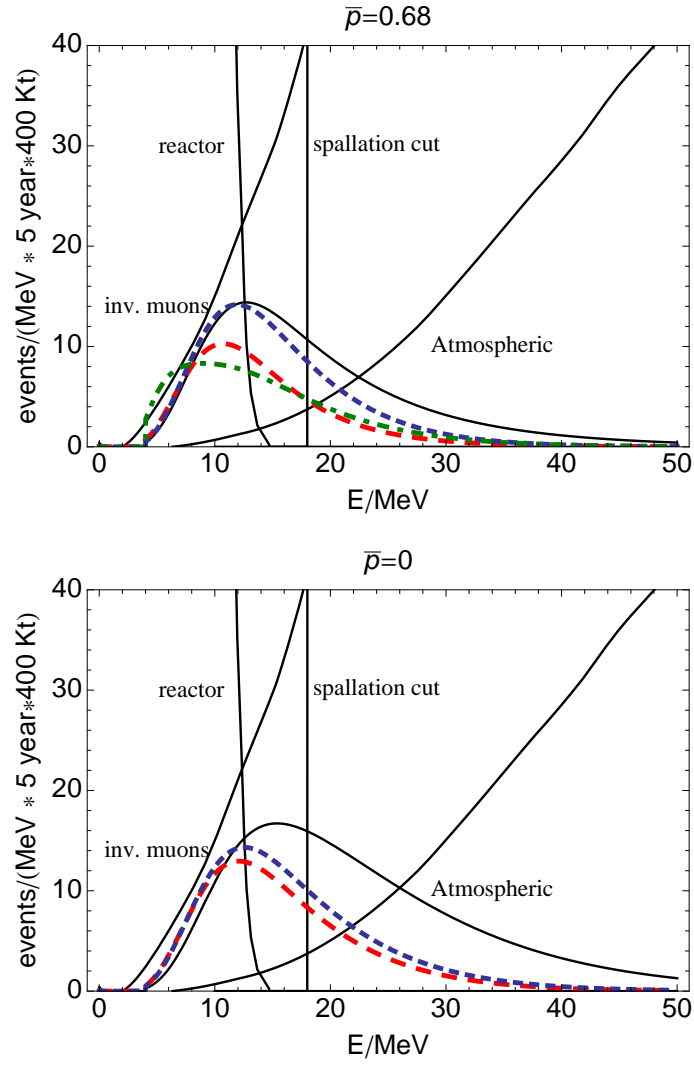


FIG. 27 Energy distribution of positrons from inverse beta decay expected at a water Cherenkov detector with a $2 \text{ Mt} \cdot \text{yr}$ exposure, located at Kamioka, for the two extreme values of \bar{p} . The solid, long dashed, short dashed and dash-dotted lines refer to the different neutrino spectra shown in fig. 16, and specifically to the models by Lawrence Livermore (LL), Arizona (TBP), Garching (KRJ) and SN1987A fit. The spectra of events from reactor neutrinos, atmospheric neutrinos and invisible muons are shown for comparison (from Fogli *et al.* (2005)). A 18 MeV energy cut (due to spallation) is shown as well.

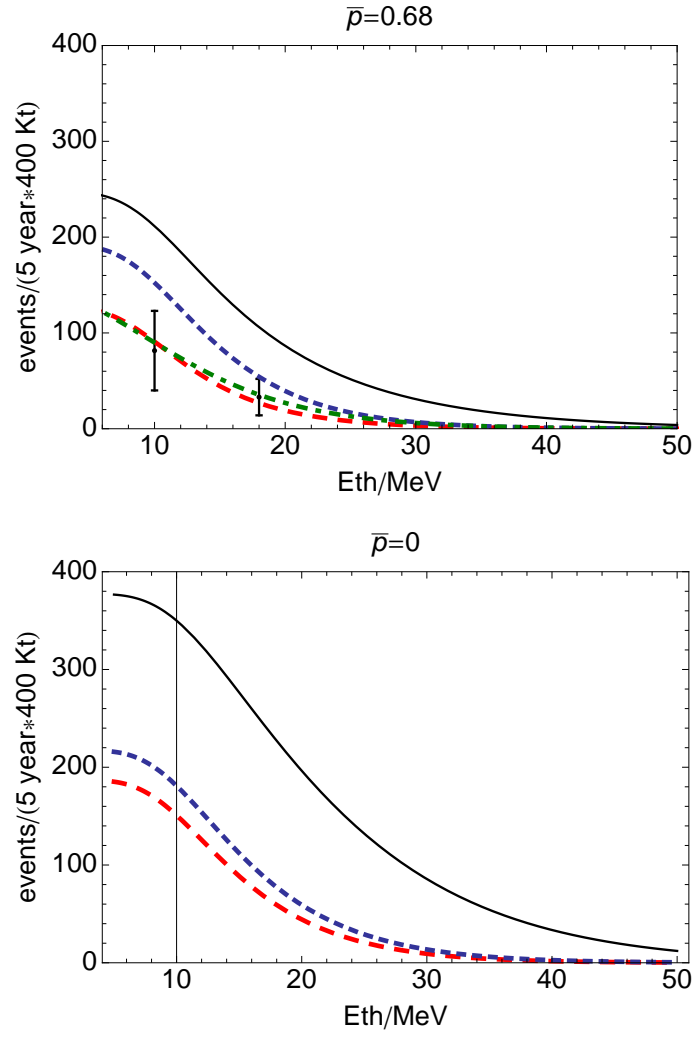


FIG. 28 Inverse beta decay events above a threshold energy E_{th} , as a function of E_{th} for the two extreme values of \bar{p} . The solid, long dashed and short dashed curves correspond to the fluxes in fig. 16 (with the same coding of colors and dashings). The vertical bars give the 90% C.L. interval predicted by imposing compatibility with SN1987A and with direct measurements of the supernova rate (Lunardini, 2006b).

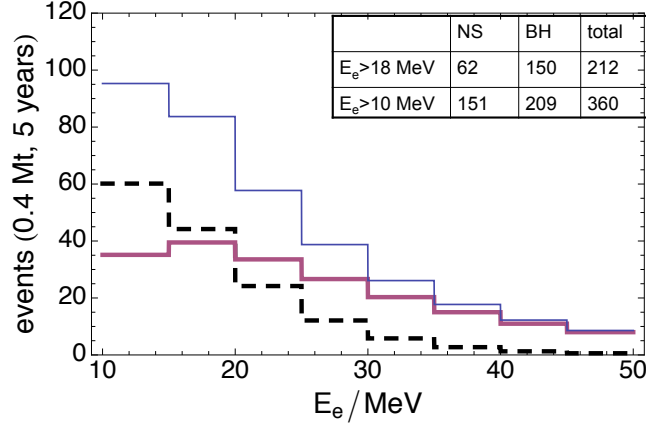


FIG. 29 From Lunardini (2009): events in water from direct black hole-forming collapses (solid thick), from neutron star-forming collapses (dashed) and the total of the two (thin line) for the best case scenario in fig. 18 (largest failed supernova flux, with the S EoS, $\bar{p} = 0.68$ and $f_{NS} = 0.78$). A 2 Mt·yr exposure is used; E_e is the positron energy. The inset gives the number of events above selected thresholds.

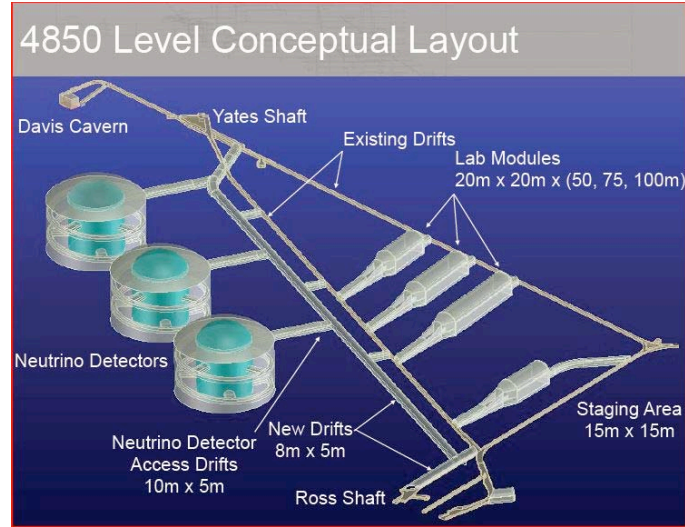


FIG. 30 DUSEL conceptual design: placement of 3 100 kt water Cherenkov chambers at 4850 ft (Diwan *et al.*, 2006) (Courtesy of D. Plate, LBNL).

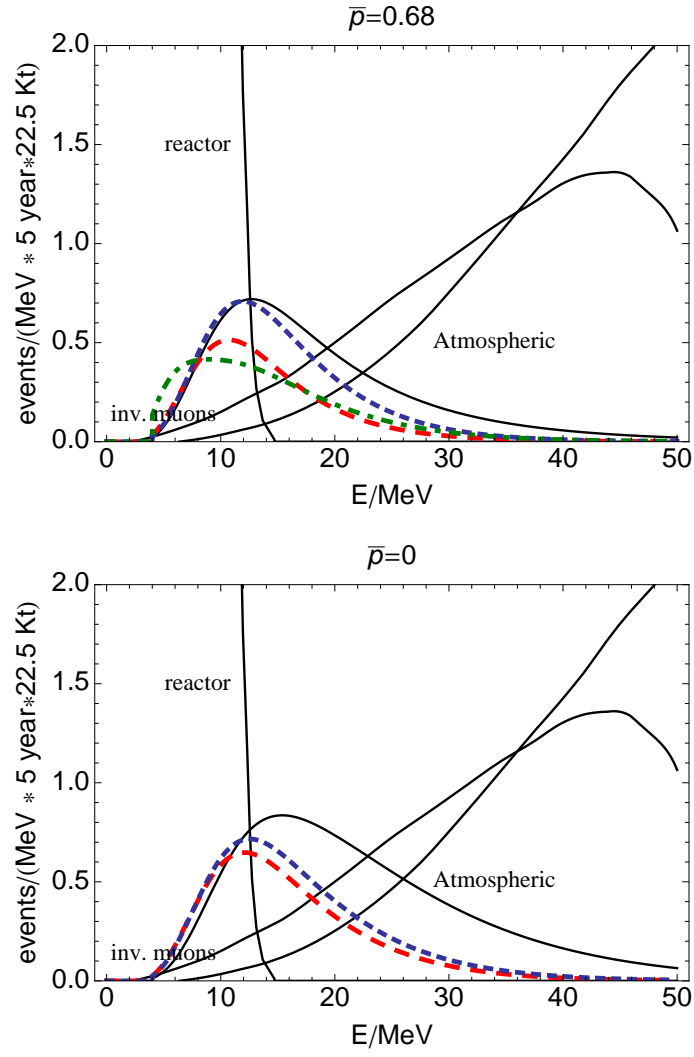


FIG. 31 The same as fig. 27 for GADZOOKS (22.5 kt water with Gd). Notice the strong reduction of the invisible muon background.

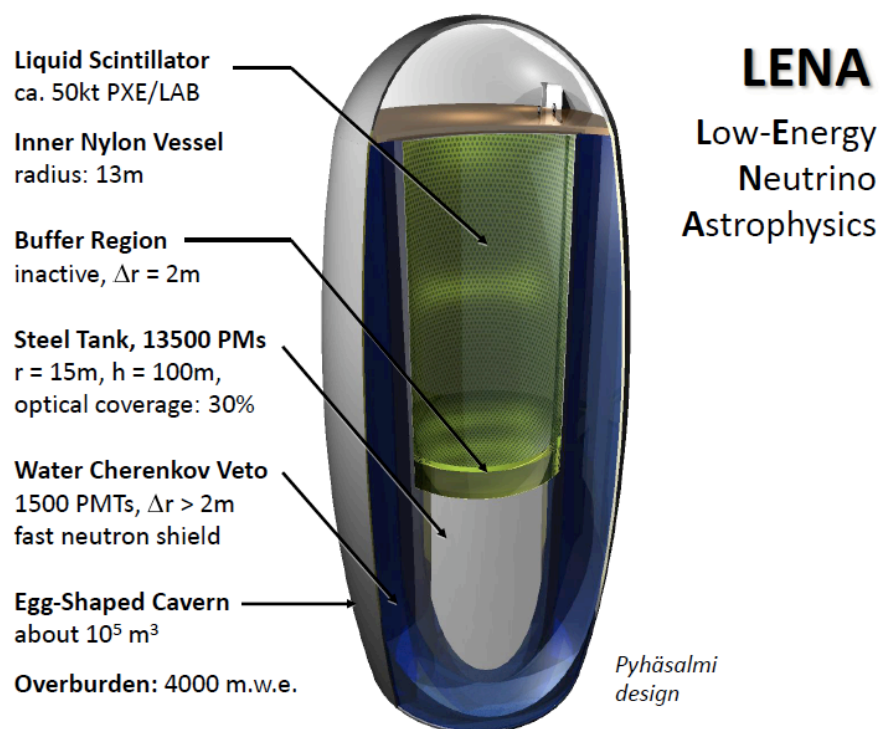


FIG. 32 LENA conceptual design for the Pyhäsalmi mine, from Lachenmaier (2009).

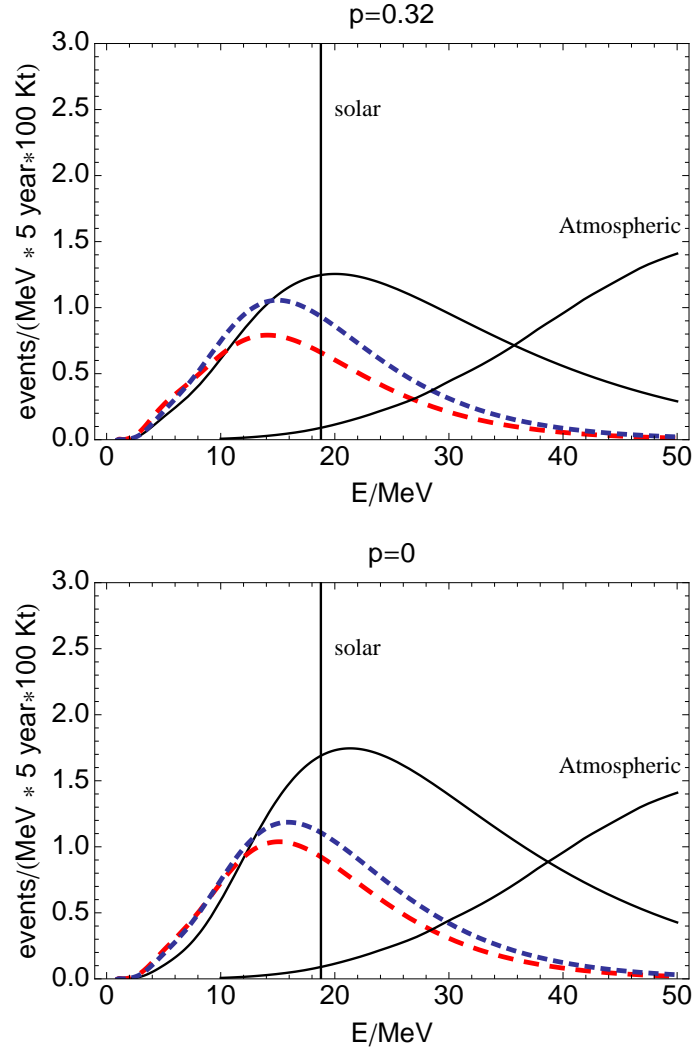


FIG. 33 Distribution of charged current ν_e events in liquid argon (Table VII) in neutrino energy for a 100 kt LAr detector located at Kamioka, for the different models of ν_e diffuse flux given in fig. 16 (same dashings and color coding), and the two extreme values of p . The spectra of events from the relevant backgrounds are shown for comparison.

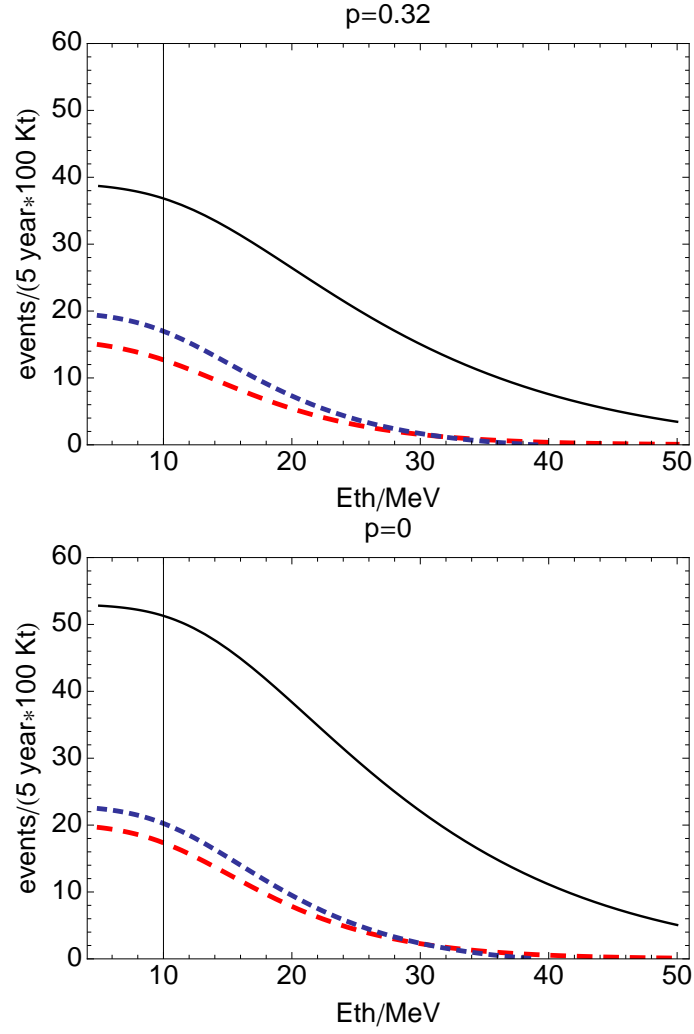


FIG. 34 ν_e CC events in liquid argon above a certain neutrino energy E_{th} , as a function of E_{th} for the two extreme values of p . The solid, long dashed and short dashed curves are from the Lawrence Livermore (LL), Arizona (TBP) and Garching (KRJ) models (see Table I). All other parameters are as in fig. 33.

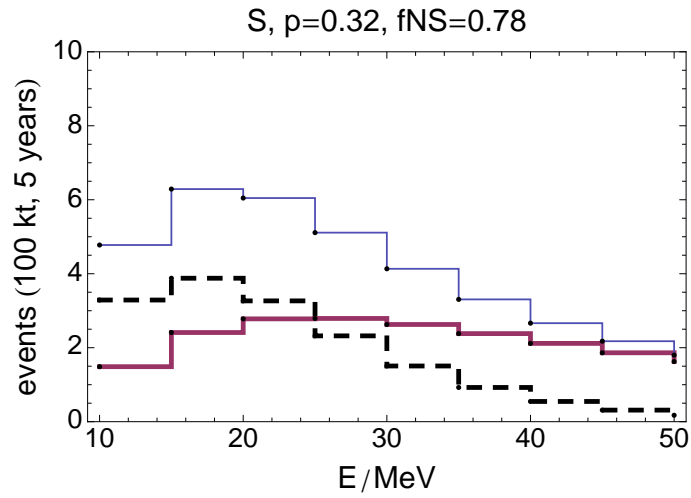


FIG. 35 From Keehn and Lunardini (2010): events in LAr from black hole-forming collapses (solid thick), from neutron star-forming collapses (dashed) and the total of the two (thin line) for the best case scenario in fig. 19 (largest failed supernova flux, with S EoS, $p = 0.32$ and $f_{NS} = 0.78$). Events are plotted in bins of neutrino energy.

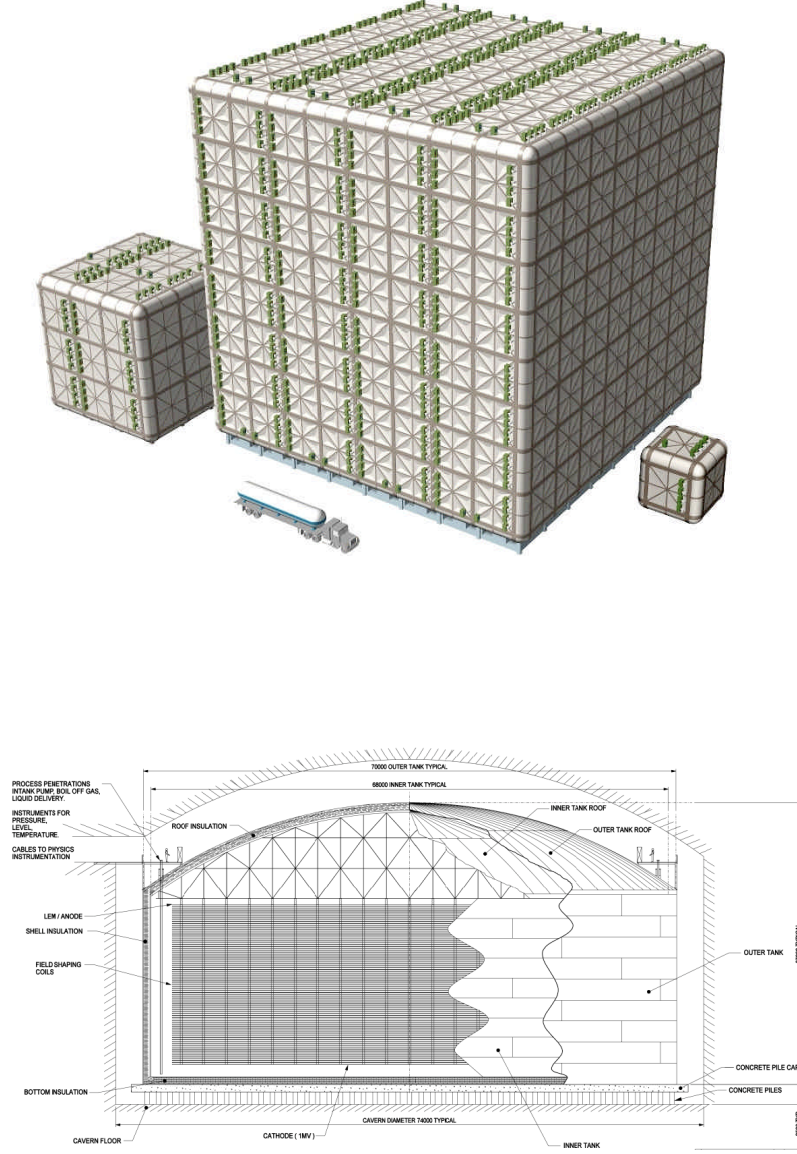


FIG. 36 Conceptual designs of two $\mathcal{O}(100)$ kt liquid argon detectors currently proposed. Upper: the US-based LANNDD (Cline *et al.*, 2006), characterized by a cellular design; the figure shows the single cell (0.8144 kt mass) and two scaled detectors, the larger made of 512 cells. Lower: the UE-based GLACIER (Ereditato and Rubbia, 2006; Rubbia, 2009b), with its characteristic domed roof.

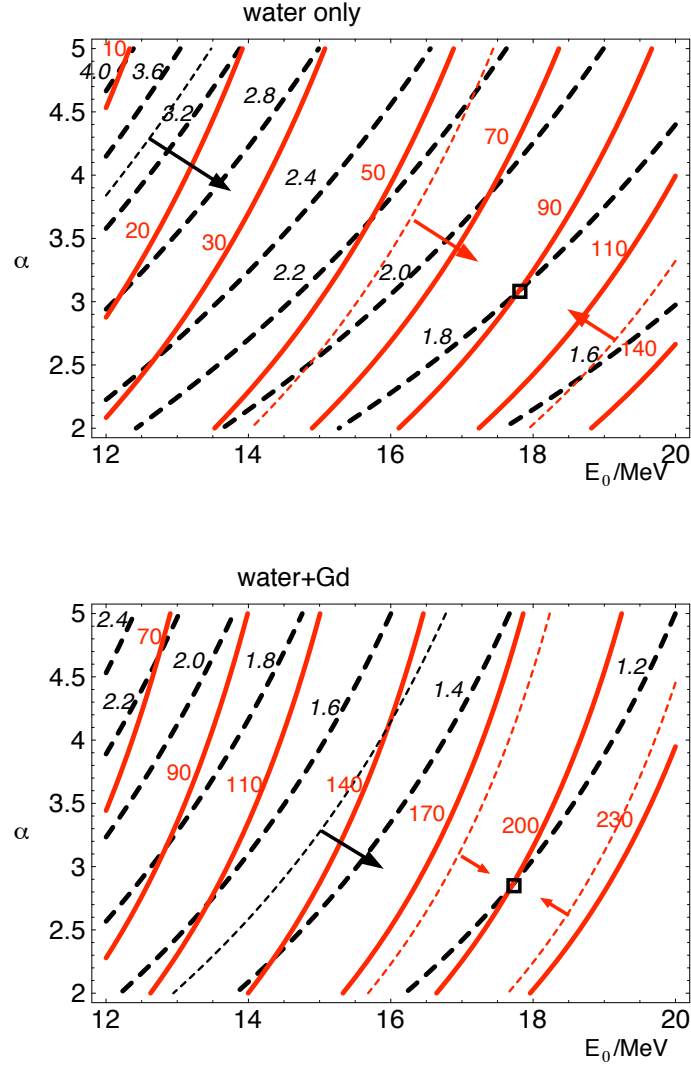


FIG. 37 From Lunardini (2007a): isocontours of the numbers of events N (solid red lines), and of the ratio r of events in the first two energy bins (Eqs. (23) and (24), long dashed black lines), at a water Cherenkov detector with $2 \text{ Mt} \times \text{yr}$ exposure, in the space of the spectral parameters $\alpha_w - E_{0w}$ (in the assumption that the spectral form in Eq. (6) applies to the $\bar{\nu}_e$ flux at Earth). In each panel a possible measurement of N and r is shown, with central values (diamond) and 1σ statistical errors (regions within the short dashed lines, marked with arrows; the wider region is the error on r). The SNR parameters and luminosity are as in fig. 16.

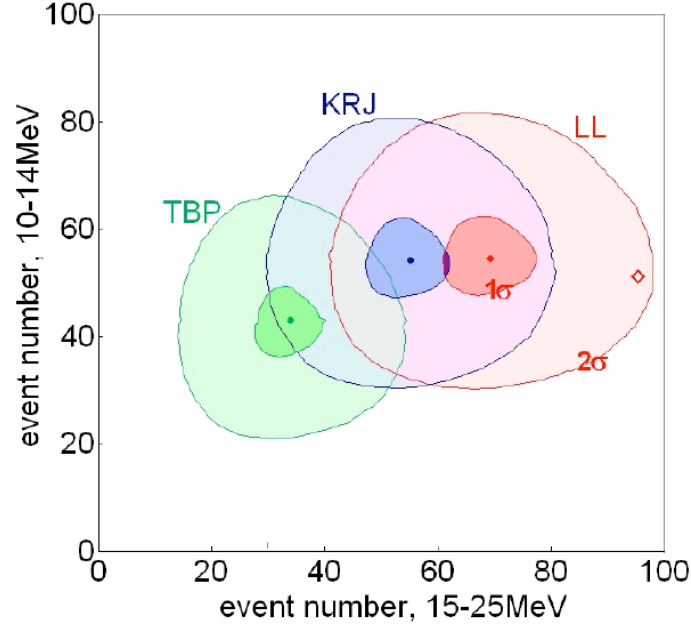


FIG. 38 From Wurm *et al.* (2007): exclusion plot for the assignment of a simulated event spectrum in LENA to a wrong DSNB model. A value of $R_{-4} = 2.1$ (see eq. (5)) and 10 years of exposure are assumed. Monte Carlo spectra created according to one of the models are compared to all possible combinations of event numbers in two energy bins. The models used are those in Table I for $\bar{p} = 0.68$ (dots). The case $\bar{p} = 0$ is included for the LL model only (diamond). Regions of more than 1 and 2 σ exclusion probability for a wrong assignment are located outside the depicted lines.

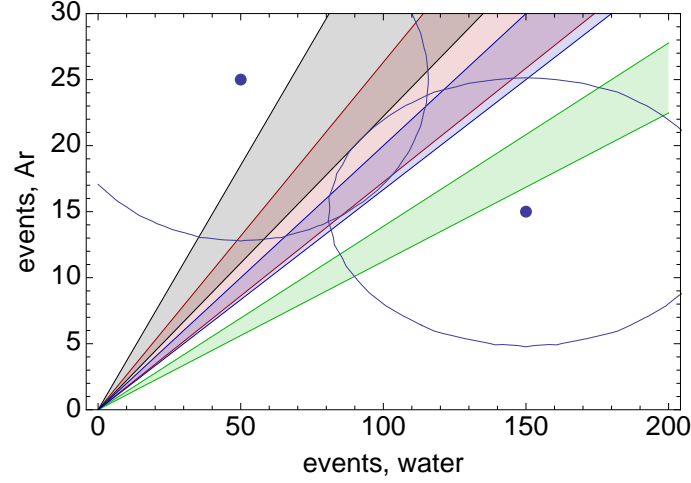


FIG. 39 Regions of the plane $N_{wa} - N_{Ar}$, with N_{wa} , N_{Ar} being the numbers of signal events in water and LAr in the energy windows $E = 19.3 - 31$ MeV and $E = 19 - 39$ MeV respectively. Each shaded area represents the region allowed for a given oscillation scenario, as in Table XV. Clockwise, they correspond to: $(\bar{p}, p) = (0.68, 0), (0.68, 0.32), (0, 0), (0, 0.32)$. The widths of these areas account for neutrino spectra varying to include those of the LL, TBP and KRJ models (Table I) and intermediate ones. The dots and contours represent the central value and 90% allowed regions (inclusive of background statistical errors) of two hypothetical measurements.

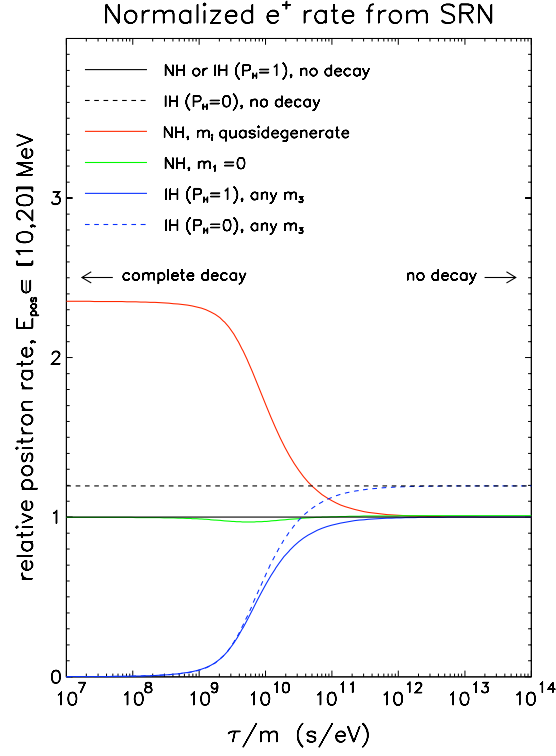


FIG. 40 From Fogli *et al.* (2004): positron event rates in water in the energy range $[10, 20]$ MeV for various decay scenarios, relative to the case of no decay with $\bar{p} \simeq 0.68$ (solid horizontal line).

Tables

Model	E_{0e}/MeV	$E_{0\bar{e}}/\text{MeV}$	E_{0x}/MeV	α_e	$\alpha_{\bar{e}}$	α_x	L_e/erg	$L_{\bar{e}}/\text{erg}$	L_x/erg
LL	11.2	15.4	21.6	3.8	3.8	1.8	4.6×10^{52}	4.9×10^{52}	5.0×10^{52}
TBP	9.1	11.4	14.1	3.8	3.7	2.2	—	—	—
KRJ	13	15.4	15.7	3.7	4.2	2.5	—	—	—

TABLE I The parameters used here, from the numerical results of the Lawrence Livermore group (LL, Totani *et al.* (1998)), of Burrows, Thompson and Pinto (Arizona group, TBP, Thompson *et al.* (2003)) and of Keil, Raffelt and Janka (Garching group, KRJ, “accretion phase model II” in Keil *et al.* (2003)). For TBP and KRJ the total neutrino luminosities are not available; the equipartition $L_e = L_{\bar{e}} = L_x = 4.9 \times 10^{52}$ ergs will be used. In the LL model α_e is not given; the same value as $\alpha_{\bar{e}}$ has been assumed.

	Normal hierarchy	Inverted hierarchy
p	$\sin^2 \theta_{12} P_H$	$\begin{cases} \sin^2 \theta_{12} & (E < E_c) \\ 0 & (E > E_c) \end{cases}$
\bar{p}	$\cos^2 \theta_{12}$	$\cos^2 \theta_{12} (1 - P_H)$

TABLE II The electron neutrino (antineutrino) survival probability, p (\bar{p}) for neutrino emerging from a supernova. Table is adapted from Dasgupta and Dighe (2008). For details, see Dasgupta and Dighe (2008); Dasgupta *et al.* (2008).

	$\phi_e^0, \phi_{\bar{e}}^0, \phi_x^0$		
	LL	TBP	KJR
total	18.4, 13.5, 9.6	22.4, 18.1, 14.6	16.0, 13.5, 13.2
$E > 11.3$ MeV	1.1, 2.2, 3.3	0.56, 1.2, 2.1	1.6, 2.2, 2.4
$E > 19.3$ MeV	0.07, 0.31, 1.10	0.018, 0.08, 0.36	0.16, 0.29, 0.46

TABLE III The unoscillated fluxes at Earth integrated above energy thresholds of interest, in $\text{cm}^{-2} \text{s}^{-1}$, for the three models in Table I.

	LL	TBP	KJR	SN1987A best fit (Eq. (17))
total	12.3	17.2	13.5	305
$E > 11.3$ MeV	2.56	1.47	2.36	1.3
$E > 19.3$ MeV	0.57	0.17	0.34	0.21

TABLE IV Integrated $\bar{\nu}_e$ flux above thresholds of interest, in $\text{cm}^{-2} \text{s}^{-1}$, for $\bar{p} = 0.68$. All parameters are as in fig. 16.

	LL	TBP	KJR
total	12.4	17.1	14.1
$E > 11.3$ MeV	2.60	1.61	2.14
$E > 19.3$ MeV	0.77	0.25	0.36

TABLE V Integrated ν_e flux above thresholds of interest, in $\text{cm}^{-2} \text{s}^{-1}$, for $p = 0.32$. All parameters are as in fig. 16.

Detector location	energy window (MeV)
Kamioka (J)	11.1 - 28.1
Frejus (F)	10.8 - 26.4
Kimballton (US)	10.6 - 28.1
Pyhasalmi (FIN)	9.7 - 25.1
Pylos (GR)	9.4 - 28.1
Homestake (US)	9.0 - 26.4
Henderson (US)	8.9 - 27.2
Hawaii (US)	8.4 - 29.0
Wellington (NZ)	8.2 - 27.2

TABLE VI The location-dependent energy window for the detection of the $\bar{\nu}_e$ component of the DSNB, defined as the interval where the signal exceeds the background fluxes of atmospheric and reactor neutrinos. The table is adapted from Wurm *et al.* (2007), where the KRJ model was used with $R_{-4} = 0.87$.

Concept	energy window (MeV)	detection processes	experiment (location)	fiducial mass (kt)	events per year
H_2O	19.3 - 30 [17.3 - 30]	$\bar{\nu}_e(\mathbf{p}, \mathbf{n})\mathbf{e}^+$	SK (Japan)	22.5	0.25 - 1.40
		$\nu_e(^{16}O, X)e^-$	DUSEL WC (USA)	300	3.3 - 18.7
		$\bar{\nu}_e(^{16}O, X)e^+$	MEMPHYS (Europe)	440	4.9 - 27.5
		$\nu_w(e^-, e^-)\nu_w$	Hyper-K (Japan)	500	5.5 - 31.2
		$\nu_w(p, p)\nu_w$ $\nu_w(^{16}O, X)\nu_w$	Deep-TITAND (Japan)	$5 \cdot 10^3$	55 - 312
$H_2O + Gd$	11.3 - 30	same as H_2O	GADZOOKS (Japan)	22.5	0.97 - 2.8
			DUSEL WC+Gd	300	12.9 - 37.2
			MEMPHYS+Gd	440	18.9 - 54.6
			Hyper-K+Gd	500	21.5 - 62.0
Scintillator	$\sim 8 - 30$	$\bar{\nu}_e(\mathbf{p}, \mathbf{n})\mathbf{e}^+$	LENA (Europe)	50	1.9 - 5.4
		$\nu_e(^{12}C, X)e^-$	Hano Hano (USA)	10	0.3 - 1.1
		$\bar{\nu}_e(^{12}C, X)e^+$ $\nu_w(e^-, e^-)\nu_w$ $\nu_w(p, p)\nu_w$ $\nu_w(^{12}C, X)\nu_w$			
Argon	$\sim 18 - 30$	$\nu_e(^{40}Ar, X)\mathbf{e}^-$	LANNDD (USA)	< 100	< 3.3
		$\bar{\nu}_e(^{40}Ar, X)e^+$ $\nu_w(e^-, e^-)\nu_w$ $\nu_w(^{40}Ar, X)\nu_w$	GLACIER (Europe)	100	0.9 - 3.3

TABLE VII Summary of running (SK only) and near-future detectors for the DSNB having mass above 10 kt. The neutrino energy windows are indicative (as they depend on a number of factors, see e.g. sec. IV.D.2) and refer to the main detection process, which is highlighted in bold. For water Cherenkov I give both the current and the improved window expected with improved background analysis (in brackets, see sec. IV.D.2). Here X stands for any final state and ν_w indicates a neutrino or antineutrino of any flavor. The intervals of event rates include the different spectral models LL, TBP and KRJ (Table I) and different oscillation scenarios. The table does not include detectors that exceed the 10 kt mass but have no capability for DSNB detection due to excessive background.

Species	Experiment	reference	energy (MeV)	limit ($\text{cm}^{-2}\text{s}^{-1}$)	C.L.
ν_e	SK	(Lunardini and Peres, 2008)	> 19.3	73.3 -154	90%
	SK (indirect)	(Lunardini, 2006a)	> 19.3	5.5	$\sim 98\%$
	SNO	(Aharmim <i>et al.</i> , 2006)	22.9 - 36.9	70	
	SK	(Lunardini, 2006a)	22.9 - 36.9	39 - 54	90%
$\bar{\nu}_e$	SK	(Lunardini and Peres, 2008; Malek <i>et al.</i> , 2003)	> 19.3	1.2 - 1.9	90%
	KamLAND	(Eguchi <i>et al.</i> , 2004)	8.3 - 14.8	3.7×10^2	90%
$\nu_\mu + \nu_\tau$	SK	(Lunardini and Peres, 2008)	> 19.3	$(1.0 - 1.4) \times 10^3$	90%
$\bar{\nu}_\mu + \bar{\nu}_\tau$	SK	(Lunardini and Peres, 2008)	> 19.3	$(1.3 - 1.8) \times 10^3$	90%

TABLE VIII Summary of the most stringent bounds on the DSNB from current detectors, with their confidence level (C.L.). The limit on the ν_e component labeled as “indirect” proceeds from the SK $\bar{\nu}_e$ limit with considerations of similarity of the ν_e and $\bar{\nu}_e$ fluxes at Earth due to neutrino oscillations in the star (Lunardini, 2006a). The results from Lunardini and Peres (2008) are given as intervals of limits, corresponding to the range of neutrino spectra used in the analysis. The SNO result is also spectrum-dependent: the quoted bound is the median of several 90% C.L. limits found with different neutrino spectra.

	Signal events				Background events	
	LL	TBP	KJR	SN1987A best fit	atmospheric	inv. muons
total	247	126	191	132		
$10 < E_e < 28$ MeV	174	86	143	82	92	851
$18 < E_e < 28$ MeV	68	22.2	44.2	27.2	76	633

TABLE IX Numbers of signal (from inverse beta decay) and background events from atmospheric neutrinos and invisible muons in energy intervals of interest at a detector of mass 0.4 Mt and livetime 5 years, for $\bar{p} = 0.68$. The total number of signal events over the whole spectrum is also given. The neutrino fluxes in fig. 16 were used; the backgrounds are for the Kamioka site (Battistoni *et al.*, 2005).

	Signal events			Background events	
	LL	TBP	KJR	atmospheric	inv. muons
total	377	186	217		
$10 < E_e < 28$ MeV	248	138	162	92	851
$18 < E_e < 28$ MeV	125	46	59	76	633

TABLE X The same as Table IX for $\bar{p} = 0$.

rock depth ft.	water equiv km-w-e	Energy thres. without (with) Gd (MeV)	Signal rate without (with) Gd relative to 18 MeV
4850	4.3	15.5 (12.0)	1.4 (2.0)
3500	3.1	17.5 (15.0)	1.1 (1.5)
3300	2.9	18.0 (15.5)	1.0 (1.4)
2000	1.8	20.5 (18.0)	0.73 (1.0)
300	0.27	25.0 (22.5)	0.36 (0.55)

TABLE XI Expected energy threshold for a water Cherenkov detector with and without Gd addition as a function of depth for detection of the DSNB, from Bernstein *et al.* (2009). The DSNB flux used in Bernstein *et al.* (2009) is close to that used here for the LL model and $\bar{p} = 0.68$ (see sec. III.B).

Detector Location		Energy Window (MeV)	DSNB Sig./Bckg. (0.5 Mt yrs)
Kamioka	(J)	11.1 - 28.1	25-49/11
Frejus	(F)	10.8 - 26.4	26-48/12
Kimballton	(US)	10.6 - 28.1	27- 52/11
Pyhäsalmi	(FIN)	9.7 - 25.1	28- 53/13
Pylos	(GR)	9.4 - 28.1	32- 57/12
Homestake	(US)	9.0 - 26.4	33- 57/13
Henderson	(US)	8.9 - 27.2	33 - 59/13
Hawaii	(US)	8.4 - 29.0	36-63/12
Wellington	(NZ)	8.2 - 27.2	36-62/12

TABLE XII Adapted from Wurm *et al.* (2007): Energy windows for DSNB observation and corresponding signal and background events for LENA at different locations after 10 years of running time. The range in the signal rates is determined by the LL and TBP model predictions for $\bar{p} = 0.68$ (sec. III.E.4). The background includes atmospheric neutrinos, reactor neutrinos and fast neutrons. 100% detection efficiency has been assumed.

	LL	TBP	KJR	atmospheric
$19 < E/\text{MeV} < 29$	11.7	4.3	6.2	2.25
$19 < E/\text{MeV} < 39$	19.6	5.6	8.2	8.6
$5 < E/\text{MeV} < 39$	30.6	14.5	19.5	9.0

TABLE XIII Rate of charged current ν_e interactions on ^{40}Ar (Tab. (VII)) in three energy windows of interest (given in terms of the neutrino energy, E) at a liquid argon detector of mass 0.1 Mt and livetime 5 years, for $p = 0.32$. All flux parameters are as in fig. 16. The atmospheric background is for the Kamioka location, and is expected to be a factor of ~ 1.5 larger at Homestake, see fig. 20.

	LL	TBP	KJR	atmospheric
$19 < E/\text{MeV} < 29$	16.6	6.1	7.8	2.25
$19 < E/\text{MeV} < 39$	28.1	8.1	10.6	8.6
$5 < E/\text{MeV} < 39$	40.7	18.8	22.5	9.0

TABLE XIV Same as Table XIII for $p = 0$.

(\bar{p}, p)	θ_{13} , hierarchy	r_N , LL model	r_N , TBP model	r_N , KRJ model
(0.68,0)	large, any	2.7	2.9	4.5
(0.68,0.32)	small, normal	3.8	4.2	5.8
(0,0)	small, inverted	5.0	6.2	6.0
(0,0.32)	large, inverted <i>no self-interactions</i>	7.2	8.9	7.8

TABLE XV The ratio r_N of the number of events in water (0.4 Mt fiducial) and LAr (100 kt fiducial) in the energy windows $E = 19.3 - 31$ MeV and $E = 19 - 39$ MeV respectively, for the different models of neutrino spectra (Table I) and several combinations of probabilities p, \bar{p} . The corresponding oscillation parameters are given according to Table II and eq. (12). “Large” (“small”) θ_{13} means $\sin^2 \theta_{13} \gtrless 3 \cdot 10^{-3}$ ($\sin^2 \theta_{13} \lesssim 10^{-5}$) or so, see sec. III.C.